Quasi-static and Dynamic Constitutive Characterization of Beryllium Bearing Bulk Metallic Glasses

Thesis by
Hugh Alan Bruck

In Partial Fulfillment of the Requirements
for the Degree of
Doctor of Philosophy

California Institute of Technology
Pasadena, CA 91125

1995
(Submitted June 16, 1994)

To the memory of my father.

The Nazis could not destroy your spirit,
and it now lives on through me.

Never again!

Acknowledgements

No thesis can be completed without the support of many individuals who deserve much appreciation and recognition. One of the most essential ingredients for a thorough and incisive research project are competent advisors, and I had two of the finest: Prof. A.J. Rosakis and Prof. W.L. Johnson. Whenever I needed guidance and moral support they were there for me, and for this I will always be grateful.

My project was also fortunate enough to have Dr. Tom Christman involved as a third advisor for a short period of time. All of the quasi-static testing was conducted under his guidance, and I will always be indebted to him for his help. My research also would not have been possible if not for the work of Dr. Atakan Peker, whose investigations in the development of bulk metallic glasses led to the discovery of the alloy used in this work. To Dr. G. Ravichandran I would like to say thanks for the use of your lab facilities, knowledge, and friendship. Also, I would like to thank Mark Walter and Weinong Chen for answering my questions and keeping the Firestone labs in such great shape.

In addition to the lessons I learned in the lab, there were many to be learned from people outside as well. Drs. Guillame Vendroux and John Lambros provided me with the diversions and friendship I needed to keep my research in perspective. Melinda Knox made it easier for me to concentrate on my research by being such a great roommate. K.C. Mcbride made Firestone a bearable place to work in through her humor and her knowledge of Caltech's beauracratic details.

I would also like to thank the people who are the foundation of my life: my mother Barbara, my father Frank, my sister Gina, and my academic father Dr. Mike Sutton. I cannot imagine having lived my life without any of you, for you gave me the strength to complete this work and the love I needed to be a human being.

Abstract

Metallic glasses were first discovered by Pol Duwez in 1960 using the fabrication technique of splat quenching. The mechanical behavior of metallic glasses were first characterized in 1969 from tensile tests conducted on thin ribbons. From these tests it was apparent that metallic glasses possessed tensile fracture strengths of approximately $\frac{E}{50}$, which approach theoretical limits. Compressive mechanical data became available in 1974 with the fabrication of small cylindrical rods of $Pd_{78}Cu_6Si_{16}$. This data indicated that the quasi-static yield behavior of metallic glasses may obey a pressure insensitive von Mises yield criterion. In 1983, Mechanical tests were conducted on $Pd_{78}Cu_6Si_{16}$ in multi-axial stress states which further confirmed the von Mises yield behavior. However, in 1988, mechanical tests performed on $Pd_{40}Ni_{40}P_{20}$ indicated that metallic glasses may instead obey a pressure sensitive Mohr-Coulomb criterion.

There is some ambiguity in interpreting the results of mechanical tests performed on metallic glasses. The data from these tests were obtained by testing specimens whose sizes do not gaurantee a well-defined stress state. Furthermore, the mechanical behavior of metallic glasses may depend on composition. In order to properly determine the yield behavior of metallic glasses in multi-axial stress states, it was necessary to fabricate specimens with geometries suitable for generating well-defined stress states.

In 1993, a new beryllium bearing bulk metallic glass with the nominal composition of $Zr_{41.25}Ti_{13.75}Cu_{12.5}Ni_{10}Be_{22.5}$ was discovered at Caltech. This metallic glass can be cast as cylindrical rods as large as 16 mm in diameter. Specimens could then be fabricated with geometries that conformed to ASTM testing standards. These specimens were then tested in quasi-static compressive, tensile, and torsional stress states at strain rates of 10^{-4} to 10^{-3}/sec in order to properly characterize the yield behavior of the metallic glass. From these tests it was determined that the beryllium bearing bulk metallic glass obeys a von

Mises yield criterion. In addition it was discovered that the ductility of this metallic glass could be altered by adding Boron and varying the quench rate.

For the first time, the dynamic compressive yield behavior of a metallic glass could be characterized at strain rates of 10^2 to 10^4/sec by using the split Hopkinson pressure bar. High-speed infrared thermal detectors were also used to determine if adiabatic heating occurred during dynamic deformation of the metallic glass. From these tests it appears that the yield stress of the metallic glass is insensitive to strain rate and no adiabatic heating occurs before yielding.

TABLE OF CONTENTS

CHAPTER 1

Introduction

1.1 Characteristics of Metallic Glasses

Metallic glasses fabricated by direct quenching from the melt were first discovered in 1960 by Klement, Willens, and Duwez at Caltech[1]. By rapidly quenching a solution of Au-Si at a eutectic composition, phase separation was prevented and the undercooled liquid state was "frozen" resulting in a completely amorphous microstructure. A "splat-cooling" technique was used to achieve the cooling rates necessary to suppress phase separation. This technique produced only a limited quantity of amorphous material. In 1969, a new technique was developed by Pond and Maddin for manufacturing continuous long lengths of thin amorphous ribbon, which made metallic glasses a commercial reality[2].

However, there was a problem in scaling up metallic glasses to bulk sizes large enough for the fabrication of structures. Because of the high quench rate requirements (10^4-10^6 K/sec), only thin ribbons and sheets with thicknesses less than 100 µm could be fabricated. It was therefore necessary to find a way to manufacture bulk metallic glasses before the structural applications of metallic glasses could be investigated.

The microstructure of a metallic glass can be characterized by the absence of long range order resulting in no crystalline microstructure. Consequently, microstructural defects found in crystalline microstructures, such as dislocations, can not be found in metallic glasses. Instead, models have been developed which describe defects in metallic glasses using concepts such as local free volume and coordination numbers. Also, because crystals do not nucleate in the amorphous matrix, there are no first-order phase transformations during solidification which results in continuous changes in the mechanical and thermodynamic properties of the metallic glass.

Experimental evidence of the amorphous microstructure in a metallic glass was first obtained by x-ray diffraction analysis. The x-ray diffraction patterns of a metallic glass are characterized by the disappearance of the sharp Bragg peaks which are indicative of a crystalline microstructure. Instead, there are just one or two very broad peaks which can also be obtained when performing x-ray analysis on a liquid. X-ray diffraction analysis does have the limitation that crystals with grain sizes less than 2 nm can not be detected; therefore, high resolution TEM was also used to verify that the microstructure was amorphous at the atomic level.

1.2 Significant Properties of Metallic Glasses

Once long lengths of amorphous ribbons were manufactured, it was possible to mechanically test metallic glasses to determine their tensile behavior[3,4]. These tests indicated that metallic glasses possessed tensile fracture strengths of approximately $\frac{E}{50}$, which are much higher than their crystalline counterparts and approach theoretical limits calculated from atomistic models. These alloys were also found to possess densities within 1-2% of their polycrystalline counterparts[5,6]. Thus, the strength-to-density ratios of metallic glasses were much higher than any commercially available alloy. This indicated that metallic glasses might be suitable for a number of structural applications. Fracture tests conducted on thin sheets also indicated that metallic glasses might possess fracture resistances comparable to their crystalline counterparts[7-9]. However, it should be observed that a valid plane strain fracture test can not be performed on thin specimens, and thus the results from thin sheets should be considered with caution. In addition, the lack of a crystalline microstructure provided metallic glasses with an excellent resistance to corrosion[10].

The metallic glasses ribbons that were mechanically tested also indicated some unique plastic behavior that had not been observed in conventional polycrystalline

alloys[3,11-13] . Although the strength of metallic glass ribbons approached theoretical limits in tension, they also appeared to possess no ductility at room temperature even though ribbons could be bent back upon themselves without fracturing and could be deformed homogeneously at elevated temperatures near the glass transition point. Further investigations of the tensile fracture surfaces indicated that the morphology and orientation were not indicative of brittle failure. Instead, they appeared to possess features which were similar to those observed on the fracture surfaces of polycrystalline alloys that failed due to shear localization. Since shear localization is a plastic instability, it was difficult to determine the inherent ductility of metallic glasses from tension tests.

In order to better understand the inherent ductility of metallic glasses, ribbons and wires were rolled and drawn at room temperature[14,15] . These experiments showed that the thicknesses and diameters of the metallic glass ribbons and wires could be reduced substantially without failing, which indicated enormous ductility. When these ribbons and wires were then chemically etched, a diffuse array of shear bands appeared that had formed during cold deformation. Thus, it was concluded that if shear band formation could be constrained, the metallic glasses would exhibit the ductility that is necessary for a number of manufacturing processes.

Annealing investigations were also conducted on the metallic glass ribbons at temperatures below the recrystallization point[16,17]. These experiments found that although the sample remained amorphous after annealing, the material sometimes lost its ductility depending on the sample's composition, annealing temperature, and annealing time. Ribbons that could be bent back upon themselves without fracturing before annealing were found to fracture after annealing. Additional investigations found that the effects of annealing embrittlement could be reversed by neutron irradiation[18] .

Because of the unique plastic behavior exhibited by the thin ribbons, it became even more important to find a way to fabricate bulk metallic glasses so that their mechanical behavior could be completely characterized. In 1969, Chen and Turnbull

discovered that $Pd_{78}Cu_6Si_{16}$ could be quenched in quartz tubes as amorphous rods up to 2 mm in diameter[19]. The cooling rate requirement for metallic glass formation of $Pd_{78}Cu_6Si_{16}$ was on the order of 10^3 K/sec, which was the lowest cooling rate requirement for metallic glass formation ascertained at the time this project was started.

The metallic glass specimens manufactured from $Pd_{78}Cu_6Si_{16}$ were large enough that uniaxial compression tests could be conducted on them. The results from these compression tests indicated that metallic glasses were elastic-perfectly plastic materials with yield stresses approaching theoretical limits[12]. In addition, the compression test specimens exhibited significant compressive ductility before catastrophic failure occurred due to fracture along shear bands. Compression tests were also conducted under hydrostatic pressure, the results of which indicated that the yield stress of metallic glasses was no more sensitive to pressure than that of a polycrystalline metal[20].

In addition to compression tests, a series of tension-torsion tests were conducted in 1983 by Kimura and Masumoto on cylindrical rods of $Pd_{78}Cu_6Si_{16}$ to try and complete the quasi-static constitutive characterization of metallic glasses[21]. Unfortunately, the size and geometry of the test specimens were not clearly indicated, which introduces some ambiguity in the validity of these results. From these tests Masumoto deduced that metallic glasses obeyed a von Mises yield condition. Annealing embrittlement tests were also conducted on notched plates of $Pd_{78}Cu_6Si_{16}$ to try and characterize the micromechanisms responsible for ductility in metallic glasses[22]. These tests indicated that annealing embrittlement was not due to suppression of slip processes but instead was due to a decrease in the micro-fracture stress below the stress required for generalized yielding.

Masumoto's work was thought to have nearly completed the quasi-static constitutive characterization of metallic glasses, until in 1989 Donovan reported results from mechanical tests performed on $Pd_{40}Ni_{40}P_{20}$ which contradicted Masumoto's findings[23]. Since $Pd_{40}Ni_{40}P_{20}$ is not as good a glass former as $Pd_{78}Cu_6Si_{16}$, the specimens

that Donovan used were not large enough for standard tension-torsion tests. A special shear test was therefore constructed which was supposed to create a state of pure shear between a pair of collinear notches that were machined into the edges of a small rod. This specimen configuration was similar to Iosipescu specimens. Combining the results of the shear test with the results from tension and compression tests, Donovan concluded that the $Pd_{40}Ni_{40}P_{20}$ metallic glass obeyed a pressure sensitive Mohr-Coulomb yield criterion.

1.3 Micromechanical Models for Metallic Glasses

Various micromechanical models have been proposed to account for the mechanical behaviour of metallic glassess. These models have spawned significant debate regarding their suitability for describing the observed mechanical properties. Some of these models have adapted descriptions of classical defects in polycrystalline materials to metallic glasses[24-26]. However, developing consistent and unique definitions of defects in amorphous structures is difficult because of the absence of long range order in these structures and remains a topic of controversy. There is also a limited amount of information available on the inelastic deformation of bulk metallic glasses in multi-axial stress states[21,23], which is necessary to critically assess the proposed micromechanical models. In addition, and unlike crystalline solids, no direct observations of such defects has been achieved by means of electron microscopy or other experimental techniques.

Micromechanical models using the concept of free volume have been developed to account for the inelastic deformation of metallic glasses. Spaepen proposed that inelastic deformation occurs because of the destruction and creation of local free volume[27]. Argon suggested that two modes of thermally activated shear transformations are responsible for differences in the mode of inelastic deformation[28]. At higher temperatures ($>0.7T_g$), a large free volume permits diffuse structural rearrangements producing a small local shear strain in a roughly spherical region. However, at lower temperatures ($<0.7T_g$) a

rearrangement resembling the nucleation of a dislocation loop is concentrated in a narrow disk shaped region due to the lack of free volume. If free volume is the micromechanism responsible for yielding in a metallic glass, then one might expect glasses to be Mohr-Coulomb materials as indicated by Donovan[23].

In addition to the free volume models, dislocation-like and disclination-like processes have also been proposed to account for inelastic deformation. Gilman postulated that dislocations of variable Burger's vectors exist in metallic glasses[24]. The Burger's vectors of such dislocations have an average magnitude which is equal to the nearest neighbor separation of atoms in the alloy. Li described the stress and strain fields of the slip bands terminating inside a sample as Somigliana dislocations[24]. The Burgers vectors of these dislocations are much larger than the nearest neighbor separations and they are created as a result of the propagation of macroscopic slip bands. Disclinations have also been used by Nelson[26] to model amorphous structures. Using the concept of disclinations, it can be proposed that local rotations of disclination cores are responsible for deformation in metallic glasses. One drawback to all of these models is the difficulty in describing defects in metallic glasses using classical defects in crystalline structures because of the lack of long range order in the amorphous structure. If dislocations and disclinations are the micromechanisms responsible for yielding in a metallic glass, then one might expect glasses to be von Mises materials as indicated by Masumoto[21].

Two-dimensional and three-dimensional computer simulations have also been used to model the inelastic deformation of metallic glasses at microscopic levels. Srolovitz, Vitek, and Egami suggest that the fundamental microscopic deformation mechanisms are the same at low and high temperatures and that the differences are due to strain localization[29]. They defined two types of defects: (1) n- and p- type defects associated with local density fluctuations, and (2) τ-defects which exist in regions of high shear stress and act as stress concentrators. Regions of inhomogeneous atomic movement which result in inelastic deformation were found to be most strongly related to τ-defects, not n- and p-

type defects. The τ-defects can therefore be visualized as microscopic shear cracks in the vicinity of which localized viscous flow develops. Takeuchi and Maeda considered a zonal slip process where a shear front propagates in a more diffuse manner than the usual dislocation glide in crystals[30] . A criterion for propagation of a shear band was given by a critical stress at the shear front. Therefore, when the internal stress at the shear front plus the applied stress reaches a critical stress, successive localized shear deformations occur in the periphery of the shear front. The results of numerical simulations tend to support the idea of dislocation- and disclination-like micromechanisms.

1.4 Motivation and Objectives

The work of Masumoto and Donovan has raised some important questions about the qausi-static constitutive behavior of metallic glasses. Were the experiments performed on specimens of sufficient size to produce a well defined stress state during mechanical testing? If the results are correct, is it possible for different metallic glasses to obey different yield criterion? Can the microfracture stress be used to explain other types of embrittlement in metallic glasses?

The goal of the work reported here was to answer these questions and gain insight into the possible micromechanisms responsible for deformation in metallic glasses by performing mechanical tests on specimens fabricated from a new bulk metallic glass with the nominal composition $Zr_{41.25}Ti_{13.75}Cu_{12.5}Ni_{10}Be_{22.5}$. This bulk metallic glass was found to be an excellent glass former with a cooling rate requirement on the order of 1 K/sec which allowed cylindrical specimens to be fabricated up to 16 mm in diameter by casting in an evacuated quartz[31]. Because of the low cooling rate requirements, bulk metallic glass compression specimens could be fabricated using a wide range of quench rates to investigate the effects quench rates have on the ductility of metallic glasses. The $Zr_{41.25}Ti_{13.75}Cu_{12.5}Ni_{10}Be_{22.5}$ metallic glass was also found to be such a good glass

former that up to 5% boron could be added to the alloy without compromising its glass formability. Therefore, effects of metalloid addition on the compressive ductility of metallic glasses were also investigated.

All of the constitutive characterization of metallic glasses has been performed in quasi-static tests. No data are currently available on the dynamic constitutive behavior of metallic glasses. It was the final goal of this work to characterize the dynamic compressive yield behavior of the $Zr_{41.25}Ti_{13.75}Cu_{12.5}Ni_{10}Be_{22.5}$ metallic glass using a split Hopkinson pressure bar. Thermal measurements were also made using high speed infrared temperature sensors to investigate whether adiabatic heating occurs during the dynamic deformation of the glass.

References

[1] Klement, K., Willens, R.H., and Duwez, P., Nature, **187**, 869 (1960).

[2] Pond, R., Jr. and Maddin, R., TMS-AIME, **245**, 2475 (1969).

[3] Masumoto, T. and Maddin, R., Acta Metallurgica, **19**, 725 (1971).

[4] Chen, H.S. and Wang, T.T., Journal of Applied Physics, **41**, 5338 (1970).

[5] Cargill, G.S., Journal of Applied Physics, **41**, 12 (1970).

[6] Chen, H.S. and Park, B.K., Acta Metallurgica, **21**, 395 (1973).

[7] Davis, L.A., Journal of Materials Science, **10**, 1557 (1975).

[8] Kimura, H. and Masumoto, T., Scripta Metallurgica, **9**, 211 (1975).

[9] Ast, D.G. and Krenitsky, D., Materials Science and Engineering, **23**, 241 (1976).

[10] Hashimoto, K., Amorphous Metallic Alloys, ed. by F.E. Luborsky, Buttersworth, London, 471 (1983).

[11] Maddin, R. and Masumoto, T., Materials Science and Engineering, **9**, 153 (1972).

[12] Pampillo, C.A. and Chen, H.S., Materials Science and Engineering, **13**, 181 (1974).

[13] Leamy, H.J., Chen, H.S., and Wang, T.T., Metallurgical Transactions, 3, 699 (1972).

[14] Masumoto, T. and Maddin, R., Materials Science and Engineering, 19, 1 (1975).

[15] Takayama, S., Materials Science and Engineering, 38, 41 (1979).

[16] Luborsky, F.E. and Walter, J.L., Journal of Applied Physics, 47, 3638 (1976).

[17] Davis, L.A., Ray, R., Chou, C.-P., and O'Handley, R.C., Scripta Metallurgica, 10, 541 (1976).

[18] Kramer, E.A., Johnson, W.L., and Cline, C., Applied Physics Letters, 35, 815 (1979).

[19] Chen, H.S. and Turnbull, D., Acta Metallurgica, 17, 1021 (1969).

[20] Davis, L.A. and Kavesh, S., Journal of Materials Science, 10, 453 (1975).

[21] Kimura, H. and Masumoto, T., Amorphous Metallic Alloys, ed. by F.E. Luborsky, Buttersworth, London, 187 (1983).

[22] Kimura, H. and Masumoto, T., Acta Metallurgica, 28, 1677, (1980).

[23] Donovan, P., Acta Metallurgica, 37, 445 (1989).

[24] Gilman, J.J., *Journal of Applied Physics*, 46, 1625 (1975).

[25] Li, J.C.M., in Rapidly Quenched Metals 4, ed. by T. Masumoto and S. Suzuki,Vol. 2, Japan Institute of Metals, 1335 (1981).

[26] Nelson, D.R., Physical Review B, 28, 5515 (1983).

[27] Spaepen, F., Acta Metallurgica, 25, 407 (1977).

[28] Argon, A.S., Acta Metallurgica, 27, 47 (1979).

[29] Srolovitz, D., Vitek, V., and Egami, T., Acta Metallurgica, 31, 335 (1983).

[30] Takeuchi, S. and Maeda, K., Key Engineering Materials, Vol. 13-15, 749 (1987).

[31] Peker, A. and Johnson, W.L., Applied Physics Letters, 63, 2342 (1993).

CHAPTER 2

Specimen Fabrication

2.1 Material Selection

The first step towards choosing a model material system for the quasi-static and dynamic constitutive characterization of metallic glasses was to establish a set of criteria for the material selection. The criteria for material selection consisted of the following:

(a) The material system should consist of components that were cheap and readily available.

(b) It should be possible to fabricate metallic glasses from the system.

(c) A technique should be available which would allow the metallic glass to be processed into bulk specimens without devitrifying the system.

(d) Bulk specimens should be fully dense, homogeneous, and free of macroscopic defects.

There were many suitable materials to select for the model system that fit one or more of the above requirements. These material systems could be fabricated in three primary forms: (1) thin ribbons and foils, (2) powders and (3) small cylindrical rods. Thin ribbons and foils (thickness < 1 mm) could be fabricated by melt spinning on the outside of a wheel and splat quenching between a pair of pistons[1,2]. Powders (particle size < 100 μm) could be fabricated by gas atomization and ball milling[3,4]. Small cylindrical rods (diameter < 2 mm) could be fabricated from only a select few material systems whose cooling rate requirements for glass formation were very low (cooling rate ~ 10^3 K/sec)[5,6].

The material systems that could be fabricated as small cylindrical rods were $Pd_{78}Cu_6Si_{16}$ and $Pd_{40}Ni_{40}P_{20}$. Although the rods that could be fabricated from these systems were almost of a size suitable for mechanical testing, palladium is prohibitively expensive and not readily available.

Powders and ribbons could be easily manufactured from a number of material systems that were relatively inexpensive and easily available. However, it was necessary to find a consolidation technique capable of producing fully dense bulk specimens from powders or ribbons without degrading the mechanical properties of the original alloy or devitrifying the system. The technique that exhibited the greatest viability for consolidation was solid state amorphization, which basically consisted of cold welding together pieces of ribbon by using diffusional bonding which created an amorphous interface in the process[7].

Solid state amorphization was thus the initial choice for fabricating bulk specimens. Since previous research had been conducted on solid state amorphization using nickel and zirconium, $Ni_{36}Zr_{64}$ seemed an ideal choice for the model system. Amorphous $Ni_{36}Zr_{64}$ ribbon 40 μm thick were easily fabricated by melt spinning. Several ribbons were pressed together inside a stainless steel sheath which was then deformed between a pair of hardened steel rollers until a limit was reached beyond which the sheath could no longer be deformed. The sheath was then folded over upon itself and the process was repeated. After repeating the process two or three times, the amorphous ribbon should have been cold welded together.

Initial attempts at cold welding layers of amorphous ribbons indicated that the interfaces did not bond uniformly even though the individual ribbons appeared to have been deformed from an initial thickness of approximately 40 μm to a final thickness of 2 μm (Figure 1). This result was attributed to the presence of oxides on the surface of the ribbons which could be removed by polishing. However, it was becoming clear that a monumental effort would be required to fabricate bulk specimens using the technique of solid state amorphization. Numerous macroscopic shear bands were also observed running through the layers of ribbon at an angle of 45[o] to the rolling direction. In addition, it was not certain after consolidating the ribbon that the composition and mechanical properties of the interface would be similar to those of the ribbons, thereby violating the homogeneity requirement. It was also possible that the deformed ribbon would not exhibit the same

mechanical behavior as the undeformed ribbon since mechanical tests conducted on cold rolled ribbon indicated that the mechanical properties of metallic glasses could be altered by large plastic deformations.
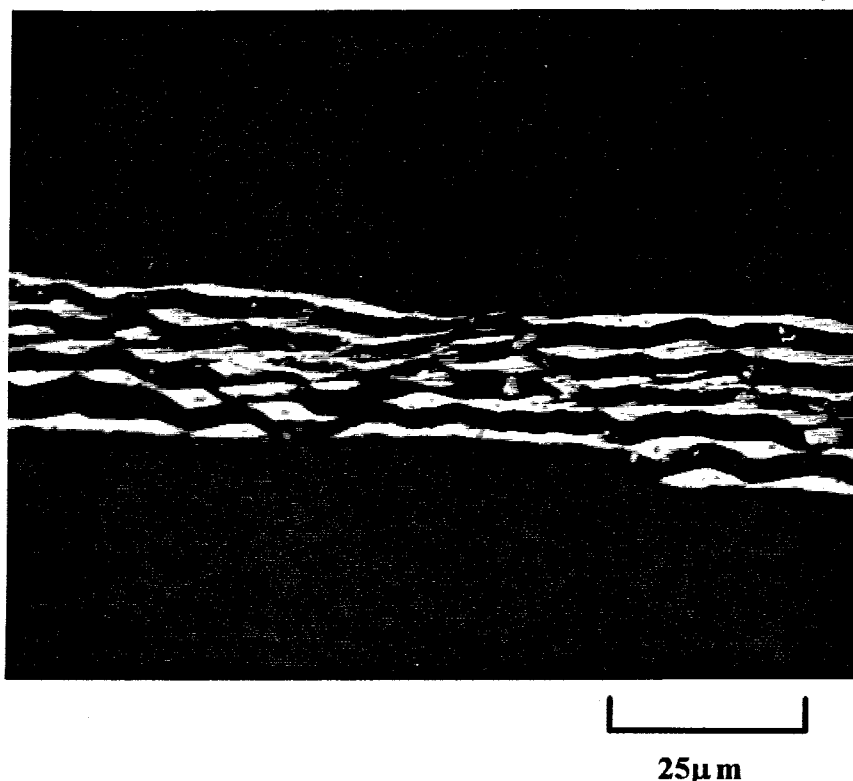

25μm

Figure 1: Attempt at mechanically bonding 5 layers of amorphous $Ni_{36}Zr_{64}$ ribbon.

2.1.1 The $Zr_{65}Ni_{10}Cu_{17.5}Al_{7.5}$ bulk metallic glass

At the time these initial investigations into using solid state amorphization to fabricate bulk amorphous specimens were concluding, an exciting development in the fabrication of bulk metallic glasses was reported by the group of Inoue and Masumoto at Tohoku University in Sendai, Japan[8]. They found that by adding the proper quantity of aluminum and copper to the Ni-Zr system, the cooling rate requirements for glass formation could be substantially reduced. In fact, the glass formability of this new amorphous alloy was even better than that of $Pd_{78}Cu_6Si_{16}$. This group reported fully

amorphous cylindrical rods up to 7 mm in diameter could be cast by injecting the molten alloy into copper molds.

It immediately became obvious that the $Zr_{65}Ni_{10}Cu_{17.5}Al_{7.5}$ system would be the ideal model system for the constitutive characterization of metallic glasses. Research efforts were then undertaken to reproduce the results of Inoue and Masumoto. These efforts were at first unsuccessful because the $Zr_{65}Ni_{10}Cu_{17.5}Al_{7.5}$ system turned out to be very sensitive to the quality of the zirconium used in the alloy. Rods 3 mm in diameter were cast from alloys which were fabricated using lumped zirconium and zirconium wire that contained up to 4.5% hafnium. X-ray diffraction analysis revealed that these rods turned out to be partially crystalline and amorphous (Figure 2). Since it was possible that the hafnium was contaminating the alloy by increasing the cooling rate requirements, turnings were obtained from zirconium crystal bars that had been zone refined and contained only trace amounts of hafnium. These turnings were then used in place of the lumped zirconium and wire, and rods 3 mm in diameter were once again cast. X-ray diffraction analysis revealed that these rods were fully amorphous (Figure 3).

After successfully reproducing the results of Inoue and Masumoto, cylindrical test specimens were prepared for quasi-static compression and tension testing. Casts were made of cylindrical rods 2.5 and 3 mm in diameter and 25.4 mm long from which smaller cylindrical specimens with length-to-diameter aspect ratios of 2 were cut for compression tests. The ends of these specimens were then polished until they were parallel to within 3 μm. A special load frame was used for the compression tests to insure uniform, uniaxial loading. End effects were reduced by placing the specimen between a pair of WC inserts coated with a high pressure grease. A typical compressive stress-strain curve for the $Zr_{65}Ni_{10}Cu_{17.5}Al_{7.5}$ metallic glass can be seen in Figure 4. It exhibits the same elastic
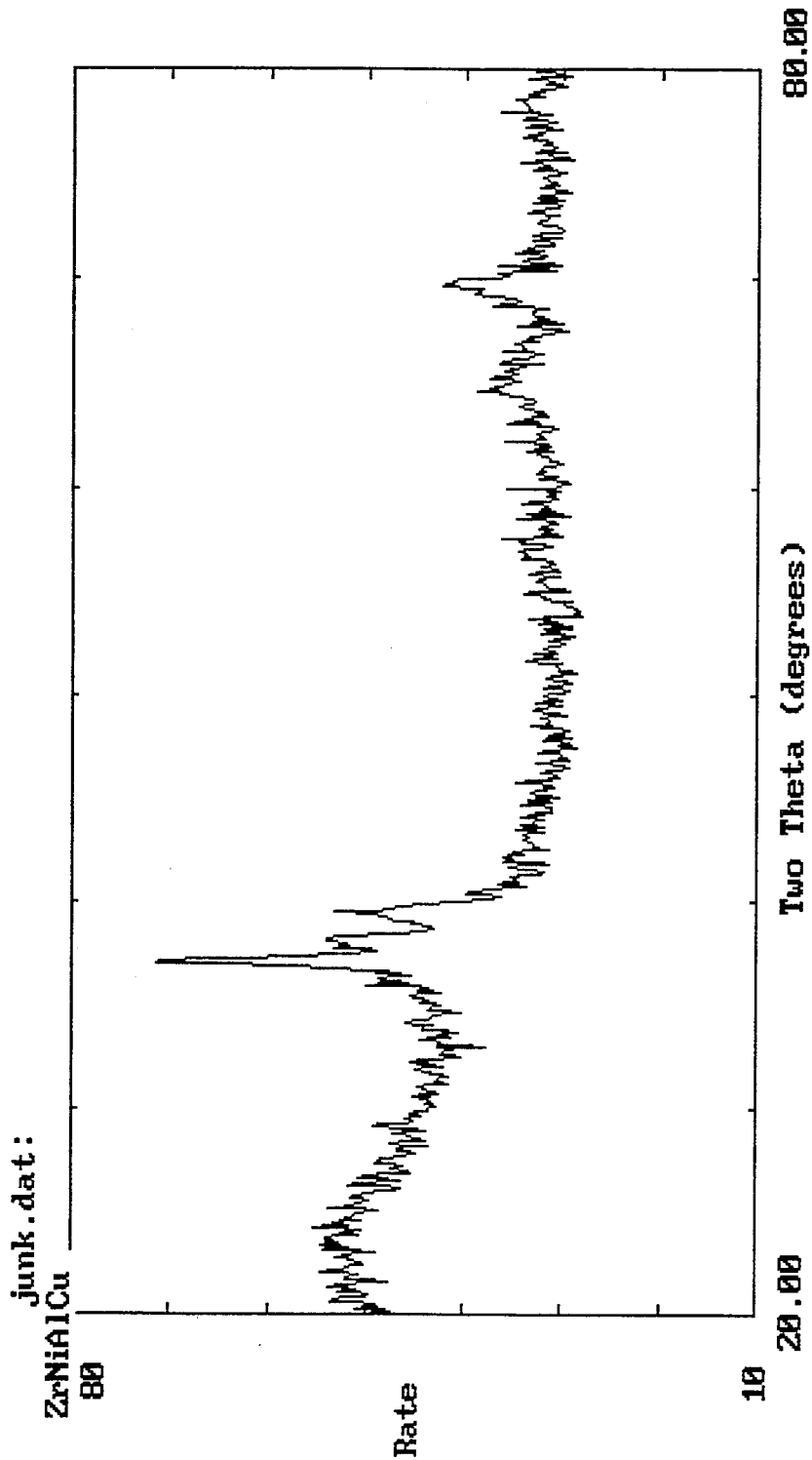
Figure 2: X-ray diffraction pattern for $Zr_{65}Ni_{10}Cu_{17.5}Al_{7.5}$ alloy using lumped zirconium.
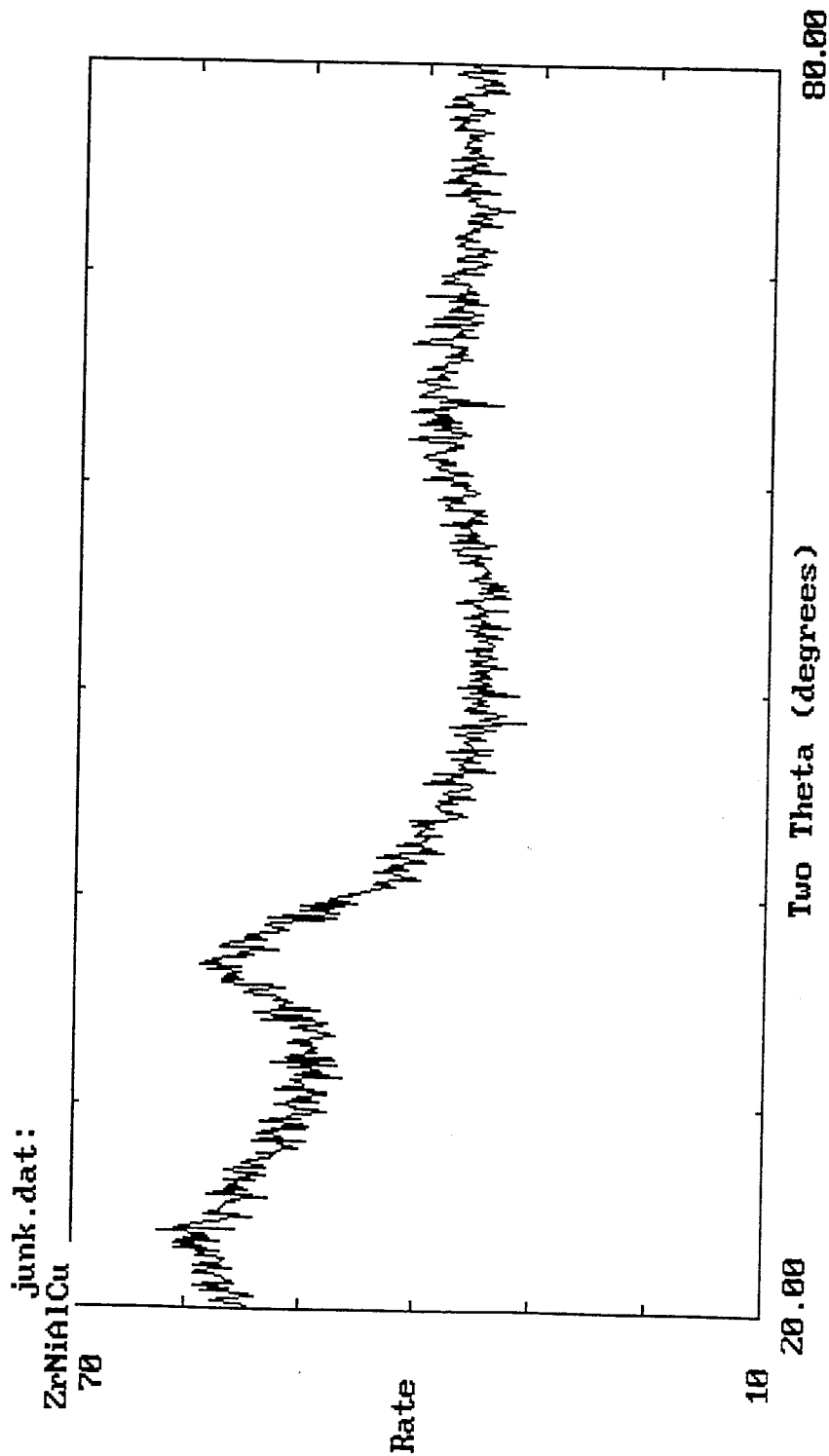
Figure 3: X-ray diffraction pattern for $Zr_{65}Ni_{10}Cu_{17.5}Al_{7.5}$ alloy using zirconium crystal bar turnings. Note the absence of Bragg peaks.
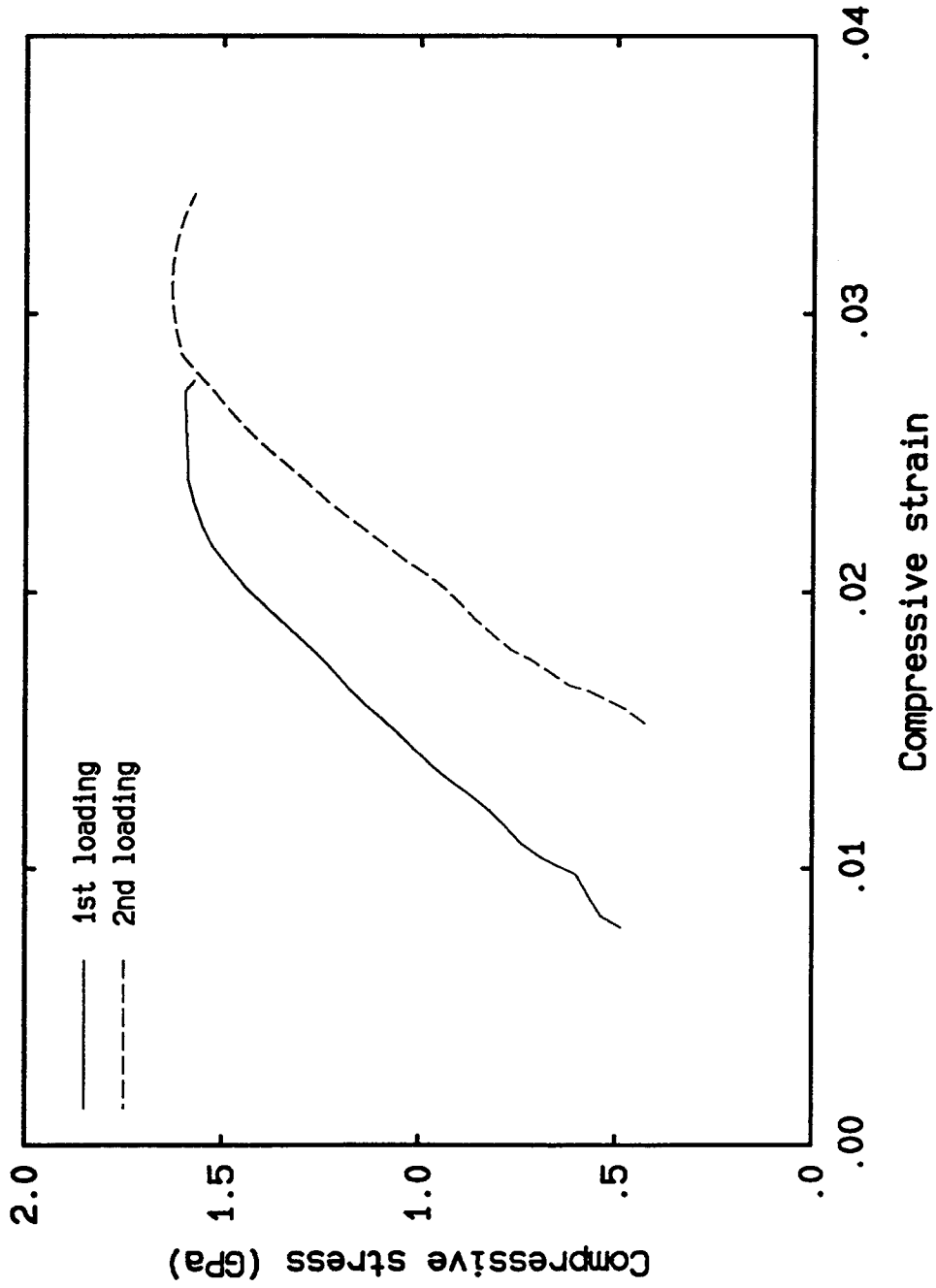
Figure 4: Stress-strain curve for 2.5 mm diameter $Zr_{65}Ni_{10}Cu_{17.5}Al_{7.5}$ metallic glass compression test specimen.

perfectly plastic yield behavior that has been observed in $Pd_{78}Cu_6Si_{16}$ and $Pd_{40}Ni_{40}P_{20}$ with a proportional limit of 1.55 ± 0.05 GPa. The plastic strain to failure was less than 2% for all specimens which indicated limited compressive ductility. Failure occurred on planes oriented approximately 45° to the loading axis, which is the angle observed for shear band formation in compression tests conducted on cylindrical rods of amorphous $Pd_{78}Cu_6Si_{16}$ (Figure 5)[9]. Thus, it appears that once again catastrophic failure may have been precipitated by a single macroscopic shear band.

1 mm
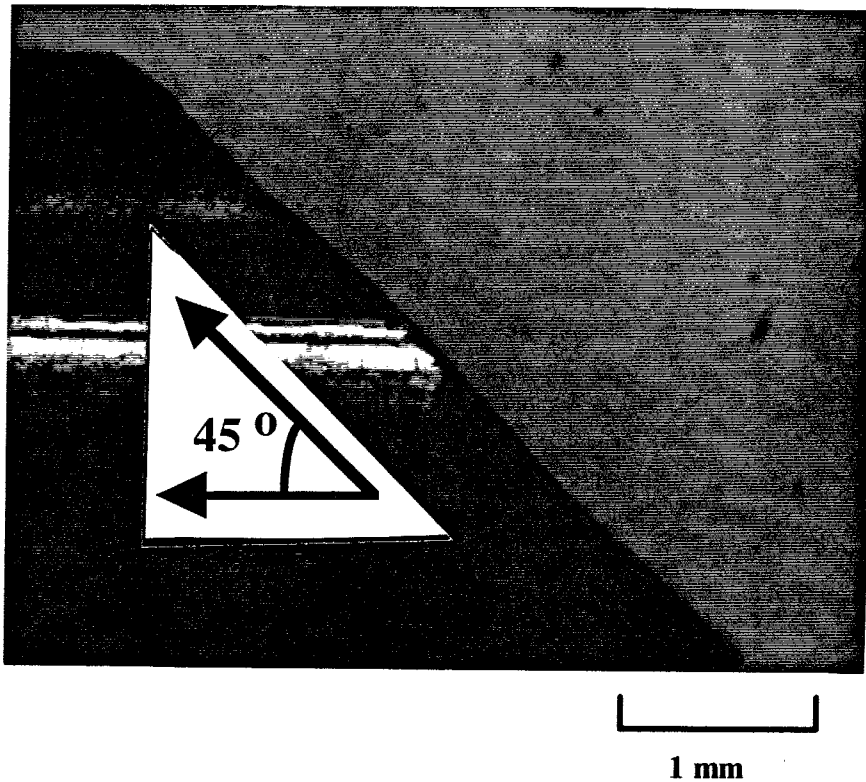
Figure 5: Fractured 3 mm diameter $Zr_{65}Ni_{10}Cu_{17.5}Al_{7.5}$ compression test specimen.

Tensile specimens were machined from 3 mm cylindrical rods into "dog-bone" geometries with 3 mm diameter grip sections and 2 mm diameter gage sections. A special set of grips were made for the tensile specimens using 7/64 inch collets held by universal joints to eliminate bending moments. Although no device was used to accurately measure
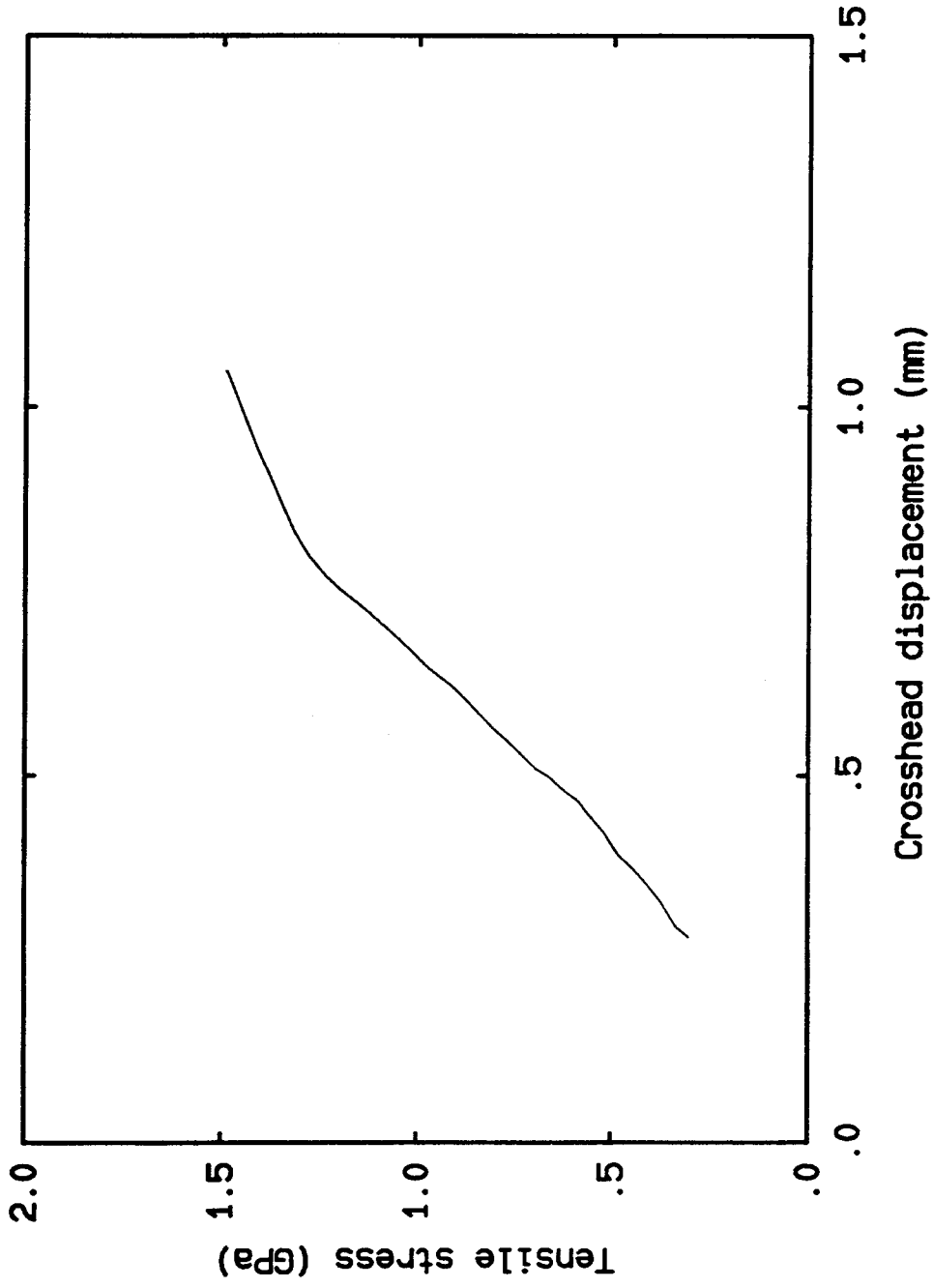
Figure 6: Stress-displacement curve for 2 mm diameter $Zr_{65}Ni_{10}Cu_{17.5}Al_{7.5}$ metallic glass tensile test specimen.

the strain in the gage sections, failure occurred in the gage section at a stress of 1.49 ± 0.02 GPa (Figure 6). In contrast to the case of the compression tests, the failure surface was oriented at an angle 55° from the loading axis, which is the angle observed for shear band formation in tensile tests conducted on cylindrical rods of amorphous $Pd_{78}Cu_6Si_{16}$ (Figure 7)[10]. Thus, it appears that the amorphous alloy may have once again experienced highly localized yielding in the form of a shear band that precipitated catastrophic failure of the specimen. So, the tensile yield stress appears to be the same as the failure stress, which is within 3% of the compressive yield stress. Thus, the $Zr_{65}Ni_{10}Cu_{17.5}Al_{7.5}$ metallic glass exhibits no anisotropy in its yield behavior.

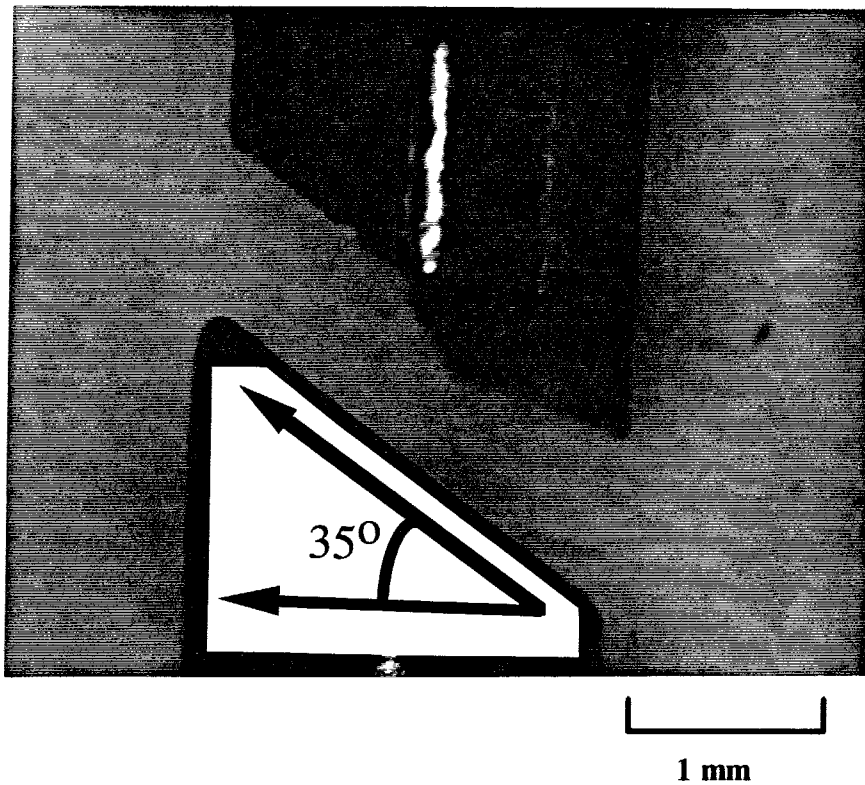**Figure 7: Fractured 2 mm diameter $Zr_{65}Ni_{10}Cu_{17.5}Al_{7.5}$ tensile test specimen.**

Before the quasi-static constitutive characterization of the $Zr_{65}Ni_{10}Cu_{17.5}Al_{7.5}$ system was complete, Peker and Johnson at Caltech discovered a bulk metallic glass that

was an even better glass former than the $Zr_{65}Ni_{10}Cu_{17.5}Al_{7.5}$ alloy[11]. This alloy was formed by removing the aluminum from the $Zr_{65}Ni_{10}Cu_{17.5}Al_{7.5}$ alloy while adding beryllium and titanium to the system. The $Zr_{65}Ni_{10}Cu_{17.5}Al_{7.5}$ alloy, although a good glass former, could not be reliably cast as a fully amorphous rod. In fact, only about 50% of the rods that were cast turned out to be amorphous. In addition, it was becoming apparent that the grips used in the tension tests would not work for torsion tests. Grips could be designed for dog-bone specimens that used threading in the grip section, but specimens larger than 3 mm cylindrical rods would be needed.

Attempts at casting fully amorphous cylindrical rods of $Zr_{65}Ni_{10}Cu_{17.5}Al_{7.5}$ that were large enough to machine threads in the grip section proved futile. Although the group of Inoue and Masumoto reported casting fully amorphous rods up to 7 mm in diameter, fully amorphous rods with diameters greater than 3 mm were impossible to produce. The $Zr_{41.25}Ti_{13.75}Cu_{12.5}Ni_{10}Be_{22.5}$ alloy turned out to be easily and reliably cast in evacuated quartz tubes as rods up to 16 mm in diameter. Thus, it was decided to abandon the $Zr_{65}Ni_{10}Cu_{17.5}Al_{7.5}$ alloy and use the $Zr_{41.25}Ti_{13.75}Cu_{12.5}Ni_{10}Be_{22.5}$ alloy instead for the dynamic and quasi-static constitutive characterization of metallic glasses.

2.2 The $Zr_{41.25}Ti_{13.75}Cu_{12.5}Ni_{10}Be_{22.5}$ Bulk Metallic Glass

A new highly processable metallic glass with the nominal composition $Zr_{41.25}Ti_{13.75}Cu_{12.5}Ni_{10}Be_{22.5}$ was discovered by Peker and Johnson at Caltech in 1992[10]. This new metallic glass was alloyed from elements with purities ranging from 99.5% to 99.9% using induction melting on a water cooled silver or copper boat under a Ti-gettered argon atmosphere (Figure 8). Typically, ingots ranging in size from 5 - 9 grams were prepared. These samples were generally found to freeze without any crystallization during preparation resulting in a glassy ingot. Their amorphous microstructure was verified using an x-ray diffractometer and high resolution transmission
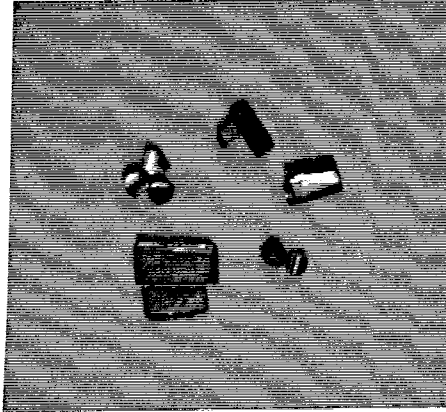
(a)
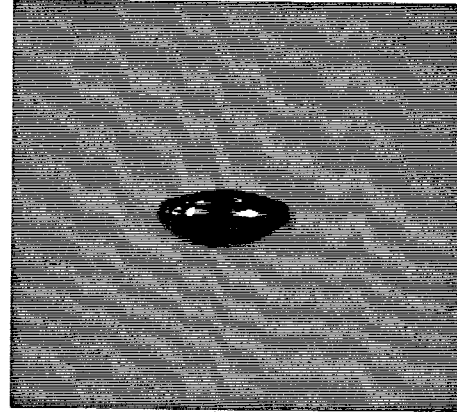
(b)
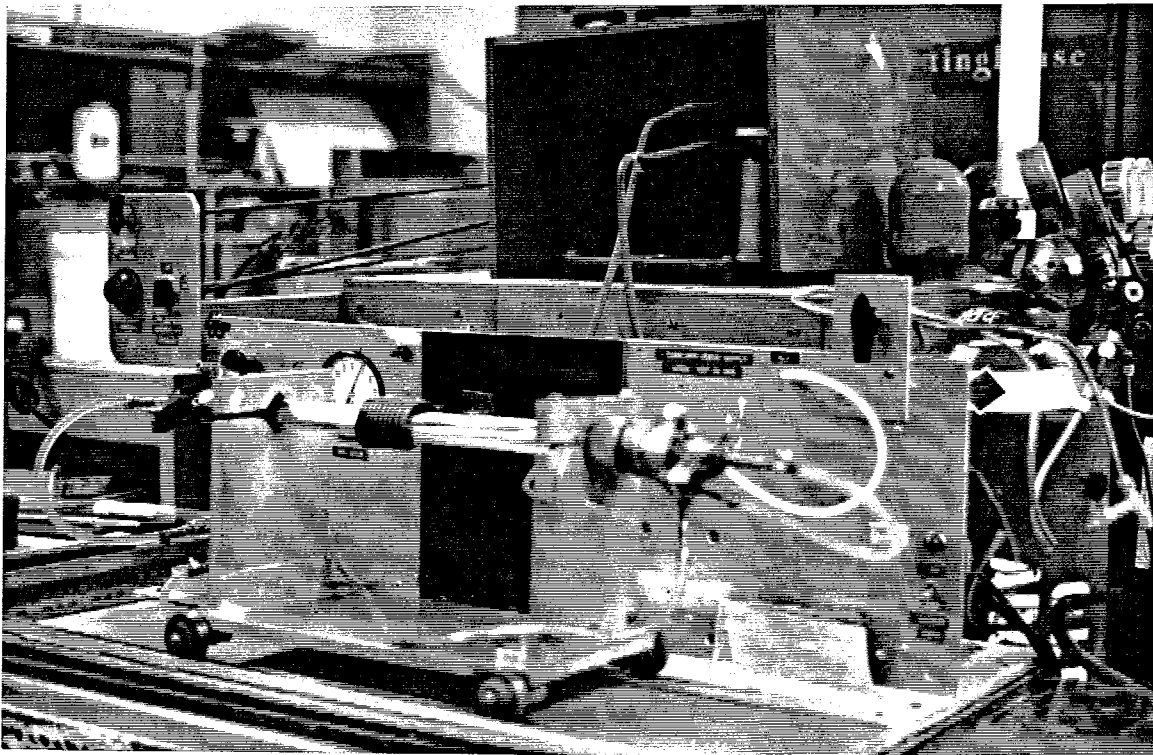
(c)

Figure 8: Alloying of $Zr_{41.25}Ti_{13.75}Cu_{12.5}Ni_{10}Be_{22.5}$ bulk metallic glass
(a) raw material, (b) alloyed ingot, (c) copper boat.

Figure 9: X-ray diffraction pattern from 7 mm diameter rod of
$Zr_{41.25}Ti_{13.75}Cu_{12.5}Ni_{10}Be_{22.5}$ **bulk metallic glass.**

(a)

(b)

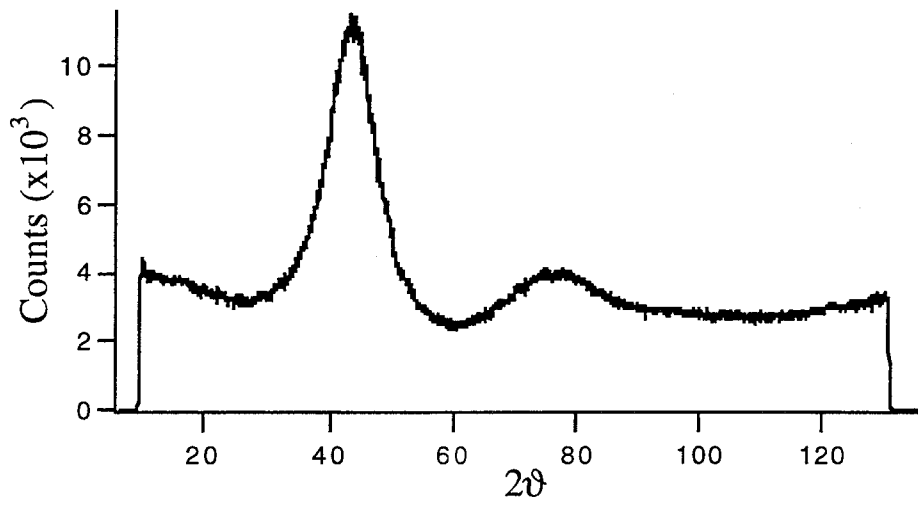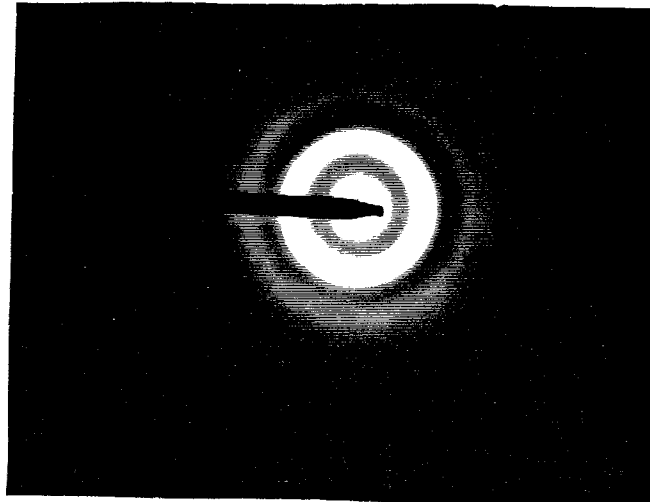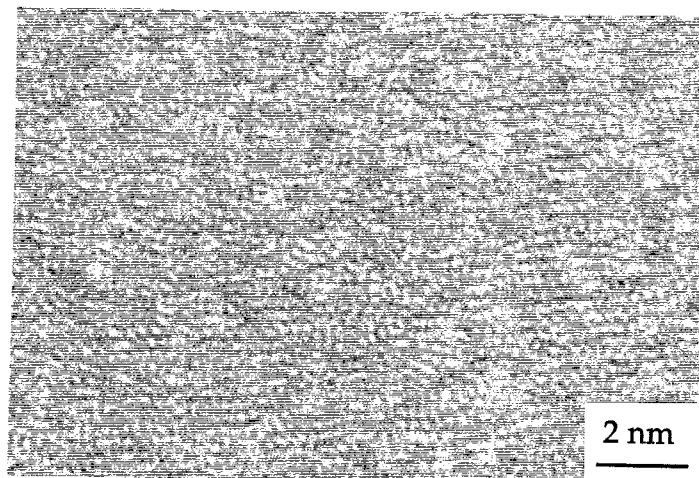Figure 10: (a) High resolution TEM diffraction pattern and (b) micrograph for 7 mm diameter rod of $Zr_{41.25}Ti_{13.75}Cu_{12.5}Ni_{10}Be_{22.5}$ bulk metallic glass.

electron microscopy (Figures 9 and 10). The x-ray diffractometer can detect crystals with grain sizes of 2 nm or greater, while the transmission electron microscopy can make images of the microstructure at the atomic level in order to corroborate the x-ray analysis.

Beryllium oxide is considered to be a hazardous material that can cause chronic beryllium disease, otherwise known as berylliosis, when inhaled by individuals who are allergic to it. Therefore, steps were taken during the processing of the $Zr_{41.25}Ti_{13.75}Cu_{12.5}Ni_{10}Be_{22.5}$ metallic glass to insure that whenever possible the unalloyed beryllium would be handled in a contained or properly ventilated environment. If properly alloyed, the hazard posed by the beryllium is considered to be minimized. However, precautionary steps were still taken when cutting or grinding the $Zr_{41.25}Ti_{13.75}Cu_{12.5}Ni_{10}Be_{22.5}$ alloy to contain the small particles created during these operations by using oil or water.

One of the most notable characteristics of the $Zr_{41.25}Ti_{13.75}Cu_{12.5}Ni_{10}Be_{22.5}$ metallic glass was the ability to add impurities to the alloy which did not compromise bulk glass formation. For example, it was discovered that up to 5 a.t. % Boron could be added to the alloy and ingots would still freeze glassy on the silver boat. This tolerance for impurities meant that the lumped zirconium and zirconium wire that compromised the glass formability of the $Zr_{41.25}Ti_{13.75}Cu_{12.5}Ni_{10}Be_{22.5}$ alloy did not affect the glass formability of the $Zr_{41.25}Ti_{13.75}Cu_{12.5}Ni_{10}Be_{22.5}$ alloy. Therefore, the cheapest form of zirconium available, zirconium plate with 99.5% purity and up to 4.5% hafnium, was used to fabricate $Zr_{41.25}Ti_{13.75}Cu_{12.5}Ni_{10}Be_{22.5}$ specimens for mechanical tests.

2.2.1 Thermal properties

In order to better understand the glass formability of the $Zr_{41.25}Ti_{13.75}Cu_{12.5}Ni_{10}Be_{22.5}$ alloys, it was necessary to characterize the thermal properties of the glassy state. Thermal analysis was carried out using a Perkin-Elmer DSC 4 scaling calorimeter. The glassy alloy was heated in an aluminum pan at rates of 20 and

4 scaling calorimeter. The glassy alloy was heated in an aluminum pan at rates of 20 and 200 K/min (Figure 11). In the 20 K/min scan, an anomaly in the heat capacity characteristic of the glass transition appears at 625 K. At higher temperatures, two crystallization events are seen the first of which occurs at 705 K. The crystallization temperatures increases substantially as the rate of heating is increased to 200 K/min scan. It was also discovered that by fluxing the sample surface with a layer of borosilicate glass or encapsulating it in a thin glass ampule the crystallization peaks could be shifted to even higher temperatures. This is apparently due to the suppression of surface oxidation and the lack of contact with the aluminum pan.
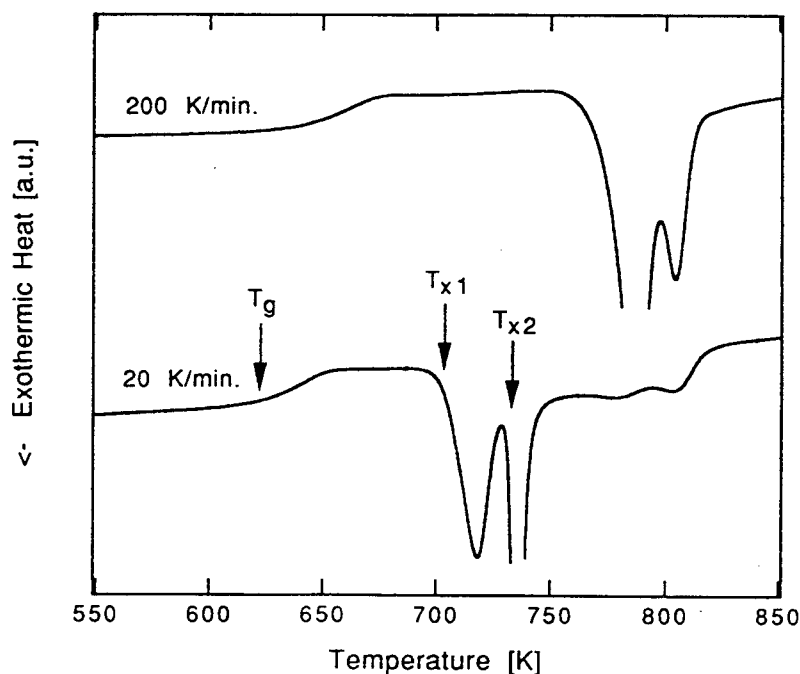

Figure 11: DSC scans of $Zr_{65}Ni_{10}Cu_{17.5}Al_{7.5}$ bulk metallic glass.

From the DSC results, it is apparent that the crystallization issue in metallic glasses is very complex. In classical nucleation theory, there are two types of crystallization: heterogeneous and homogeneous. In heterogeneous nucleation, crystals inside or on the

be much higher than those for homogeneous nucleation. Homogeneous nucleation, on the other hand, depends solely on the composition of the molten alloy. By suppressing heterogenous nucleation, homogeneous nucleation would represent the limiting nucleation rate for crystal growth in a molten alloy. Thus, a true measure of the glass formability of an alloy can only be obtained by preventing contact of the molten alloy with crystals. This becomes an important issue in the fabrication of amorphous specimens from the $Zr_{41.25}Ti_{13.75}Cu_{12.5}Ni_{10}Be_{22.5}$ alloy.

The melting temperature of the $Zr_{41.25}Ti_{13.75}Cu_{12.5}Ni_{10}Be_{22.5}$ alloy was also obtained using a Seteram SDC 2000 K. A solidus temperature of 937 ± 3 K was measured for the alloy with a liquidus temperature of 993 ± 5 K. The solidus temperature is believed to be a eutectic temperature, and from comparison of the endothermic signals of the solidus and liquidus line, the alloy appears to be close to a eutectic composition. Using the glass transition temperature and melting temperature, it is possible to calculate the reduced glass transition temperature, $t_g = T_g/T_m$ (where T_g is the calorimetrically defined glass transition temperature and T_m is the alloy melting point). For this alloy $t_g = 0.67$, which is higher than the value of 0.66 reported for the good glass forming alloy $Pd_{40}Ni_{40}P_{20}$.

From classical nucleation theory it can be seen that by increasing the value of t_g the homogeneous nucleation rate can be lowered. Thus, the nose of the transformation curve on a TTT diagram for the amorphous alloy is shifted to the right (Figure 12). In order to suppress homogeneous nucleation, it is necessary to quench the alloy rapidly so that the nose of the transformation is not intersected during cooling. The nose of the transformation curve for conventional metallic glasses typically lies 4 to 6 orders of magnitude to the left of the nose for the $Zr_{41.25}Ti_{13.75}Cu_{12.5}Ni_{10}Be_{22.5}$ alloy's transformation curve. The quench rates that are therefore required to suppress homogeneous nucleation in conventional metallic glasses are on the order of 10^4-10^6 K/sec while the quench rates for the $Zr_{41.25}Ti_{13.75}Cu_{12.5}Ni_{10}Be_{22.5}$ alloy are on the order

of 1 K/sec. By relaxing the cooling rate requirements for metallic glass formation, the size of metallic glass specimens that can be fabricated increases substantially.
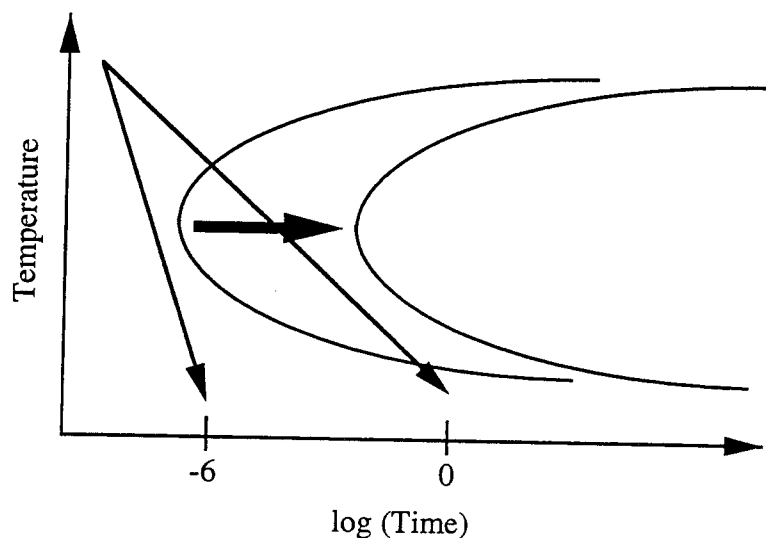
Figure 12: Shift of TTT diagram for $Zr_{41.25}Ti_{13.75}Cu_{12.5}Ni_{10}Be_{22.5}$ alloy.

Another factor which may influence the crystallization of the $Zr_{41.25}Ti_{13.75}Cu_{12.5}Ni_{10}Be_{22.5}$ alloy is the complexity of the five component system. For example, the atomic radii of the elemental constituents vary over a large range. The atomic radius of beryllium is 0.111 nm, those of nickel and copper are 0.124 and 0.128 nm, while those of zirconium and titanium are 0.160 and 0.147 nm. These differing sizes are expected to limit the solubilities of these elements in crystalline phases having a small number of nonequivalent positions in the unit cell. Masumoto and Inoue have also suggested that atomic size differences in the multicomponent alloys lead to efficient packing of atoms in the glassy phase which lowers the ground state energy difference between the amorphous and crystalline phases thereby suppressing nucleation[7,12].

2.2.2 Elastic properties

Before mechanical tests were conducted on the $Zr_{41.25}Ti_{13.75}Cu_{12.5}Ni_{10}Be_{22.5}$ metallic glass, the elastic properties of the alloy were measured using ultrasonic techniques. Measurements were made on a 7 mm diameter cylindrical rod 10 mm in length whose ends were mechanically polished with 600 grit SiC abrasive paper using a V-block to insure flat and parallel surfaces. By measuring the length of the specimens with a micrometer, the surfaces were found to be parallel within 3 µm.

Ultrasonic measurements were made using a Parametrics Model 5052UA ultrasonic analyzer connected to an oscilloscope for data analysis. Two ultrasonic transducers were placed on the ends of the rod. One transducer was used to measure the dilitational wave speed while the other measured shear wave speeds. Wave speeds were calculated by measuring the time it took for a pulse to travel from one end of the specimen to the other and back, and then dividing by twice the specimen length.

Elastic properties can be calculated from the measured wave speeds using the following equations[13]:

$$c_S = \sqrt{\frac{\mu}{\rho}}$$

$$c_L = \sqrt{\frac{\lambda + 2\mu}{\rho}}$$

where c_S is the shear wave speed, c_L is the dilitational wave speed, μ is the shear modulus, λ is Lame's constant, and ρ is the density. The elastic properties are often given in terms of

Young's modulus, $E = \dfrac{\mu(3\lambda + 2\mu)}{(\lambda + \mu)}$, and Poisson's ratio, $\nu = \dfrac{\lambda}{2(\lambda + \mu)}$. The specimen's density was measured using the hydrostatic weighing technique.

For the $Zr_{41.25}Ti_{13.75}Cu_{12.5}Ni_{10}Be_{22.5}$ metallic glass, $c_S = 2337 \pm 13$ m/s, $c_L = 4913 \pm 25$ m/s, and $\rho = 6.11 \pm 0.01$ g/cm^3. The elastic properties are therefore:

$$\mu = 33 \pm 1 \text{GPa}$$
$$E = 90 \pm 1 \text{ GPa}$$
$$\nu = 0.354 \pm 0.003$$

The amorphous material is slightly more compliant than crystalline Zr, which has a Young's modulus of 98-99 GPa and a Poisson's ratio of 0.35-0.38 at room temperature[14,15].

2.3 Fabrication of Specimens for Mechanical Testing

Before specimens could be fabricated, specimen sizes had to be determined that would yield well-defined stress fields. Standards for compression and tension testing have been established by the American Society for the Testing of Materials (ASTM). For high strength materials, ASTM standard E9-67 recommends compression specimens be fabricated with length-to-diameter ratios of 1.5 to 2.0 for mechanical testing. For tension testing, specimens should be fabricated in dog-bone geometries with dimensions specified by ASTM standard E8-68. No standards are given for specimens to be used in torsion tests.

Compression test specimens could be easily fabricated with the same casting technique used to manufacture compression test specimens from ZrNiCuAl. Rods with diameters of 2.5 and 3 mm and 25.4 to 30 mm in length were fabricated using approximately 1.5 to 2.5 grams of alloy (Figure 13). The alloy was placed in a nozzle that was made from Vycor tubing with an inner diameter of 7 mm and a thickness of 1 mm (Figure 14). The tube was placed in contact with a copper mold inside a chamber that was first evacuated then backfilled with helium or argon at an absolute pressure of 9-10 in Hg. The alloy was then melted using an induction heater and injected into the copper mold using a back pressure of 10-30 in Hg.

Figure 13: A 2.5 mm diameter rod of $Zr_{41.25}Ti_{13.75}Cu_{12.5}Ni_{10}Be_{22.5}$ bulk metallic glass cast in copper mold.

Figure 14: Vycor nozzle and copper mold used to cast cylindrical rod in Figure 13.

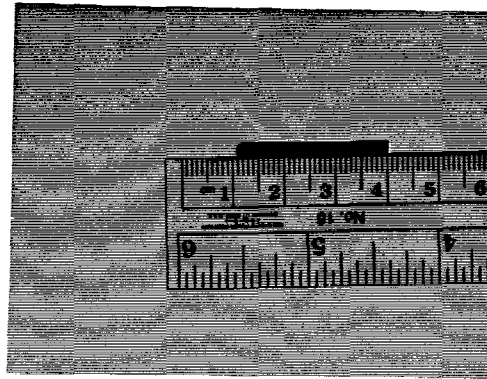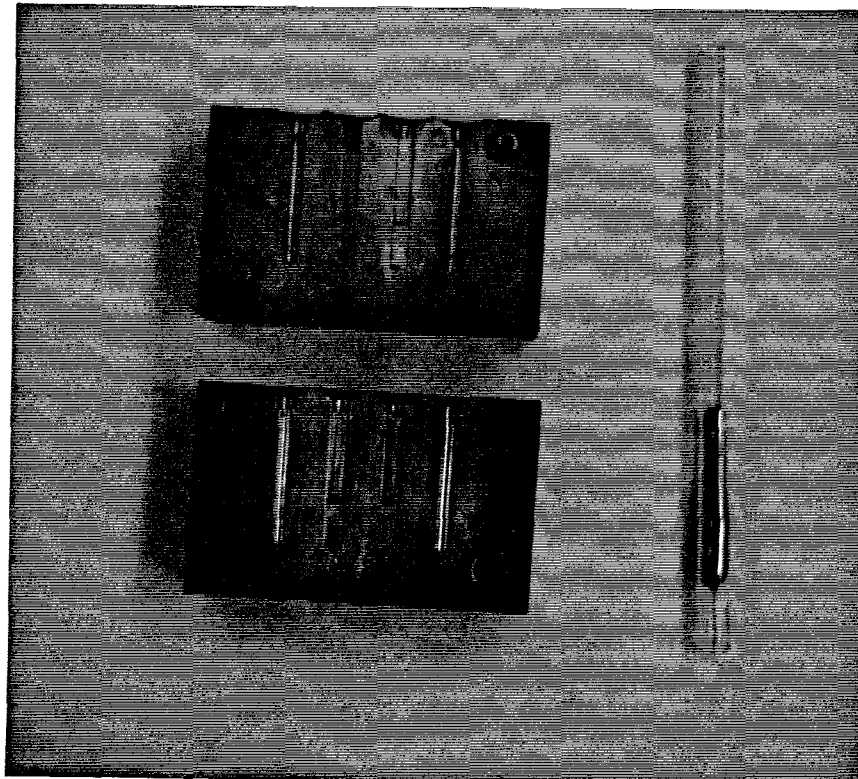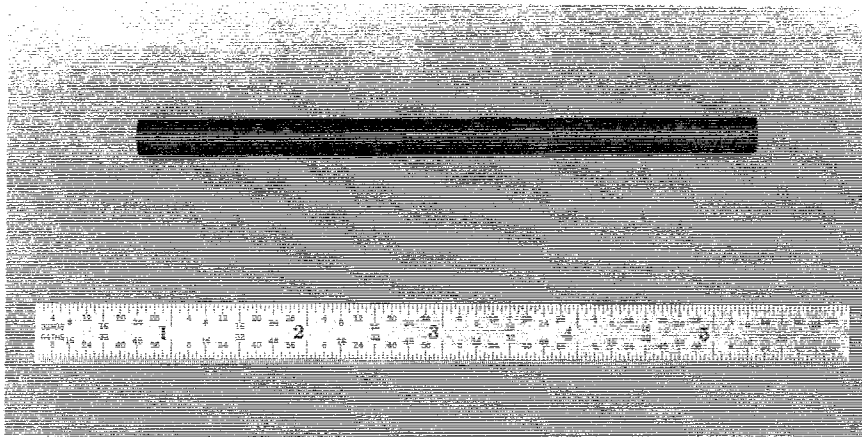**Figure 15: A 7 mm diameter rod of $Zr_{41.25}Ti_{13.75}Cu_{12.5}Ni_{10}Be_{22.5}$ bulk metallic glass cast in evacuated Vycor tube.**
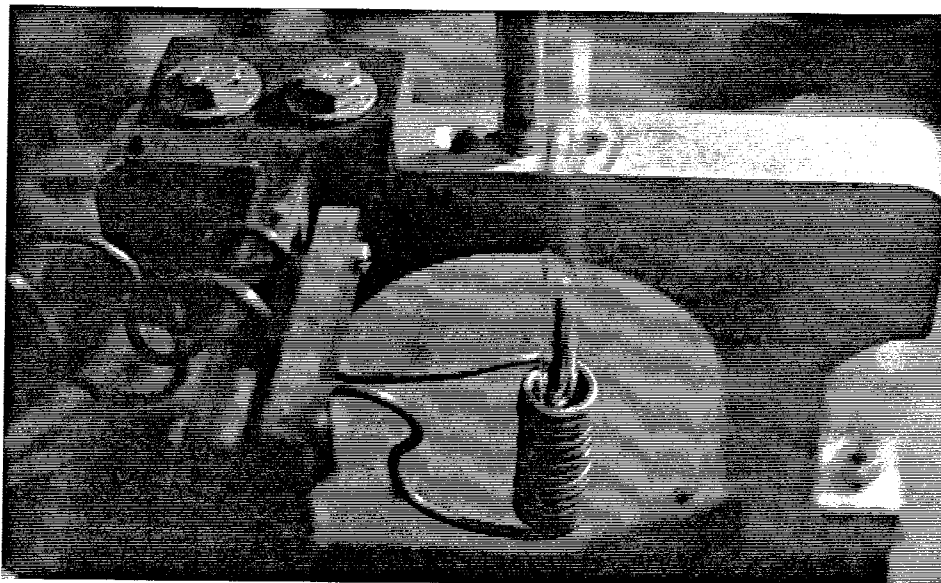
Figure 16: Evacuated Vycor tube used to cast cylindrical rod in Figure 15.

Vycor is a type of quartz which was chosen as the nozzle material because of its high reactivity temperature (1200 K) and its excellent fracture resistance. Since the melting temperature of the alloy was well below the reactivity temperature of Vycor, it is possible to melt the alloy inside a Vycor tube for an extended period of time without contaminating the melt. Thus, it became evident that large cylindrical rods of the alloy could be fabricated by simply melting the alloy in an evacuated Vycor tube and quenching in water (Figures 15 and 16). These rods could then be cut into compression test specimens or machined into dog-bone specimens for tension tests (Figure 17).
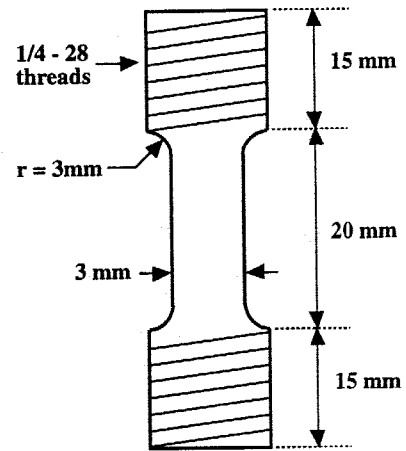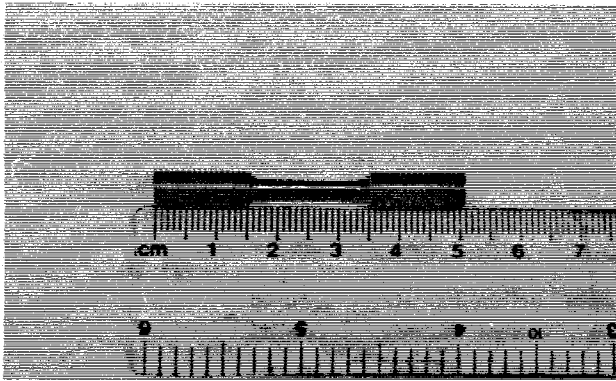
Figure 17: Dog-bone specimen used for tension and torsion tests.

Attempts were made to cast large cylindrical specimens by injecting the molten alloy into a copper mold. However, large quantities of molten alloy (> 6 g) tended to flow out of the quartz tube under their own weight and freeze just after entering the copper mold. Reducing the diameter of the nozzle helped to control the melt, but the cast

specimens were riddled with defects because of the reduced flow rates. The casting technique which used the evacuated Vycor tubes produced specimens with fewer defects, so that technique was used to fabricate large compression test specimens and dog-bone specimens for tension tests. During the quenching process, the Vycor tubes were slowly submerged into a bucket of water while stirring. This quenching technique produced a two-dimensional solidification front that passed through the molten alloy minimizing the production of shrink-hole cavities.

After the specimens were fabricated, their amorphous structure was verified by placing thin cross sections cut from the specimens in an Inel CPS-120 x-ray diffractometer having a large angle position sensitive detector with a resolution of 0.03° (Figure 9). Because of heterogeneous nucleation, the cylindrical rods cast in the copper molds had a crystalline outer surface usually with a depth of 25 μm. This surface had to be removed using 240 grit SiC abrasive paper before performing the x-ray analysis. The specimens fabricated in the evacuated Vycor tubes appear to form an amorphous flux on the outer surface that could be easily broken off with a hammer before performing the x-ray analysis.

In order to minimize the number of procedures that would be used to fabricate specimens for mechanical testing, the dog-bone geometry used for tensile test specimens was also used for the torsional test specimens. When a torsional moment is applied to a cylindrical rod, an inhomogeneous stress state of pure shear is established in the rod. This stress state attains a maximum value on the outer surface and vanishes at the center of the rod. By using a balance of moments which is detailed in Chapter 3, it is possible to obtain the material's constitutive behavior in pure shear using the dog-bone geometry. It is also possible to use the dog-bone geometry to determine the material's constitutive behavior in a combined stress state of tension and torsion.

Once procedures had been established for fabricating bulk metallic glass specimens to be used in mechanical tests, the next step was to perform the actual tests. It seemed

logical that the first set of tests should characterize the material's quasi-static compressive behavior, since the results from these tests could be used to verify results from compression tests performed on other metallic glass alloys. The characterization of the material's quasi-static constitutive behavior could then be completed by performing mechanical tests in stress states of pure tension and pure torsion. Finally, the dynamic compressive behavior of the bulk metallic glass could be characterized and compared with the quasi-static results.

References

[1] Liebermann, H.H. and Graham, C.D., IEEE Transactions on Magnetics, **MAG-12**, 921 (1976).

[2] Harbur, D.R., Anderson, J.W., and Maraman, W.J., Transactions of TMS-AIME, **245**, 1055 (1969).

[3] Grant, N.J., Rapid Solidification Processing Principles and Technologies, ed. by R. Mehrabian, B.H. Kear and M. Cohen, Claitor's Publishing Division, Baton Rouge, LA, 230 (1978).

[4] Koch, C.C., Cavin, O.B., McKamey, C.G., and Scarbrough, J.O., Applied Physics Letters, **43**, 1017 (1983).

[5] Chen, H.S. and Turnbull, D., Acta Metallurgica, **17**, 1021 (1969).

[6] Maitrepierre, P.L., Journal of Applied Physics, **41**, 498 (1970).

[7] Atzmon, M., Verhoeven, J.D., Gibson, E.D., and Johnson, W.L., Applied Physics Letters, **45**, 1052 (1984).

[8] Zhang, T., Inoue, A., and Masumoto, Materials Transactions of JIM, **32**, 1005 (1991).

[9] Pampillo, C.A. and Chen, H.S., Materials Science and Engineering, **13**, 181 (1974).

[10] Kimura, H. and Masumoto, T., Amorphous Metallic Alloys, ed. by F.E. Luborsky, Buttersworth, London, 187 (1983).

[11] Peker, A. and Johnson, W.L., Applied Physics Letters, **63**, 2342 (1993).

[12] Zhang, T., Inoue, A., and Masumoto, T., Materials Letters, **15**, 379 (1993).

[13] Malvern, L.E., Introduction to the Mechanics of a Continuous Medium, Prentice-Hall Inc., Englewood Cliffs, NJ (1969).

[14] Smithell's Reference Book, ed. by E.A. Brandes and E.B. Brook, Butterworth-Heinemann, Linacre House, Jordan Hill, Oxford, **15-3** (1992).

[15] ASM Metals Handbook Desk Edition, ed. by H.E. Boyer and T.L. Gail, American Society for Metals, Metals Park, Ohio, **14.13** (1985).

CHAPTER 3

Quasi-static Constitutive Characterization of $Zr_{41.25}Ti_{13.75}Cu_{12.5}Ni_{10}Be_{22.5}$ Bulk Metallic Glasses

3.1 Compression Tests

3.1.1 Experimental procedure

The first quasi-static mechanical test that was performed on the $Zr_{41.25}Ti_{13.75}Cu_{12.5}Ni_{10}Be_{22.5}$ metallic glass was in uniaxial compression. Specimens were fabricated as 2.5, 3, and 7 mm diameter cylindrical rods as detailed in Chapter 2. In order to establish a homogeneous, uniaxial compressive stress state, specimens were prepared according to ASTM standards which recommend using length to diameter ratios of 1.5 to 2 in compression tests conducted on high strength materials (Figure 18). If higher aspect ratios are used, it is possible that the specimens may prematurely buckle or bend biasing the yield stress towards values that are lower than they would be for a homogeneous, uniaxial compressive stress state. Using lower aspect ratios would increase the triaxiality of the stress field because of end effects thereby creating a state of plane strain compression in the interior of the specimen. The preparation of compression test specimens were completed by mechanically polishing the ends of the specimens with the 600 grit SiC abrasive paper using the V-block.

Compression tests were conducted in an MTS 319.25 axial-torsional load frame using a special frame that was designed according to ASTM standard E9-67 to insure that the specimens experienced only uniaxial loading (Figure 19). End effects were reduced by placing specimens between a pair of WC inserts coated with "Molygraph Extreme Pressure Multi-purpose" grease. Compressive strains in the specimens were calculated from the displacement of the crosshead after correcting for the compliance of the load

train. All compression tests were conducted using constant crosshead velocities which resulted in strain rates varying from 10^{-3} to 10^{-4}/sec.
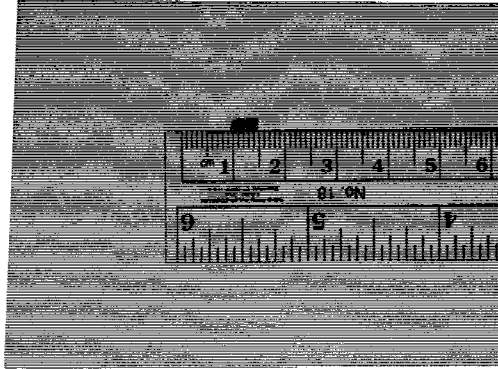

Figure 18: A 2.5 mm diameter compression specimen.

3.1.2 Experimental results

Typical compressive stress-strain curves for 2.5, 3, and 7 mm diameter specimens can be seen in Figure 20. These curves indicate that the $Zr_{41.25}Ti_{13.75}Cu_{12.5}Ni_{10}Be_{22.5}$ metallic glass exhibits the elastic-perfectly plastic compressive response observed in tests previously conducted on metallic glasses with plastic deformation initiating at an elastic strain of approximately 2%, which is the same as $\frac{\sigma_y}{E}$ where E is calculated from utrasonic techniques. However, unlike previous tests there is a notable absence of serrated yielding in the $Zr_{41.25}Ti_{13.75}Cu_{12.5}Ni_{10}Be_{22.5}$ metallic glass which has also been observed in compression tests conducted on metallic glasses at low temperatures and at higher quasi-static strain rates. Masumoto has proposed a model for the mechanics of serrated flow which indicates that absence of serrated yielding is most likely due to the large compliance of the load frame used in this work and the rates at which the specimens were deformed[3].

The compressive yield stress for 2.5 and 3 mm specimens was measured to be 1.93 ± 0.03 GPa while for the 7 mm specimens it was measured to be 1.87 ± 0.03 GPa. The yield stress was defined as the stress at the plateau of the stress-strain curve. This yield
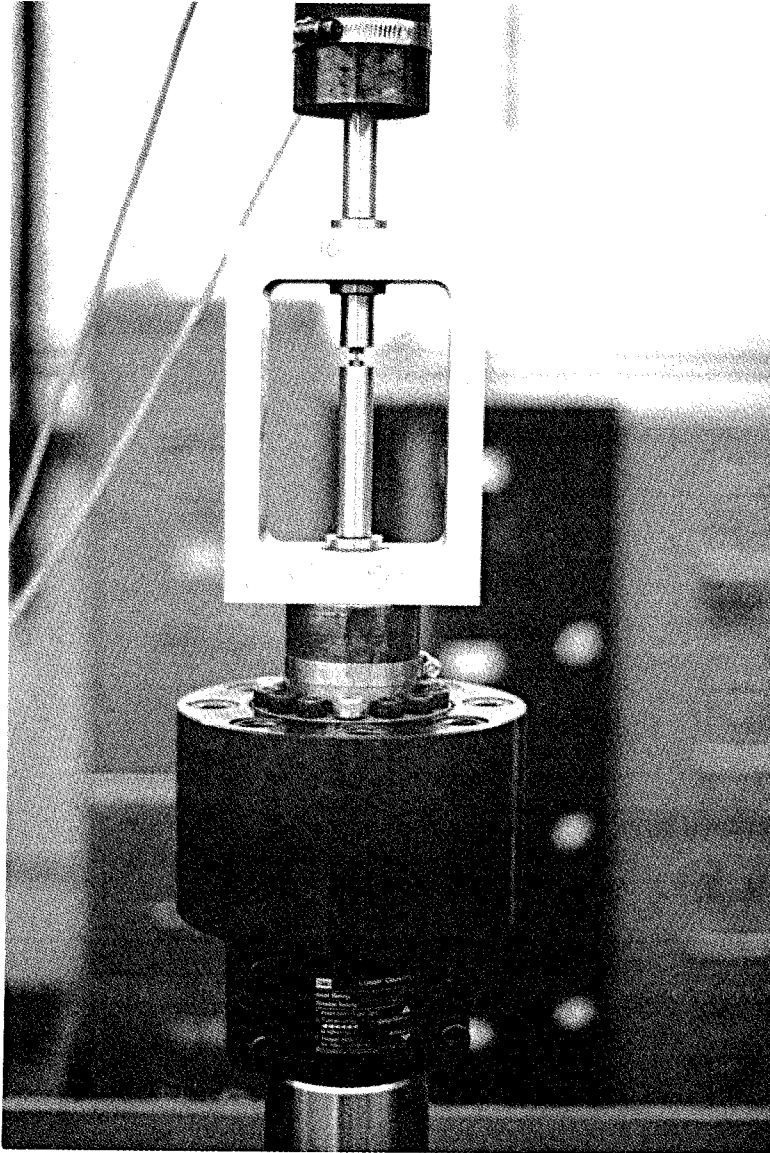
Figure 19: Test frame used for quasi-static compression tests.

stress is approximately 3 to 4 times higher than the yield stress for polycrystalline zirconium alloys.
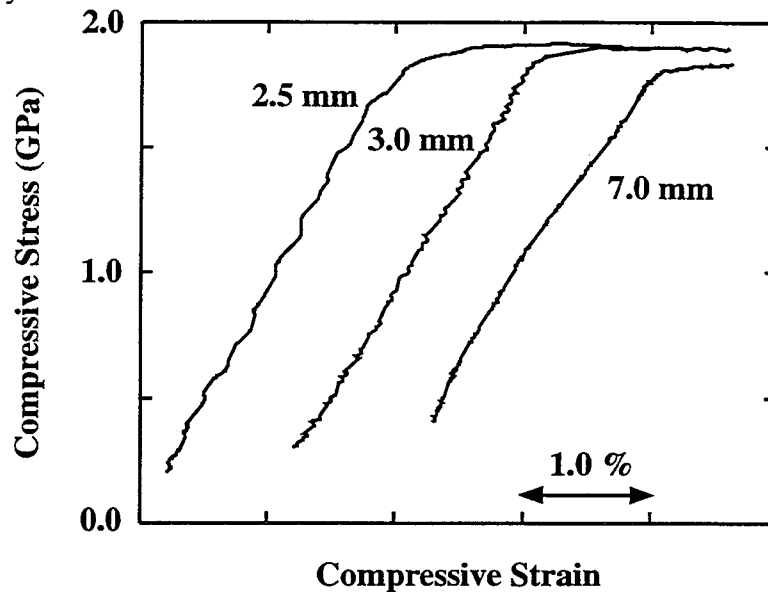
Figure 20: Stress-strain curves from quasi-static compression tests.

In every compression test, catastrophic failure occurred on a plane which was oriented at an angle approximately 45° from the loading axis (Figure 21). As mentioned previously, this is the same angle that has been observed for shear band formation in compression tests conducted on cylindrical rods of $Pd_{78}Cu_6Si_{16}$[1]. Consequently, catastrophic failure was believed to have been precipitated by shear localization. Masumoto has proposed that the angle at which these shear bands occur are predicted by slip line field theory for an elastic-perfectly plastic, von Mises material in plane strain compression[2,3]. However, this is also the angle slip lines form in a state of uniaxial compression.

Scanning electron micrographs were also obtained of the fracture surfaces (Figure 22). The only morphology that appears on the failure surface are vein-like patterns. These features are identical to those observed on the failure surfaces of other metallic glass specimens tested in compression. An explanation for these features has been proposed which asserts that the viscosity of the material within a shear band is reduced considerably because of adiabatic heating generated by the enormous plastic deformations within the

Figure 21: Orientation of fracture surface for 2.5 mm diameter quasi-static compression test specimen.

Figure 22: Scanning electron micrograph of compressive fracture surface.
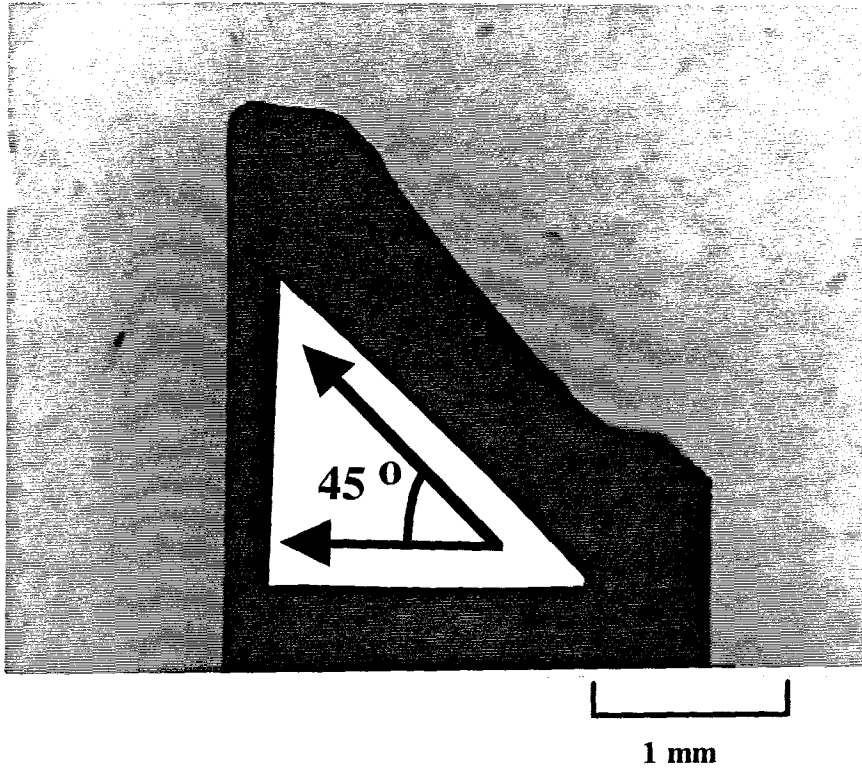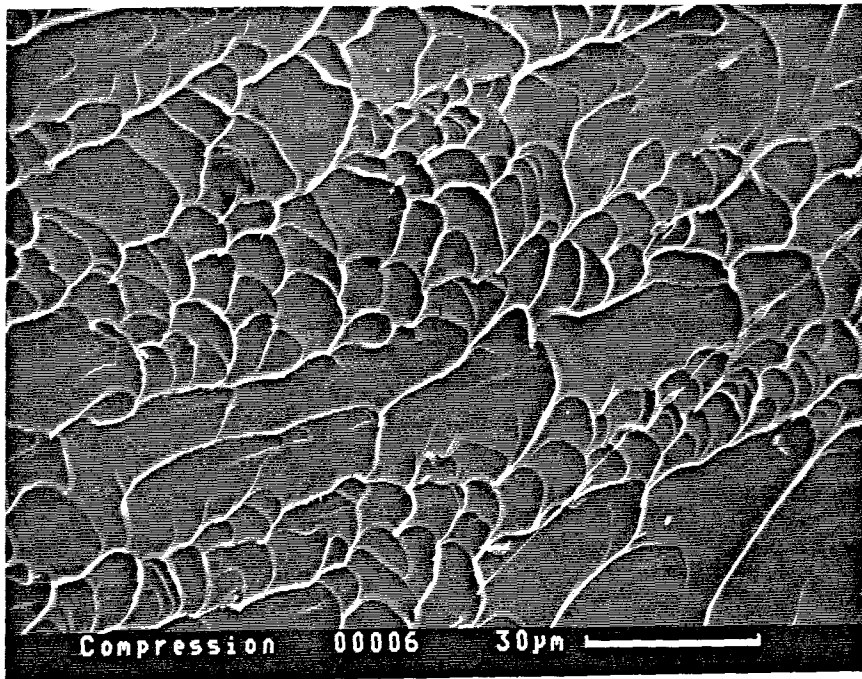
shear band which precedes catastrophic failure[4]. As the material separates, pores are opened up leaving behind the vein-like morphology. This hypothesis has been confirmed by shear experiments performed on a viscous material that has been placed between glass slides[5]. After the slides are sheared apart, a vein-like morphology is revealed on the separated surfaces.

3.1.3 Plane strain compression

Another stress state that can be tested in compression tests is plane strain, where plane strain is defined as a two-dimensional state of strain. A state of plane strain compression can be achieved by lowering the aspect ratio and removing the grease from the ends of the specimen in order to increase the triaxiality of the stress field. For the plane strain compression tests, specimens with diameters of 3 mm and 7 mm were used with length to diameter aspect ratios of 0.5 to 0.8.

Plane strain compression for this set of experiments will be approximated in cartesian coordinates as follows:

$$\varepsilon_{xx} = 0, \tag{3.1a}$$
$$\sigma_{yy} = 0. \tag{3.1b}$$

The only nonzero components of stress are σ_{zz} and $\sigma_{xx} = v\sigma_{zz}$, where the z-direction is the direction of compressive loading and lies along the axis of the cylinder.

A typical stress-strain curve for a 3 mm diameter rod tested in a state of plane strain compression can be seen in Figure 23. The yield stress for plane strain compression was 2.12 ± 0.05 GPa. For materials whose flow is insensitive to hydrostatic pressure, the apparent yield strength would be expected to increase compared to the uniaxial value as the triaxiality of the stress field increases. In addition to the increase in yield strength, the plane strain compression specimens also exhibited an enormous increase in ductility that will be discussed in the following section.
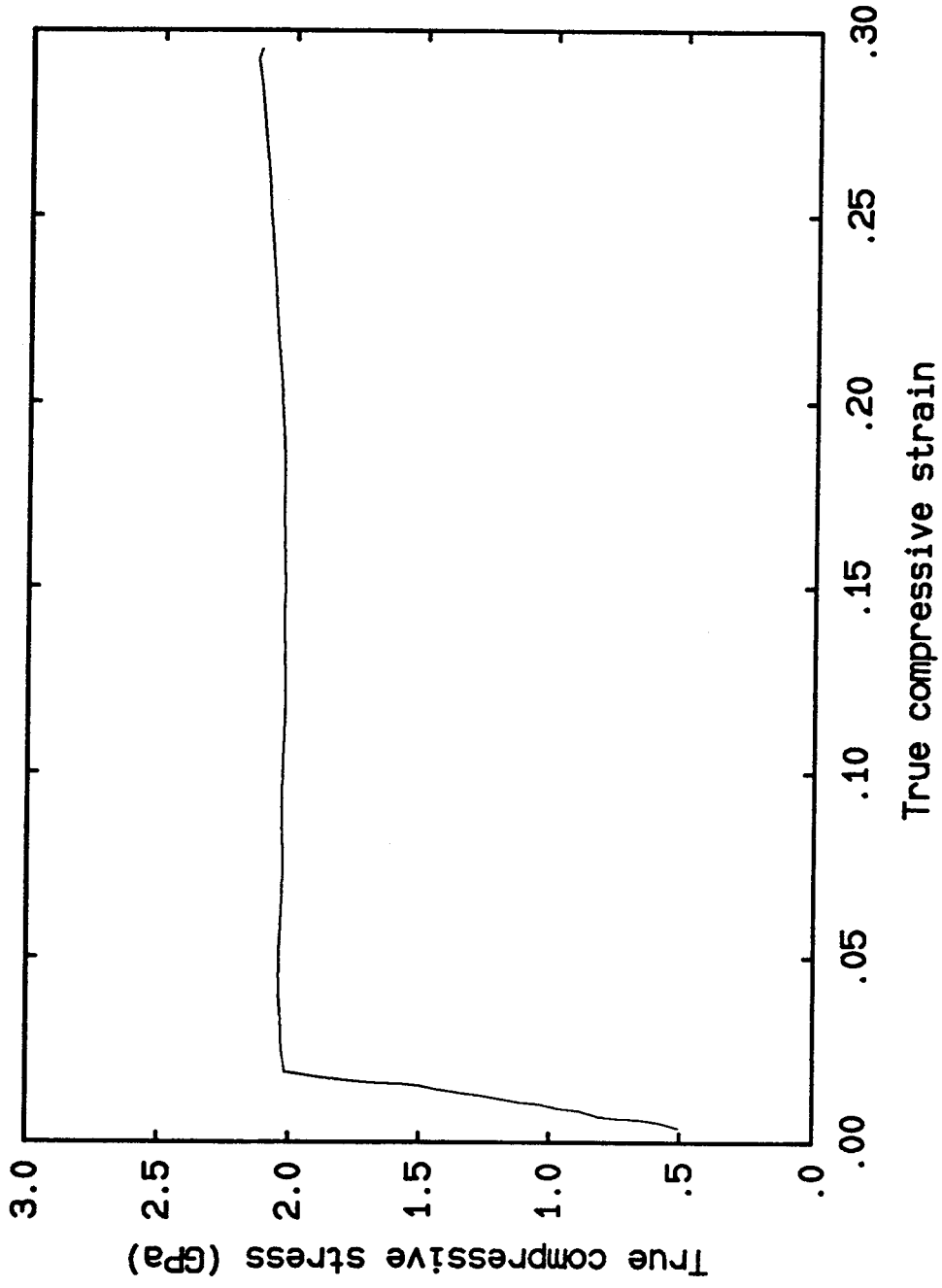
Figure 23: Stress-strain curve for 2.5 mm diameter plane strain compression test specimen.

The observed increase in yield stress from the uniaxial to the plane strain stress states is consistent with the observations made by Kimura and Masumoto when they lowered the aspect ratios of their compression test specimens[6]. However, Donovan conducted plane strain compression tests using a special test designed by Watts and Ford that indicated no change in the compressive yield stress of $Pd_{40}Ni_{40}P_{20}$[7]. His result is consistent with the Mohr-Coulomb yield criterion that Donovan proposed for $Pd_{40}Ni_{40}P_{20}$[8]. A similar conclusion can not be supported on the basis of the results from the present work.

3.2 Compressive Ductility

3.2.1 Effects of quench rates on compressive ductility

The plastic strains to failure were also measured for each compression test specimen in order to gain an understanding of the material's compressive ductility. These results can be seen in Figure 24 for the 2.5, 3 and 7 mm rods respectively. Although there is considerable scatter in the data, a trend appears of decreasing plastic strain to failure with increasing specimen diameter. In fact, there appears to be almost no measureable plastic strain in the 7 mm diameter rods.

It can be argued that the quench rates are being lowered in the core of the specimen as the diameter increases. Attempts were made to explain this embrittlement phenomenon by distinguishing differences in the microstructure of the specimens using x-ray diffraction analysis and density measurements. However, no differences were detected in the density measurements to within 0.1%, while for x-ray diffraction analysis no differences were detected to within 0.1°. At these resolutions, it is possible that the differences in the microstructure that are responsible for the embrittlement phenomenon might not be distinguishable.

The effects of quench rate on ductility in Fe-based glasses have been studied by Chen and Polk[9] and Chi, Chen and Miller[10]. They observed that the more rapidly an alloy
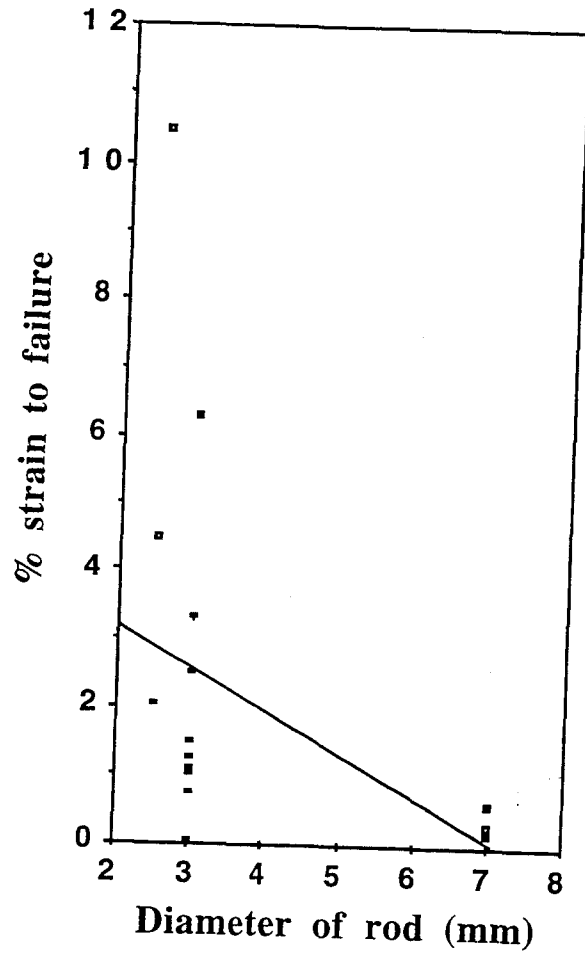
Figure 24: Variation of compressive strain to failure with specimen diameter, indicating a dependence on the average quench rate.

was quenched, the more ductility it appeared to have. The differences in ductility were attributed to the more rapidly quenched alloy possessing more free volume and a less relaxed structure. The differences in structure were confirmed by Differential Scanning Calorimetry. No attempt was made to explain the mechanisms for the influence of the quenching rate on the embrittlement behavior.

Although no experimental evidence of microstructural differences in rods quenched at various rates could be resolved in this investigation, experimental investigations of density changes under plastic deformation have been conducted on other metallic glasses and have yielded conflicting data. One set of results indicates density is reduced under plastic deformation, while another pair of investigations indicate density increases. From Srolovitz, Vitek, and Egami's work, it appears that initially, density may decrease, then after a large amount of inelastic deformation, the density will increase as local free volume is annihilated by the deformation[11].

3.2.2 Effects of metalloid addition on compressive ductility

Lowering the quench rates increased ductility, but at the same time it decreased the size of test specimens. So, an attempt was made to find a way to suppress the castrophic failure of the specimens due to shear banding which could be used for specimens of any dimension. Since the $Zr_{41.25}Ti_{13.75}Cu_{12.5}Ni_{10}Be_{22.5}$ metallic glass could tolerate large amounts of impurities without compromising the material's glass formability, it was proposed that by adding metalloids to the material, the covalent bonding that would be introduced might resist the propagation of the shear bands and suppress failure. Therefore, a series of compression tests were performed where boron was added to the metallic glass and the ductility was measured.

The addition of boron to the metallic glass was not an inconsequential task. Initially, attempts were made to alloy the boron with the metallic glass on the silver boat, but the boron never fully alloyed with the glass. The reason for this appeared to be that

Figure 25: Variation of compressive strain to failure with boron concentration.
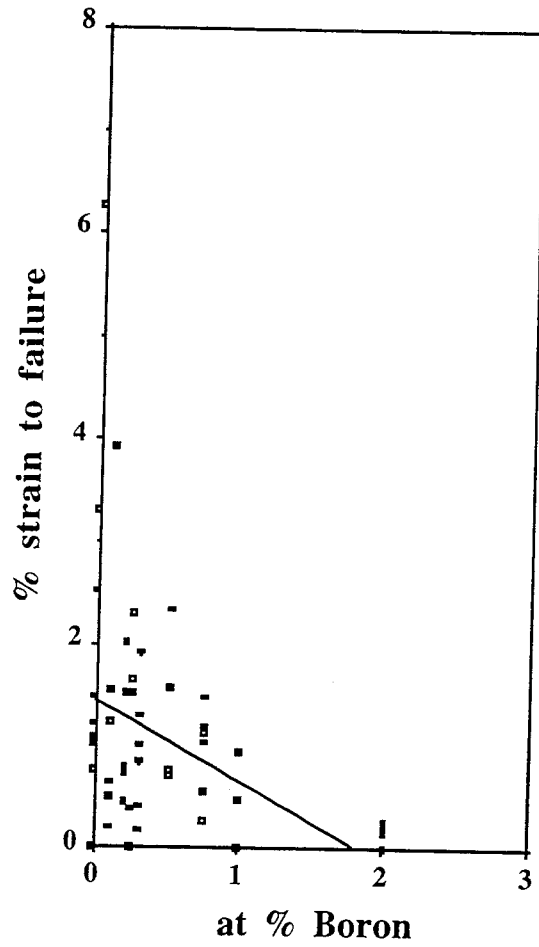
when using induction heating, the melt temperature of the glass dropped so quickly during the alloying process that the boron did not have time to alloy with the glass. Therefore, an alloying technique had to be used which could elevate the temperature of the melt to levels where the boron would have time to alloy. One technique which could accomplish this task was arc melting. Since arc melting can achieve much higher currents in the melt than induction heating, the temperature of the melt can be increased by hundreds of degrees. However, one drawback to increasing the melt temperature to these levels is the vapor pressure of beryllium increases substantially thereby allowing more beryllium to degas from the melt and increasing the hazard posed by the beryllium. This required that the hazard be minimized by limiting the number of ingots that would be alloyed using this technique.
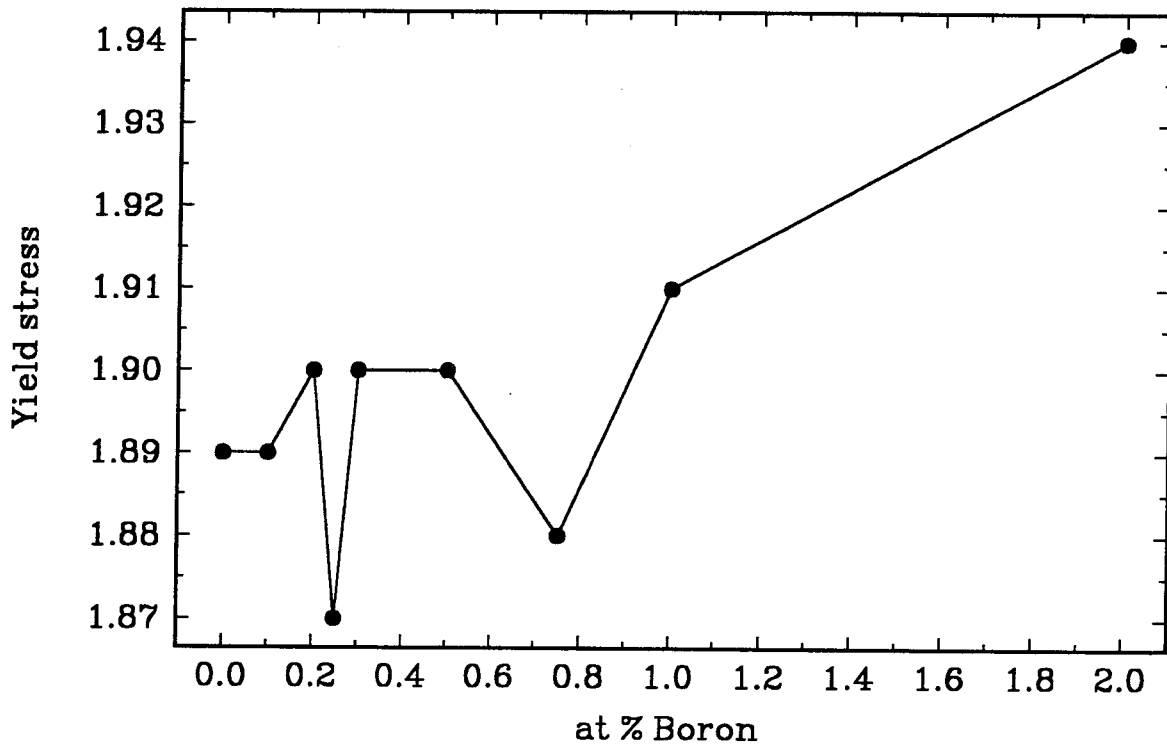
Figure 26: Variation of yield stress with boron concentration.

Once a technique was discovered to alloy boron with the $Zr_{41.25}Ti_{13.75}Cu_{12.5}Ni_{10}Be_{22.5}$ metallic glass, specimens were fabricated with compositions of $(Zr_{41.25}Ti_{13.75}Cu_{12.5}Ni_{10}Be_{22.5})_{1-x}B_x$ where x was varied from 0 to 2 a.t. %. These specimens were then tested in compression and their yield strengths and strain to failures were measured (Figures 25 and 26). Once again the scatter in the strain to failure measurements is significant; however, there appears to be an overall trend that the strain to failure decreases as the concentration of boron increases while the yield strength exhibits only a slight increase. In fact, above 1 a.t. % boron the strain to failure appears to disappear completely. So, instead of increasing the ductility of the metallic glass, the addition of the metalloid appears to be embrittling it.

Johnson and Williams have observed that increasing the concentration of metalloids, such as Boron, in an amorphous alloy significantly increases the Vicker's hardness of the alloy and eventually embrittles the alloy at some critical concentration[12]. In their work, the density of the alloys was measured in order to calculate the partial atomic volume of the Boron. The partial atomic volume of the Boron was found to decrease with increasing Boron concentration, approaching values close to those expected for a close-packed metallic arrangement. From this data, it was postulated that excess volume quenched into the metalloid-free amorphous alloy was progressively filled by boron addition with complete filling occurring somewhere near the upper limit of boron concentration for which an amorphous phase can be obtained by liquid quenching. Since only 0-2 at.% Boron was added to the amorphous metal alloy used in this work, while Johnson and Williams used 10-24 at.% Boron, it is possible that the strength differences they observed were due to significant compositional changes in the alloy. These compositional changes can affect the electronic bonding around a given atom by altering coordination numbers, bond strength, bond types, and bond lengths. The stronger the electronic bonding is around a given atom, the more difficult it is to move that atom. If the atom were associated with a defect, then the defect would become more difficult to move.

From Nelson's work, it is apparent that structural relaxation increases coordination numbers which results in more bonding[13]. Consequently, it would require more stress to move defects in a relaxed structure. The increase in strength reported for Boron addition in amorphous metal alloys could therefore be attributed to changes in the bonding structure around defects. Since the elastic properties of the amorphous metal alloy depend on the electronic bonding structure within the alloy, the addition of Boron would also be expected to alter the elastic properties of the alloy by increasing the moduli of elasticity.

3.2.3 Effects of the plane strain stress state on compressive ductility

From the results of the plane strain compression tests, it appears that the ductility of the $Zr_{41.25}Ti_{13.75}Cu_{12.5}Ni_{10}Be_{22.5}$ metallic glass is substantially greater than from the uniaxial compressive strain results. In fact, a 3 mm diameter rod was deformed in a state of plane strain compression by a true plastic strain of 30% without experiencing catastrophic failure due to shear banding or softening. For a 7 mm diameter rod the plastic deformation was not as impressive, only 3%; however, this is substantially greater than the embrittled deformation observed from the uniaxial compression tests (Figure 27).

It is difficult to determine what could be responsible for the increased ductility in the $Zr_{41.25}Ti_{13.75}Cu_{12.5}Ni_{10}Be_{22.5}$ metallic glass observed in the plane strain compression tests. One possible explanation is the shear band dominated deformation that would be responsible for catastrophic failure in the uniaxial compression test is constrained in the plane strain compression tests because the aspect ratios are below 1. This argument is very crude, and although some constraint exists it will be seen that a more detailed explanation for the ductility increase can be offered by considering the effect of constraint on the microstructural fracture mechanisms. Another possibility is that the increased hydrostatic pressure in the plane strain stress state inhibits fracture processes and increases ductility, which has been observed in the technique of "hydrostatic extruding" where brittle metals
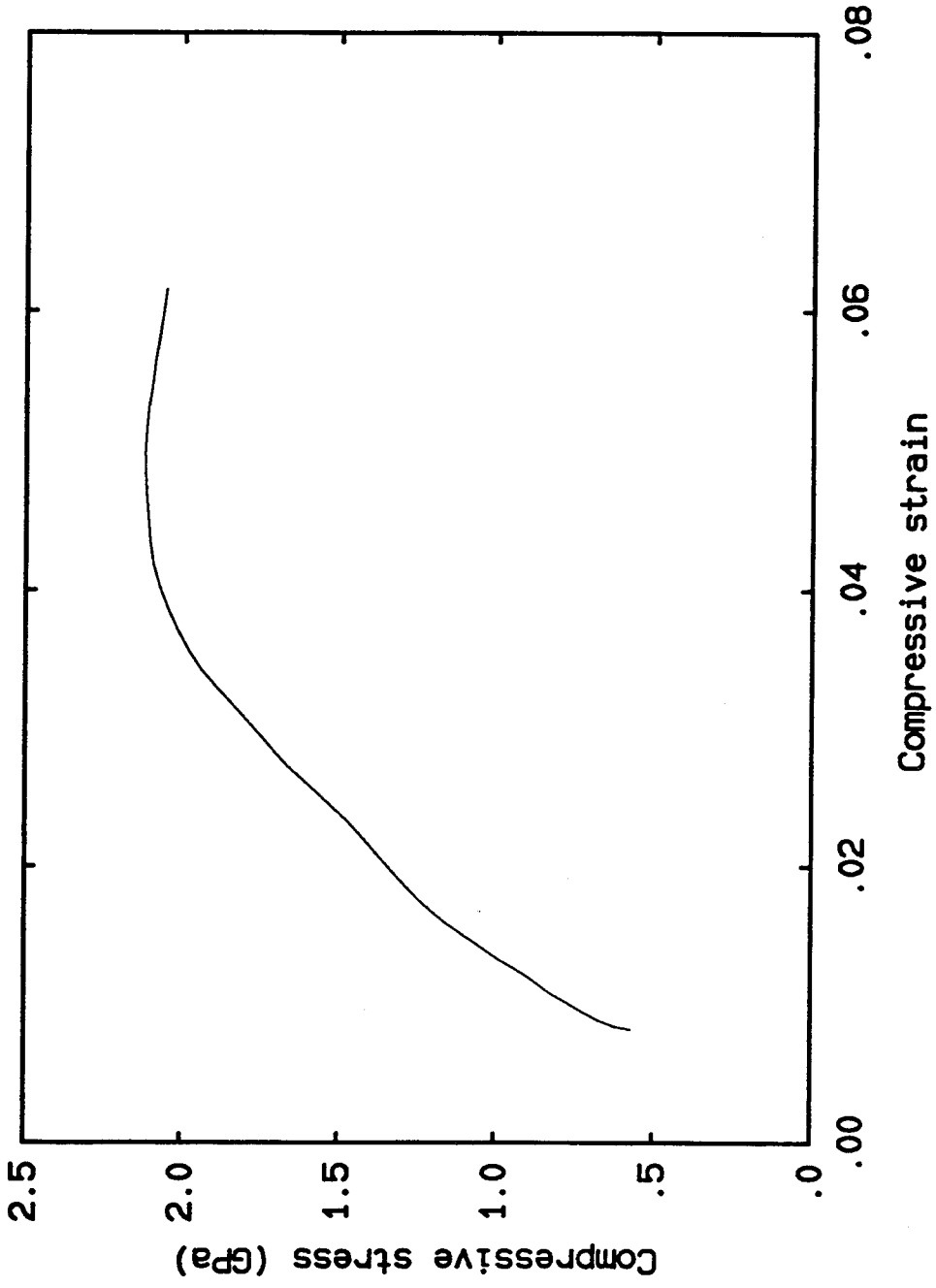
Figure 23: Stress–strain curve for 7 mm diameter plane strain compression test specimen.

can be plasticly formed using high compressive hydrostatic pressure[14] and has also been observed in compression tests conducted on rocks under hydrostatic pressure[15].

Some insight into the ductility of metallic glasses can be inferred from tensile tests that were conducted by Masumoto on notched bars of the metallic glass $Pd_{78}Cu_6Si_{16}$ which indicated that the plastic constraint factor approached the upper limit predicted by slip line fields assuming a von Mises' criterion[3]. From this information, it was concluded that the $Pd_{78}Cu_6Si_{16}$ metallic glass was a 'perfect' ductile material under general constrained yielding. Thus, it may be surmised that the increased ductility in the plane strain compression tests is evidence that the $Zr_{41.25}Ti_{13.75}Cu_{12.5}Ni_{10}Be_{22.5}$ metallic glass is also a 'perfect' ductile material.

3.2.4 The critical tensile criterion

In addition to the notched bar tensile tests, Masumoto also conducted bend tests on notched bars of the metallic glass $Pd_{78}Cu_6Si_{16}$ that were annealed for various periods of time[16]. Masumoto felt that the loss of ductility in metallic glasses could not be explained as an inhibiting of the slip process without first considering the mechanics of fracture. From the bend tests Masumoto proposed that the micro-fracture stress could be used as a structure-sensitive parameter to describe ductility in metallic glasses, where the microfracture stress is the tensile stress required to initiate propagation of a microscopic defect.

The idea of a micro-fracture stress is derived from the critical tensile criterion, which is expressed in the simple form[17]:

$$\sigma_f = \sigma_{yymax} = K_{e,p}\sigma, \qquad (3.2)$$

where $K_{e,p}$ are the elastic stress concentration factor and the plastic intensification factor, depending on the geometry of the elastic-plastic stress distribution beneath the notch root. σ is the stress applied where the defect occurs; σ_f is the micro-fracture stress; and σ_{yymax} is the maximum tensile stress ahead of the defect. Equation (3.1) says, "fracture occurs

when the maximum tensile yield stress (σ_{yymax}) ahead of a defect attains the critical value of tensile stress required to produce fracture (σ_f)." If the maximum tensile stress ahead of a defect is less than the microfracture stress, then the material will yield ahead of the defect before the tensile stress attains the critical value to initiate propagation of the defect (σ_f).

Therefore, the loss of ductility can be expressed as a decrease in micro-fracture stress due to changes in the amorphous microstructure. Although all of the specimens used in the bend tests would be considered amorphous matrices from DSC scans, the decrease in the micro-fracture stress was consistent with the nucleation of fcc clusters in the amorphous matrix and also with a slow increase in the number of the fcc phase both of which were detected by x-ray analysis. These phase transformations have been generally characterized in the crystallization of $Pd_{78}Cu_6Si_{16}$ alloys. Using these ideas it is possible that the observed dependence of ductility on quench rate and metalloid addition can be related to phase transformations in the $Zr_{41.25}Ti_{13.75}Cu_{12.5}Ni_{10}Be_{22.5}$ alloy. It is also possible that these phase transformations can be characterized by changes in the local free volume, which would be consistent with the observations of changes in the amorphous microstructure due to quench rate and metalloid addition. But independent of the semantics in describing the microstructure, it is clear that DSC and x-ray diffraction scans should be obtained on the $Zr_{41.25}Ti_{13.75}Cu_{12.5}Ni_{10}Be_{22.5}$ metallic glass in order to characterize its phase transformations and relate the microstructure to the ductility of the glass.

It is also possible to conclude from the critical tensile criterion that ductility of a metallic glass is determined from the competition between slip processes and fracture mechanisms. Therefore, the ductility of a metallic glass will not only be determined from its microfracture stress, which is microstructurally dependent, but also on the sensitivity of the fracture processes in the glass to the applied stress field. As an example, consider the cases of uniaxial and plane strain compression. Since failure occurs due to shearing, a

critical shear criterion should be used instead of a critical tensile criterion where fracture occurs when the maximum shear yield stress exceeds the micro-fracture shear stress. Using a two-dimensional analysis, the maximum shear stress, τ_{max}, for each stress state can be written:

$$\tau_{max} = \begin{cases} \dfrac{\sigma}{2} & \text{, for uniaxial compression} \\ \dfrac{\sigma(1-v)}{2} & \text{, for plane strain compression} \end{cases} \qquad (3.3)$$

where σ is the compressive stress. When yielding occurs, the maximum shear stress calculated using the von Mises criterion is:

$$\tau_{max} = \begin{cases} \dfrac{\sigma}{2} = \dfrac{\sqrt{3}\tau_y}{2} & \text{, for uniaxial compression} \\ \dfrac{\sigma(1-v)}{2} = \dfrac{\sqrt{3}\tau_y(1-v)}{2\sqrt{(1-v+v^2)}} & \text{, for plane strain compression} \end{cases} \qquad (3.4)$$

where τ_y is the shear yield stress and v is Poisson's ratio. For the $Zr_{41.25}Ti_{13.75}Cu_{12.5}Ni_{10}Be_{22.5}$ metallic glass, the maximum shear stress at yield for the plane strain case will be 70% of the maximum shear stress at yield for the uniaxial case. In fact, the maximum shear stress for the plane strain case will not exceed the maximum shear stress for the uniaxial case until $v < 0$. Consequently, metallic glasses will exhibit more ductility in stress states like plane strain compression than in uniaxial compression because the plane strain stress state is not as conducive to fracture as the uniaxial stress state. This simplified analysis illustrates the type of approach that needs to be taken to characterize the yield behavior of metallic glasses. However, before a proper criterion can be developed, the fracture processes in metallic glasses must be thoroughly investigated to determine their behavior in multi-axial stress states.

3.3 Tension Tests

3.3.1 Experimental procedure

As was described in section 2.3, tensile test specimens were prepared from 7 mm diameter cylindrical rods of the $Zr_{41.25}Ti_{13.75}Cu_{12.5}Ni_{10}Be_{22.5}$ metallic glass that had been cast in evacuated quartz tubes. These rods were machined into a dog-bone geometry with dimensions proportional to ASTM standard E8-68 for tension testing. The exact dimensions of these test specimens can be seen in Figure 17.

Tension tests were performed in the same MTS 319.25 axial-torsional load frame as the compression tests; however, the specimens were threaded into grips that were connected by universal joints to the load frame in order to reduce the bending moments transmitted to the specimen (Figure 28). Uniaxial strain gages from the Micromeasurements Group were glued on the surface of the specimen's gage section in order to obtain one-dimensional surface strains. All of the tensile tests were conducted using constant crosshead velocities which resulted in strain rates varying from 10^{-4} to 10^{-3}/sec.

3.3.2 Experimental results

Many of the tensile specimens that were tested had a shrink-hole cavity within the gage section of the specimen that invalidated the tests results because of premature failure. These shrink-hole cavities were formed during fabrication even though a quenching technique was used to minimize their formation. However, about 20% of the specimens had failure surfaces which were free of internal defects. A stress-strain curve from a tensile test specimen whose failure was not precipitated by internal defects can be seen in Figure 29. Failure occurs at a stress of 1.89 ± 0.03 GPa and an elastic strain of 1.8% with no yielding apparent before failure.

Although the tensile test specimen appears to be brittle with no apparent macroscopic ductility, scanning electron micrographs of the fracture surface revealed the vein-like morphology that was characteristic of viscous failure in a shear band (Figure 30).
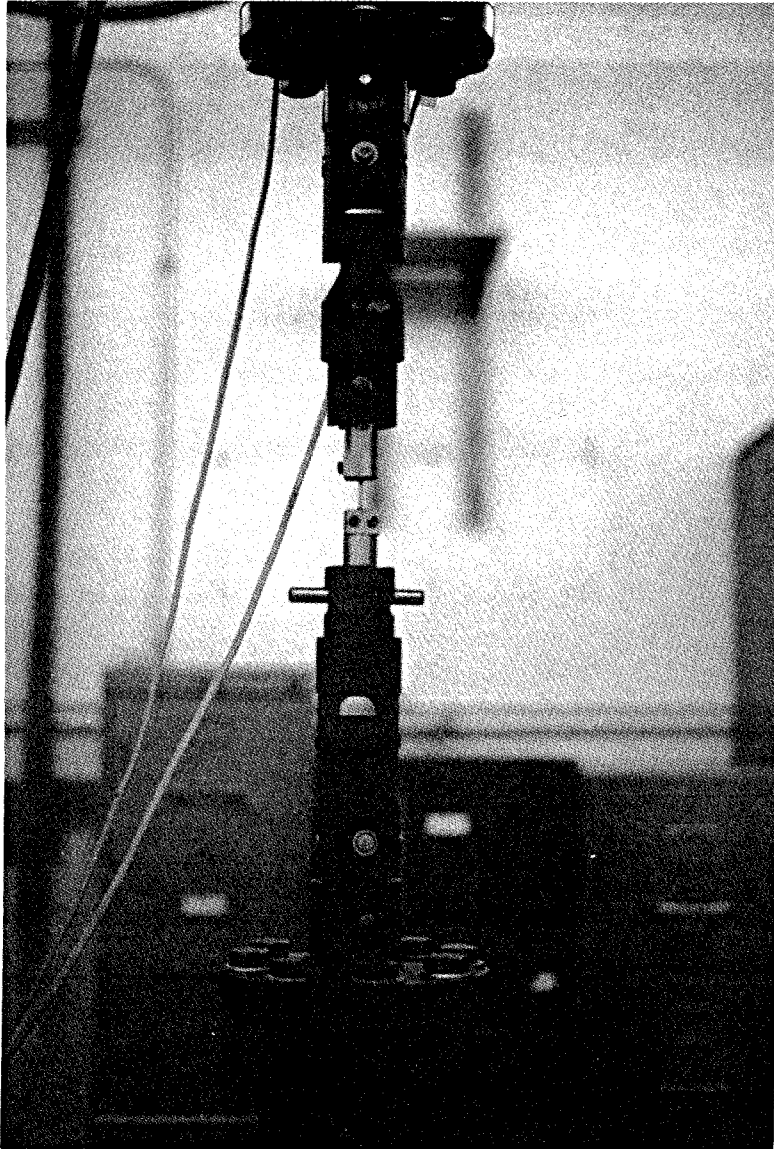
Figure 28: Grips used for quasi-static tension tests.

Also, the fracture surface is inclined at an angle of 55° to the loading axis, the same angle observed for shear band formation in tensile tests conducted on cylindrical rods of amorphous $Pd_{78}Cu_6Si_{16}$ (Figure 31)[3]. Therefore, even though the material appears to be brittle, there is evidence that the tensile specimen yielded locally in a shear band prior to failure. Masumoto has proposed that these angles are predicted by slip line field theory for an elastic-perfectly plastic, von Mises material in plane stress tension. However, these shear bands form in a state of uniaxial tension where the slip line angle is predicted to be 45°, the same as for uniaxial compression.
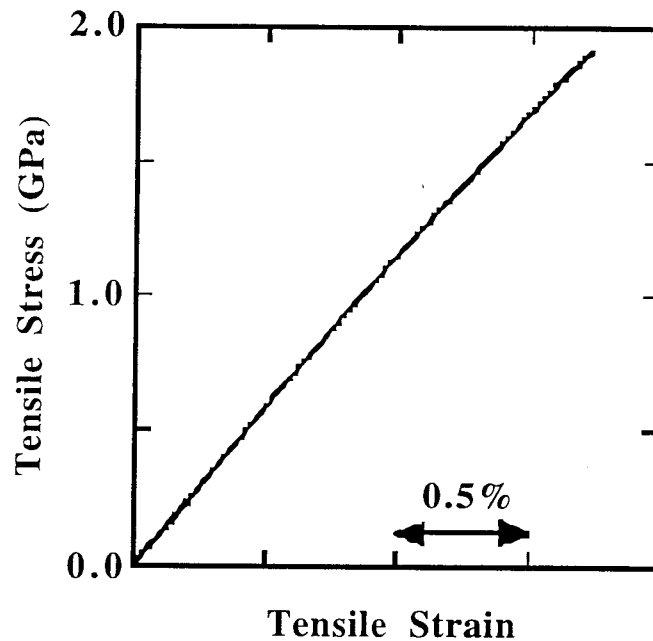
Figure 29: Stress-strain curve from quasi-static tension test.

The localized yielding in the shear band causes necking of the tensile specimen which leads to catastrophic failure because of the ensuing stress concentration. Consequently, the tensile yield stress of the metallic glass is equivalent to the failure stress in Figure 29. The tensile yield stress of the $Zr_{41.25}Ti_{13.75}Cu_{12.5}Ni_{10}Be_{22.5}$ metallic glass is approximately equal to the compressive yield stress of the glass, which means that the yield behavior of the $Zr_{41.25}Ti_{13.75}Cu_{12.5}Ni_{10}Be_{22.5}$ metallic glass exhibits no anisotropy.

Figure 30: Orientation of fracture surface for quasi-static tensile test specimen.

Figure 31: Scanning electron micrograph of tensile fracture surface.

3.4 Torsion Tests

3.4.1 Experimental procedure
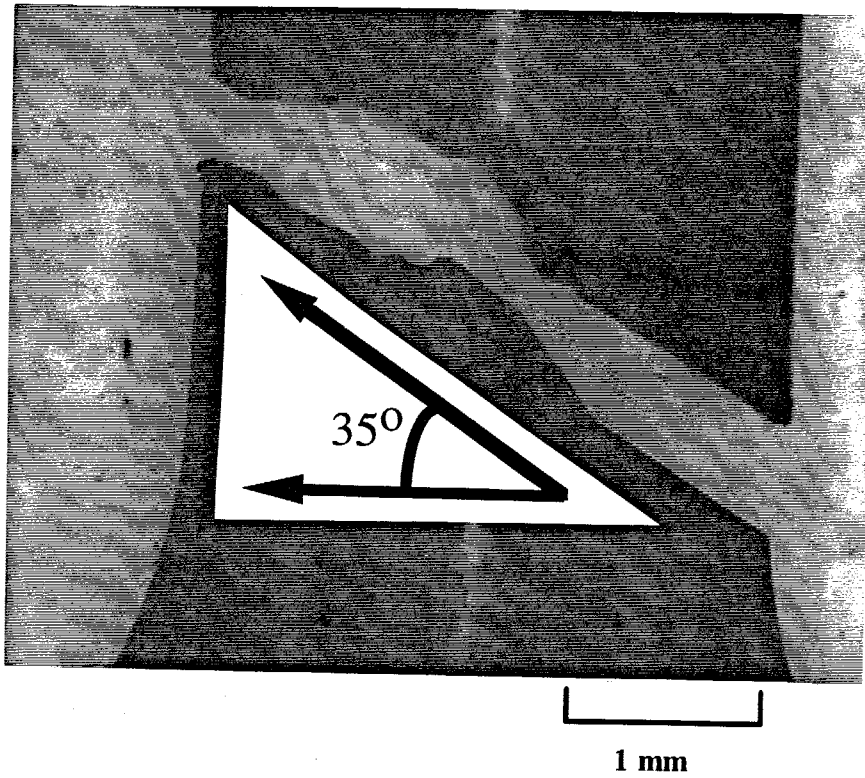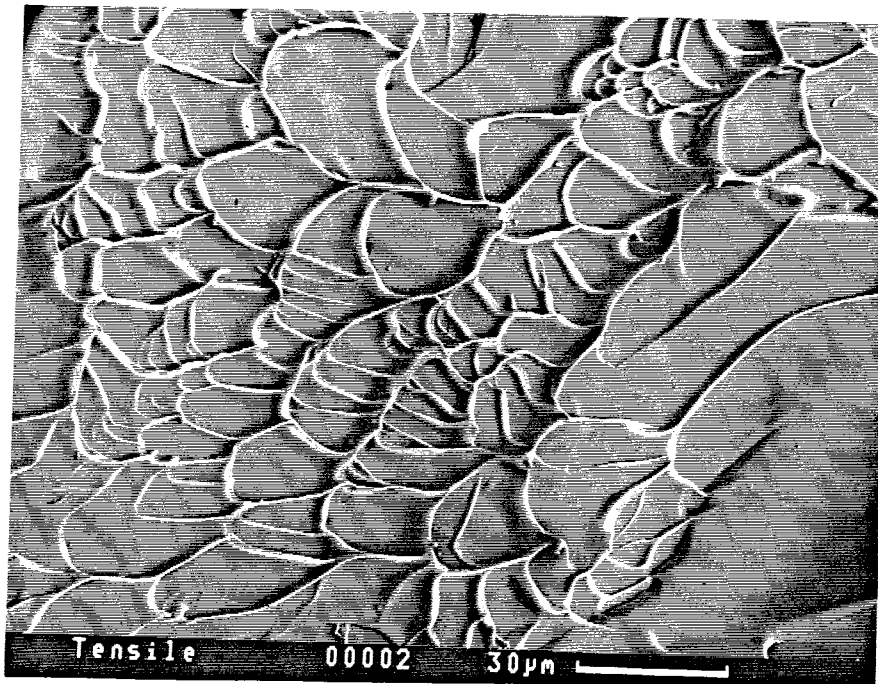
Torsion tests were conducted using the same specimens as in the tension tests. Surface strain measurements were made using rectangular strain gage rosettes from the Micromeasurement Group. Torsion specimens were loaded using the same grips as in the tension tests. Because the specimens were threaded, hardened steel inserts were placed in the grips to contact the bottom of the specimens and prevent them from being screwed in during loading. Torsion tests were conducted at a constant angular velocity which results in strain rates varying from 10^{-4} to 10^{-3}/sec. The MTS load frame was also placed in load control with the load nominally set at zero to gaurantee that the specimen experienced only pure torsional loading.

3.4.2 Experimental analysis

The shear stress state for a cylindrical rod under torsion is inhomogeneous, with the shear stress varying from a maximum value on the outer surface to zero at the center of the rod. It is therefore necessary to analyze the shear stress distribution in the rod assuming the elastic-perfectly plastic behavior observed in compression and tension tests, and determine the relationship of the shear stress distribution to the applied torsional moment. The shear stress can be related to the applied torsional moment, M_T, by balancing moments for an elastic-perfectly plastic rod as follows:

$$M_T = 2\pi \left\{ \int_b^R \tau_y r^2 dr + \int_0^b \tau(r) r^2 dr \right\}, \tag{3.5}$$

where R is the radius of the rod, b is the radial position for the plastic zone boundary, τ_y is the yield shear stress, r is the radial position, and $\tau(r)$ is the elastic shear stress.

One can calculate the shear strain, $\gamma(r)$, from the deformation of the rod as follows:

$$\gamma(r) = \frac{\vartheta r}{L},$$ (3.6)

where ϑ is the angle of rotation imposed on the rod and L is the length of the rod. The shear strain can then be used to calculate the elastic shear stress ($\tau(r) = \mu\gamma(r)$). Rearranging these equations and calculating the integral, one finds:

$$M_T = \pi\tau_o \left\{ \frac{2}{3}R^3 - \frac{b^3}{6} \right\},$$ (3.7)

where τ_o is the shear stress at the surface of the rod which is equal to $\mu\vartheta R/L$ when the rod is fully elastic and equal to τ_y after yielding has occurred.

3.4.3 Experimental results

The resulting stress-strain curve for a typical torsion test can be seen in Figure 32. From this curve, it appears that yielding is initiated at $\gamma_y \sim 0.019$ and failure occurs at $\gamma_f \sim 0.021$. The ductility appears to be limited for torsion test specimens fabricated from 7 mm diameter rods cast in evacuated quartz tubes, but it is consistent with the ductility observed in compression tests conducted on specimens cut from 7 mm diameter rods that were fabricated using the same quench technique. From equation (3.5), the failure strain, γ_f, on the outer surface can be used to predict the radial position of the plastic zone boundary at failure, b_f, as follows:

$$b_f = \frac{\gamma_y}{\gamma_f}R,$$ (3.8)

where γ_y is the strain at which yielding is initiated on the outer surface. Therefore, for a rod 1.5 mm in radius, the radial position of the plastic zone boundary at failure is approximately 1.36 mm.

Because of the limited extent of yielding in the torsional experiments ($b \sim 0.9R$), the shear stress at the surface of the rod was calculated neglecting yielding in equation (3.6) as follows:

$$\tau(R) = 2M_T \, \pi^{-1} \, R^{-3}. \qquad (3.9)$$

The shear stress increases monotonically in Figure 32 and does not reach a plateau value because of the limited ductility and the inhomogeneous torsional stress state. The shear yield behavior has serrated features similar to those observed in compressive tests conducted on other metallic glasses. The shear yield strength was taken to be the point at which the shear response deviates significantly from linearity, a value of 1.03 GPa. The shear yield stress is approximately equal to $\frac{\mu}{32}$, which approaches the theoretical shear strength limit of $\frac{\mu}{30}$ calculated from atomistic models.
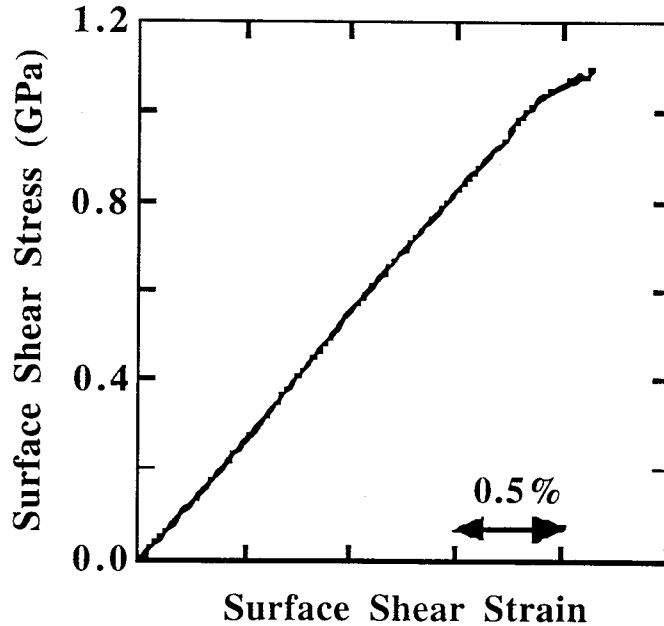

Figure 32: Stress-strain curve from quasi-static torsion test.

The extent of yielding at failure in an elastic-perfectly plastic rod under torsional load can also be calculated from equation (3.6) as follows:

$$b^3 = 4R^3 - 6M_T\pi^{-1}\tau_y^{-1}.$$

(3.10)

Plugging equation (3.8) into equation (3.9) yields:

$$b^3 = R^3 (4 - 3\tau(R)\tau_y^{-1}).$$

(3.11)

From Figure 32, the failure stress in shear is 1.10 GPa, which results in the radial position of the plastic zone boundary at failure being 1.39 mm. The consistency in predicting the radial position of the plastic zone boundary based on equations (3.7) and (3.10) supports the assumption of elastic-perfectly plastic constitutive behavior.
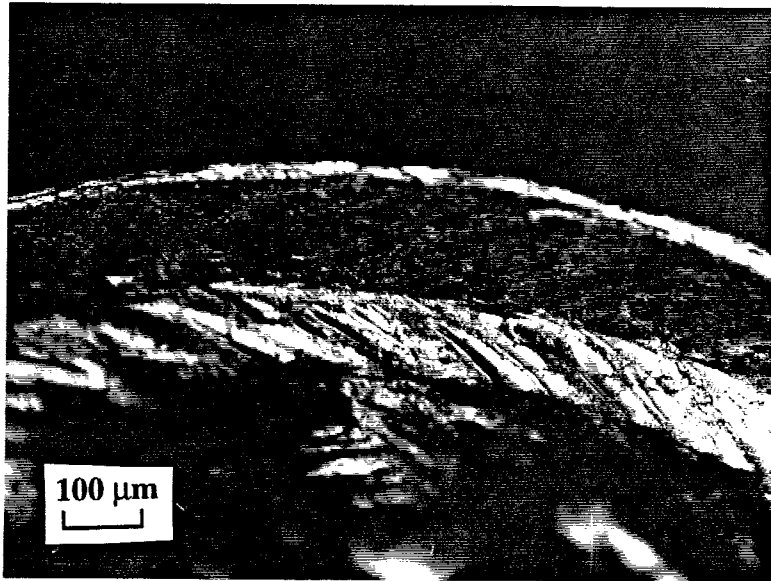

Figure 33: Optical micrograph of torsional fracture surface.

An optical micrograph of the torsional fracture surface, Figure 33, reveals a thin, smooth band near the outer surface. Circular-smooth regions have also been observed by

Masumoto ahead of notches in amorphous $Pd_{78}Cu_6Si_{16}$ fracture specimens because of constrained slipping[3]. The band terminates at a radial position of approximately 1.35 mm, equivalent to the previous plastic zone calculations. If the specimen were polycrystalline instead of amorphous, it would be possible to etch this surface and see the dislocations responsible for plastic deformation. However, since this is not possible it can only be surmised that this band represents the extent of constrained torsional yielding in the specimen.

The fracture surface is oriented at an angle of approximately 90° to the loading axis, which is the angle predicted by slip line theory for an elastic-perfectly plastic von Mises material loaded in torsion (Figure 34). Scanning electron micrographs of the fracture surface revealed the vein-like morphology that was characteristic of viscous failure in a shear band (Figure 35). These observations are consistent with the observed yield behavior in uniaxial compression, but in the case of uniaxial tension the shear band angles did not correspond to the predictions of slip line field theory.

3.5 Von Mises yield criterion

After determining the quasi-static yield strength of the $Zr_{41.25}Ti_{13.75}Cu_{12.5}Ni_{10}Be_{22.5}$ metallic glass in compression, tension and torsion, an appropriate yield criterion had to be chosen for the material. Since the orientation of the fracture surfaces for uniaxial compression and torsion indicated that the metallic glass might be a von Mises material, the von Mises yield criterion seemed a natural choice.

For isotropic, pressure insensitive solids, the von Mises yield criterion is as follows:

$$(\sigma_1 - \sigma_2)^2 + (\sigma_1 - \sigma_3)^2 + (\sigma_2 - \sigma_3)^2 = 6k^2 \quad , \tag{3.12}$$

where σ_1, σ_2, and σ_3 are the principal stresses and k is a constant. For each of the four quasi-static stress states that were tested in this work, k can be evaluated as follows:
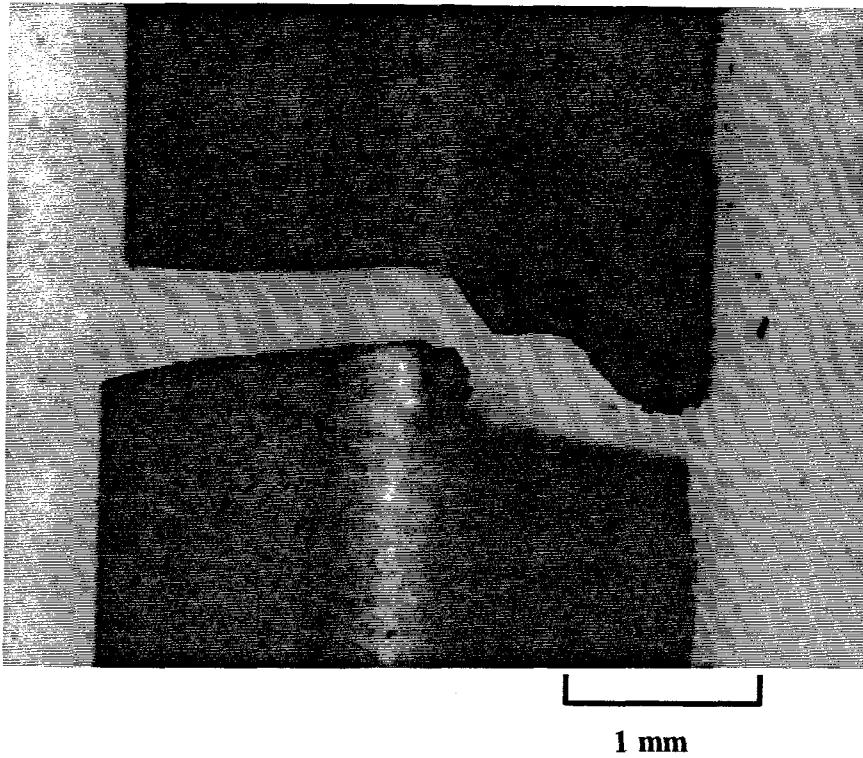
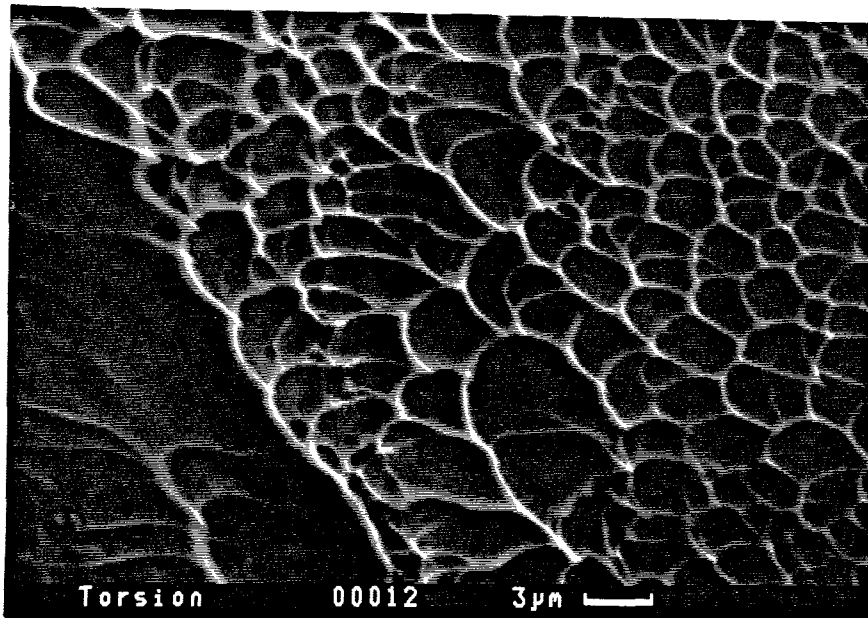**Figure 34: Orientation of fracture surface for quasi-static torsional test specimen.**

Figure 35: Scanning electron micrograph of torsional fracture surface.

Uniaxial normal stress: $k = \dfrac{\sigma_y}{\sqrt{3}}$,

Plane strain compression: $k = \sigma_y \sqrt{\dfrac{(1 - \nu + \nu^2)}{3}}$, (3.12)

Torsion: $k = \tau_y$.

From the yield stresses that were measured for each stress state, the resulting values of k were:

Uniaxial compression: $k = 1.10$
Plane strain compression: $k = 1.07$
Tension: $k = 1.09$
Torsion: $k = 1.03$

The values of k calculated for the $Zr_{41.25}Ti_{13.75}Cu_{12.5}Ni_{10}Be_{22.5}$ metallic glass from the four stress strates are all within 7% of each other. From these results it appears that the $Zr_{41.25}Ti_{13.75}Cu_{12.5}Ni_{10}Be_{22.5}$ metallic glass obeys a von Mises yield criterion. Consequently, the yield behavior of the glass can be considered isotropic and pressure insensitive.

The orientation of the shear bands in uniaxial tension does not appear to support the pressure insensitive yield behavior of the glass. In fact, it tends to support Donovan's conclusions that the yield behavior of metallic glasses obeys a pressure sensitive Mohr-Coulomb criterion. Another possibility is that the yield behavior may be pressure insensitive while the orientation of shear bands is not. Furthermore, the orientation of the shear bands may only be sensitive to tensile hydrostatic pressure and not compressive since the shear bands formed in compression and torsion tests lie along planes of maximum shear. It is also not clear how cracks are initiated and propagate in metallic glasses, so the orientation of the fracture surfaces may not at all be related to the formation of shear bands.

This issue cannot be resolved from the work presented here, and would require detailed investigations of the orientation of shear bands with respect to hydrostatic pressure or tests conducted on geometries for which slip line field solutions are known. It may also be useful to perform three-dimensional numerical simulations of amorphous atomistic models to determine the effects of stress state on shear band orientation. Although there is a plethora of evidence supporting the von Mises yield behavior of metallic glasses, the issue of shear band orientation remains the primary source of conflict.

References

[1] Pampillo, C.A. and Chen, H.S., Materials Science and Engineering, **13**, 181 (1974).

[2] Kachanov, L.M., Fundamentals of the Theory of Plasticity, MIR Publishers, Moscow, (1974).

[3] Kimura, H. and Masumoto, T., Amorphous Metallic Alloys, ed. by F.E. Luborsky, Buttersworth, London, 187 (1983).

[4] Leamy, H.J., Chen, H.S., and Wang, T.T., Metallurgical Transactions, **3**, 699 (1972).

[5] Pampillo, C.A. and Reimschuessel, A.C., Journal of Materials Science, **9**, 718 (1974).

[6] Kimura, H. and Masumoto, T., Amorphous Metallic Alloys, ed. by F.E. Luborsky, Buttersworth, London, 187 (1983).

[7] Watts, A.B. and Ford, H., Proceedings of the Institute of Mechanical Engineering B, **1**, 448 (1952).

[8] Donovan, P., Acta Metallurgica, **37**, 445 (1989).

[9] Chen, H.S. and Polk, D.E., Journal of Non-Crystalline Solids, **15**, 174 (1974).

[10] Chi, G.C., Chen, H.S., and Miller, C.E., Journal of Applied Physics, **49**, 1715 (1978).

[11] Srolovitz, D., Vitek, V., and Egami, T., Acta Metallurgica, **31**, 335 (1983).

[12] Johnson, W.L. and Williams, A.R., Physical Review B, **20**, 1640 (1979).

[13] Nelson, D.R., Physical Review B, **28**, 5515 (1983).

[14] Atkins, A.G. and Mai, Y.-W., <u>Elastic and Plastic Fracture: metals, polymers, ceramics, composites, biological materials</u>, Ellis Horwood Limited, New York (1988).

[15] Patterson, M.S., <u>Experimental Rock Deformation-The Brittle Field</u>, Springer-Verlag, New York (1978).

[16] Kimura, H. and Masumoto, T., <u>Acta Metallurgica</u>, **28**, 1677 (1980).

[17] Knott, J.F., <u>Fundamentals of Fracture Mechanics</u>, Butterworths, London, 77 (1974).

CHAPTER 4

Dynamic Compressive Behavior of $Zr_{41.25}Ti_{13.75}Ni_{10}Cu_{12.5}Be_{22.5}$ Bulk Metallic Glasses

4.1 Kolsky Bar Testing Technique

In many manufacturing processes and impact problems, materials are subjected to dynamic loading. It is therefore necessary to understand the dynamic behavior of a material to be used in these applications. Bulk metallic glasses have especially shown promise as such a material. However, there is no experimental mechanical data available on the dynamic behavior of bulk metallic glasses.

In order to underestand the dynamic behavior of materials, it is necessary to design a test where the dynamic loading and response of a material is well characterized. One such technique is the split Hopkinson pressure bar, which was first introduced by Kolsky in 1949[1]. This technique will be referred to in this investigation as the Kolsky bar.

The basic principle of the Kolsky bar is illustrated below (Figure 36). The set-up basically consists of two elastic pressure bars, $\overline{AB}$ known as the incident or input bar and $\overline{CD}$ known as the transmitter or output bar. A specimen is placed between the two bars. A striker bar impacts the input bar at $\overline{A}$. This sets up a pressure pulse within the incident bar with a strain $\varepsilon_I(t)$. When this pulse reaches $\overline{B}$, the end of the incident bar, part of the wave is reflected with a strain $\varepsilon_R(t)$ and part of the wave is transmitted to the ouput bar with a strain $\varepsilon_T(t)$. Strain gages are placed in the middle of the elastic pressure bars to provide the time resolved signals of the incident, reflected, and transmitted pulses. The pulse is reflected from the interface of the bar and specimen at $\overline{B}$ due to impedance mismatch.

When the specimen is deforming uniformly, the strain rate $\dot{\varepsilon}$ within the specimen is proportional to the reflected wave's amplitude. Similarly, the stress within the sample is
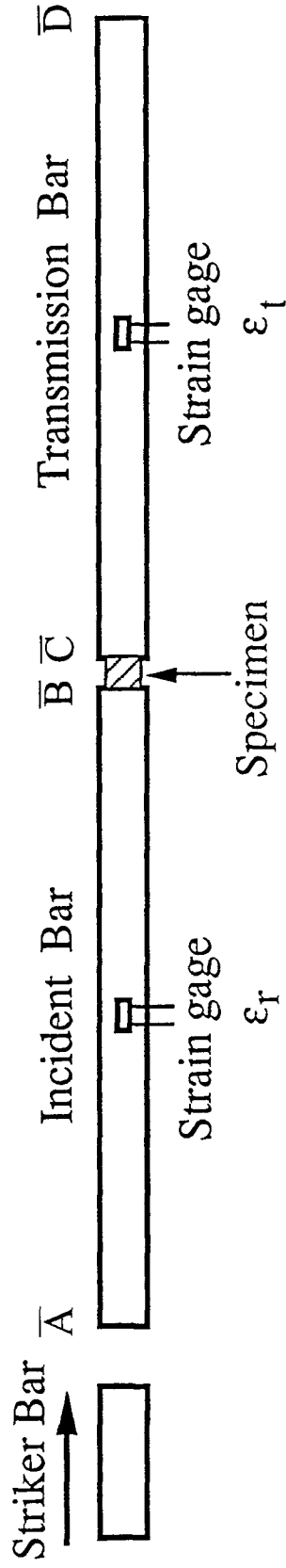
Figure 36: Kolsky bar used for dynamic compression tests.

proportional to the amplitude of the transmitted wave. This can be shown by the following analysis (Figure 37).
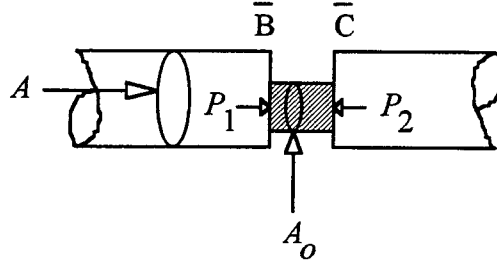
Figure 37: Stress and strain analysis of homogeneously deformed specimen in the Kolsky bar.

where A is the cross sectional area of the elastic bars and A_O is the cross sectional area of the specimen. The strain rate in the deforming specimen is:

$$\frac{d\varepsilon}{dt} = \dot{\varepsilon}(t) = \frac{v_1(t) - v_2(t)}{L}, \tag{4.1}$$

where v_1 and v_2 are particle velocities at $\overline{B}$ and $\overline{C}$ respectively, and L is the length of the specimen. From characteristic relations for one-dimensional wave propagation assuming no wave dispersion occurs, one has[1]:

$$v_1 = c_o(\varepsilon_I - \varepsilon_R), \tag{4.2a}$$

$$v_2 = c_o\varepsilon_T, \tag{4.2b}$$

where, $c_o = \sqrt{\dfrac{E}{\rho}}$ is the longitudinal bar wave velocity for the elastic bars, E is the Young's modulus of the elastic bars, and ρ is the density of the elastic bars. From equations (4.1) and (4.2):

$$\dot{\varepsilon}(t) = \frac{c_o}{L}\left[\varepsilon_I(t) - \varepsilon_R(t) - \varepsilon_T(t)\right]. \tag{4.3}$$

The average stress in the specimen is:

$$\sigma(t) = \frac{P_1(t) + P_2(t)}{2A_o}, \tag{4.4}$$

where P_1 and P_2 are the forces at the incident bar/specimen and specimen/transmitter bar interfaces respectively. Assuming that no wave dispersion occurs:

$$P_1 = EA_o \, [\varepsilon_I(t) + \varepsilon_R(t)], \qquad (4.5a)$$

$$P_2 = EA_o \varepsilon_T(t). \qquad (4.5b)$$

From equations (4.4) and (4.5):

$$\sigma(t) = \frac{EA_o}{2A}[\varepsilon_I(t) + \varepsilon_R(t) + \varepsilon_T(t)]. \qquad (4.6)$$

When the specimen is deforming uniformly (homogeneously) the stress at the incident bar/specimen interface equals the stress at the trnsmitter bar/specimen interface. From equation (4.5):

$$P_1(t) = P_2(t), \qquad (4.7)$$

which implies that:

$$\varepsilon_I(t) + \varepsilon_R(t) = \varepsilon_T(t). \qquad (4.8)$$

From equations (4.3), (4.6), and (4.8):

$$\sigma(t) = \frac{EA_o}{A}\varepsilon_T(t), \qquad (4.9)$$

$$\dot{\varepsilon}(t) = -\frac{2c_o}{L}\varepsilon_R(t). \qquad (4.10)$$

Integrating equation (4.10), we obtain the time history of the strain as follows:

$$\varepsilon(t) = \int_0^t \dot{\varepsilon}(\tau) \, d\tau. \qquad (4.11)$$

The stress-strain behavior is completely determined by measuring $\varepsilon_T(t)$ and $\varepsilon_R(t)$ on the elastic pressure bars using strain gages.

4.2 High Speed Infrared Thermal Measurements

High speed, non-contact techniques have been developed for measuring temperature fields on the surfaces of deforming objects[2,3]. These techniques use detectors

to measure the infrared thermal signatures generated by the deforming object. An Offner imaging system first employed by Zehnder and Rosakis was used for the dynamic compression tests to focus the surface of the compression specimens onto a single infrared detector. The Offner system has a fixed 1:1 magnification, so that optics were used with a focal length of approximately 160 mm and an object distance of 320 mm in order to protect the optics by keeping them a sufficient distance away from the test specimen.

A single EG&G J15D12 HgCdTe infrared detector with dimensions 100 μm square and a temperature range of approximately 300 to 1000 K was used to detect the temperature (Figure 36). The HgCdTe detector was cooled with liquid nitrogen, and the voltage from the detector was outputted to a preamp with a band pass of 5 Hz to 1 MHz, well beyond the detector's cutoff frequency of 400 kHz. Because the sensor had a very high signal-to-noise ratio, the preamp was connected to an amplifier set at 20X and a filter set at 10 kHz which in turn was connected to a Nicolet 440 digital oscilloscope that was also connected to the strain gages on the Kolsky bars.

The HgCdTe detector integrates wavelengths ranging from 2 μm to 12 μm. The voltage produced by the detectors is related to the energy emitted by the specimen through an integral depending upon the emissivity of the material, $\varepsilon(\lambda,T)$, the spectral responsivity of the HgCdTe detector, $R(\lambda)$, and the black body radiation $P(\lambda)$, as follows[3]:

$$v(T,T_o) = A A_D \beta \int_{2\,\mu m}^{15\,\mu m} R(\lambda)[P(\lambda,T)\varepsilon(\lambda,T) - P(\lambda,T_o)\varepsilon(\lambda,T_o)]d\lambda, \quad (4.12)$$

where the integration variable λ is the wavelength of the radiation, A is the amplification, A_D is the detector area, and β is the fraction of energy transmitted to the detectors by the optical system (related to the aperture). When evaluated for HgCdTe detectors, this relationship is nearly linear on a log-log plot of voltage versus temperatures. In order to determine this relationship for the $Zr_{41.25}Ti_{13.75}Cu_{12.5}Ni_{10}Be_{22.5}$ metallic glass, a 1.5 mm thick plate specimen with a thermocouple clamped to its surface was heated in an oven.

The voltage output from the detectors and the thermocouple readings were then recorded as the specimen cooled. This calibration data was then plotted on a log-log plot, and the linear relationship was determined (Figure 38). This relationship was then used to convert the voltage record from the detector into a temperature measurement.
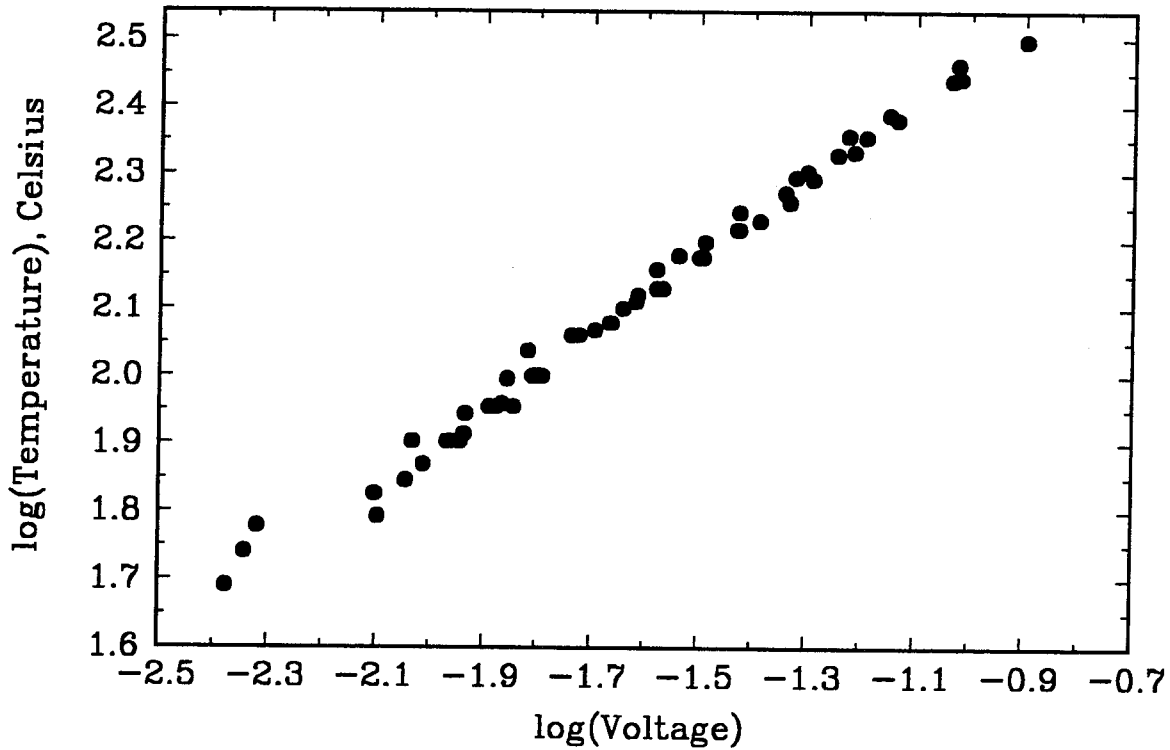
Figure 38: Thermal calibration curve for $Zr_{41.25}Ti_{13.75}Cu_{12.5}Ni_{10}Be_{22.5}$.

4.3 Experimental Procedure

The split Hopkinson bar and thermal measurement system used for the dynamic testing of the $Zr_{41.25}Ti_{13.75}Cu_{12.5}Ni_{10}Be_{22.5}$ metallic glass can be seen in Figure 39. The elastic bars were made of C350 maraging steel with a yield stress of 2.5 GPa. The bars were 1.22 meters in length and 1.27 cm in diameter. A striker bar was used that was manufactured from the same material as the elastic bars and with the same diameter, but
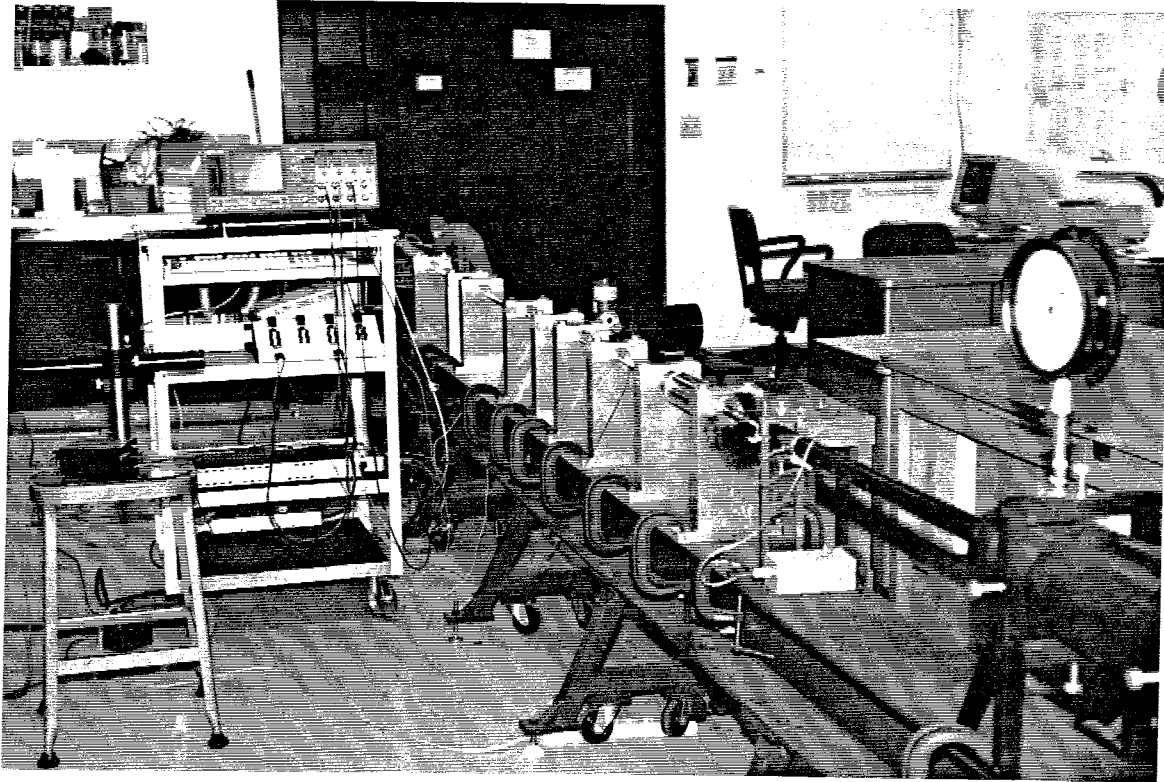
(a)
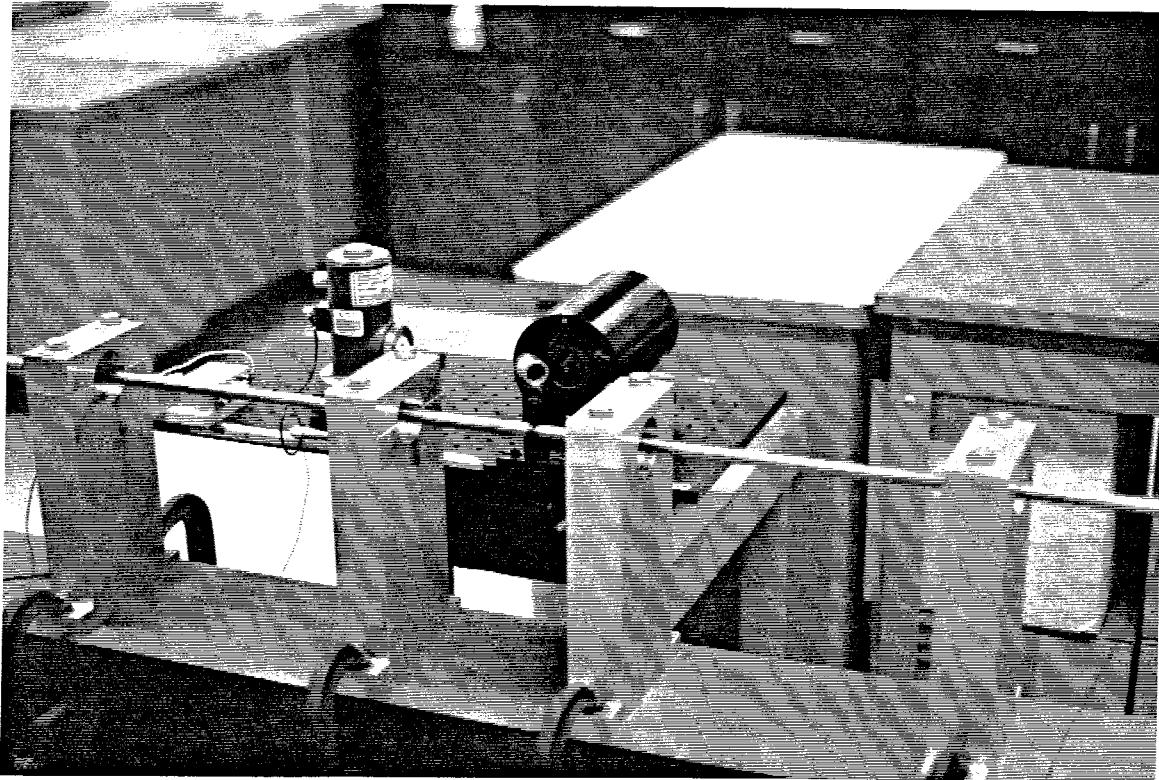
(b)

Figure 39: (a) Kolsky bar, (b) Thermal measurement system.

is only 10 cm in length. Strain gages from Micromeasurements Group were placed midway from the ends of the elastic bars to measure the strain response on the surface of the bar from the propagating waves. The strain gages were attached to quarter Wheatstone bridges whose voltage outputs were measured with a Nicolet 440 digital oscilloscope using a sampling rate of 5 megahertz.

Sometimes when the striker bar impacts the incident bar, there is some misalignment which can cause a variation in the amplitude of the incident stress pulse often referred to as "ringing." Consequently, there is some dispersion of the stress pulse that is detected by the strain gages well after the stress pulse has passed underneath the strain gage. This makes it extremely difficult to detect the start of the reflected wave when it passes through the same strain gage.

In order to reduce dispersion from the incident stress pulse, a copper insert was placed between the striker bar and the incident bar as proposed by Nemat-Nasser *et al.* The resulting stress pulse generated by using the copper inserts was a ramp function instead of the step function generated when the copper inserts are removed. The period of the stress pulse was nearly quadrupled by the presence of the copper inserts. Theoretically, the length of the stress pulse would be twice the length of the striker bar, which implies that the stress pulse generated using copper inserts would be eight times the length of the striker bar. A constraint on the length of the stress pulse is it should be less than the length of the bar if there is to be no overlap of incident and reflected signals underneath the strain gage when it is positioned midway from the ends of the bar. So, the striker bar should be less than 15 cm in length if the stress pulse is to be less than the length of the elastic bar, which dictated that the 10 cm long striker bar be used.

Striker bar velocities varied from 5 m/s to 20 m/s, which generated strain rates in the specimen of 300 to 6000/s depending on the length of the specimen. One problem with using the copper inserts was the stress pulses generated by their deformations were of insufficient amplitude to obtain strain rates in the specimen greater than about 2000/sec to

3000/sec depending on the length of the specimen. In order to obtain the higher strain rates, it was necessary to remove the copper inserts.

Test specimens fabricated for the quasi-static compression tests were also used for the dynamic compression tests. Specimens with diameters of 2.5 mm and aspect ratios ranging from 1.5-2.0 were used because quasi-static tests indicated that these specimens had the greatest ductility. End effects were reduced by placing specimens between a pair of WC inserts coated with "Molygraph Extreme Pressure Multi-purpose" grease.

4.4 Experimental Results

Strain gage data and the thermal measurements from a typical Kolsky bar test on the $Zr_{41.25}Ti_{13.75}Cu_{12.5}Ni_{10}Be_{22.5}$ metallic glass can be seen in Figures 40 and 41. The stress-strain curve and strain-strain rate curve reduced from these signals can be seen in Figures 42 and 43. Yield stresses were obtained for a variety of strain rates and plotted in Figure 44. Catastrophic failure of dynamic compression specimens occurred due to shear banding along a plane oriented $45°$ to the loading axis, identical to the failure observed in quasi-static tests.

Thermal measurements indicated that temperatures varied dramatically after the specimen failed reaching peak values of approximately 500 $°C$. Since the specimen failed by shear banding, it is possible that the variations in the thermal trace are due to the shear band pasing through the detector and that the peak values correspond to the maximum temperature reached within the shear band after deformation. This temperature is approaching the melting point of the $Zr_{41.25}Ti_{13.75}Cu_{12.5}Ni_{10}Be_{22.5}$ metallic glass, which would imply that the deformation within the shear band is so intense that the material within the band could be melting. It has also been observed that there is a temperature of 100 $°C$ which is sustained for a period of time after the specimen has yielded. Since the

homogeneous plastic deformation is too limited to account for this temperature rise, it could be due to the formation of micro-shear bands.

This is the first time transient thermal measurements have been made on a metallic glass during a shear banding event. However, more definite conclusions could be made about the origin of the thermal measurements if an array of detectors had been used to detect the inhomogeneous thermal distribution that would be associated with shear banding.
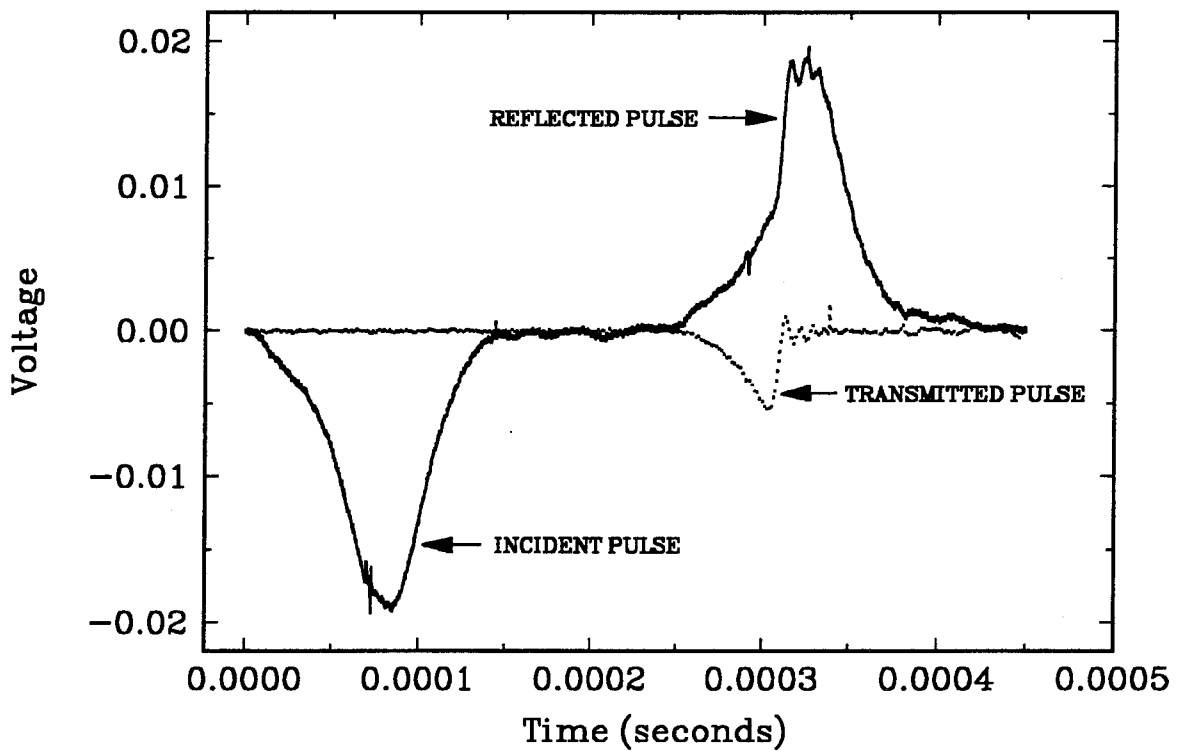

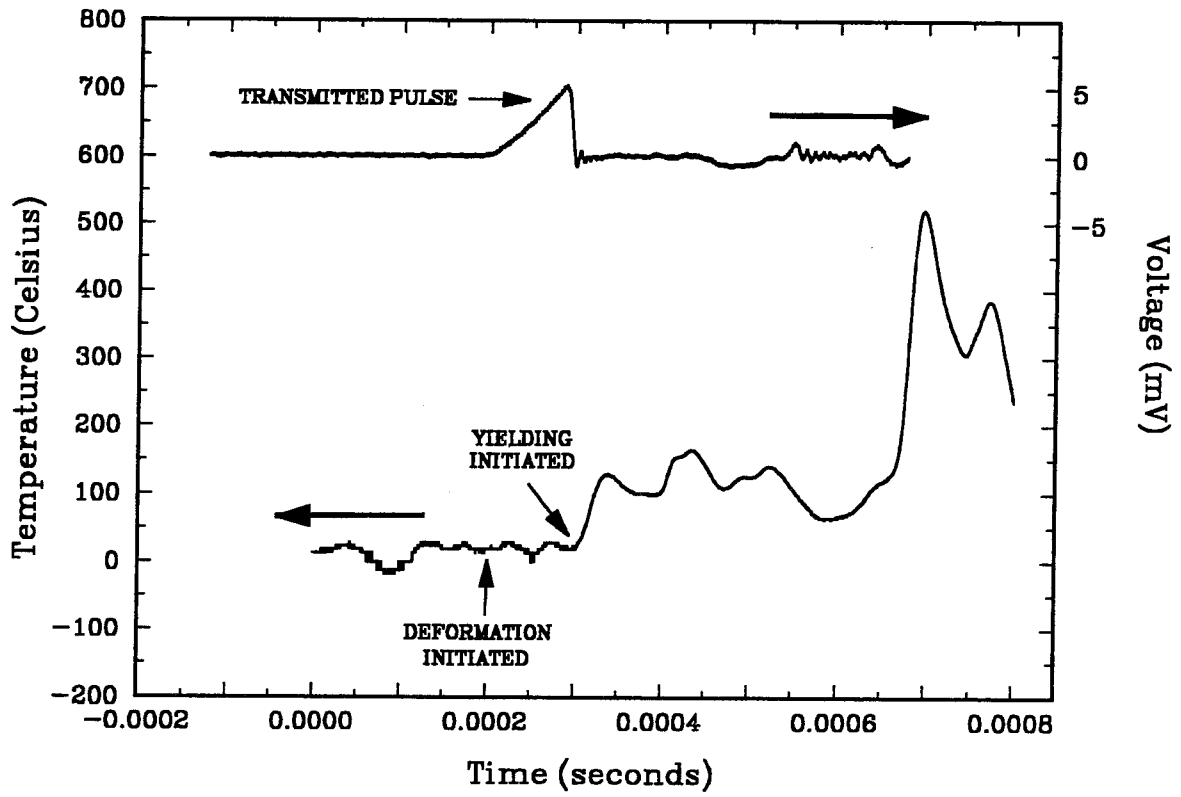Figure 40: Strain gage signals from dynamic compression test.

Figure 41: Temperature and loading recorded from dynamic compression test.
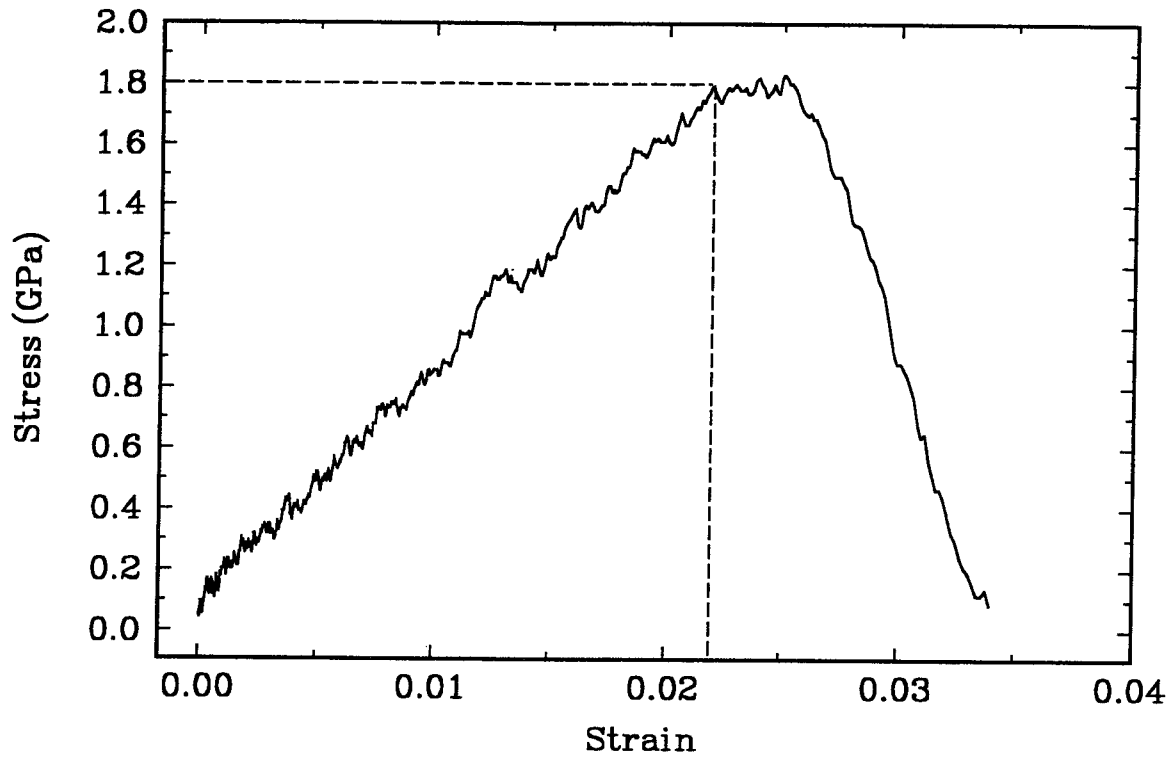
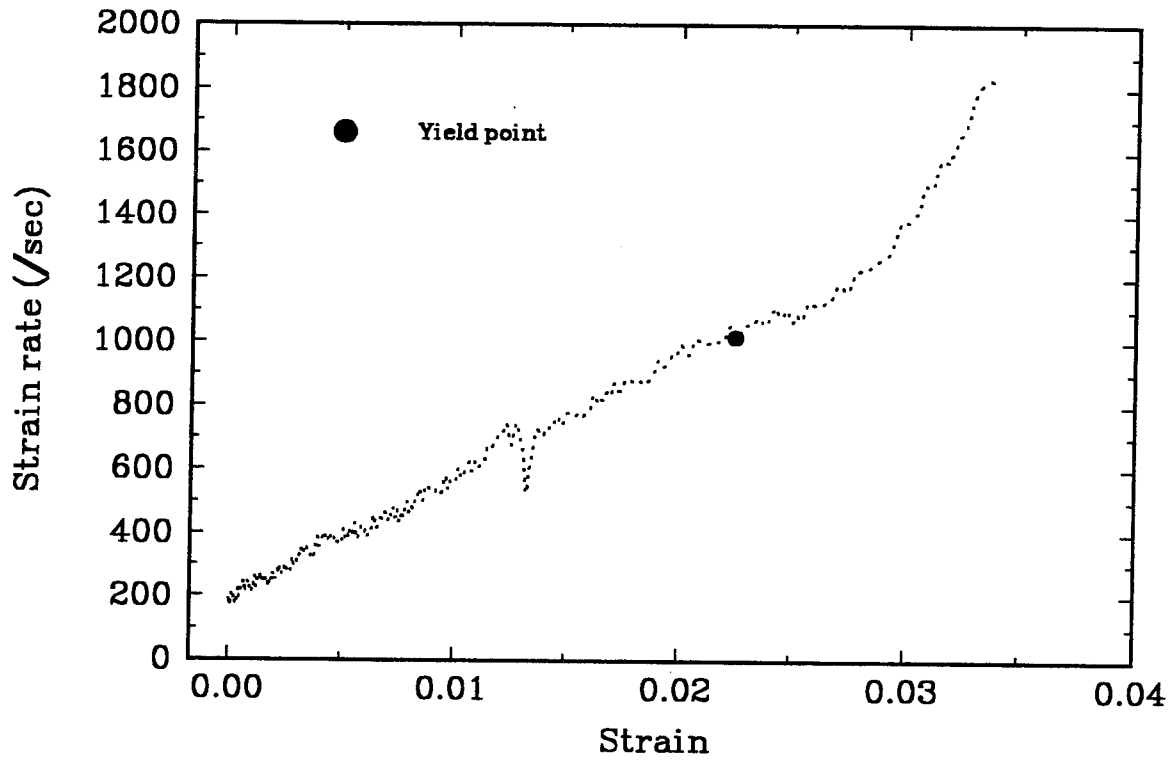**Figure 42: Stress-strain curve reduced from strain gage signals in Figure 40.**

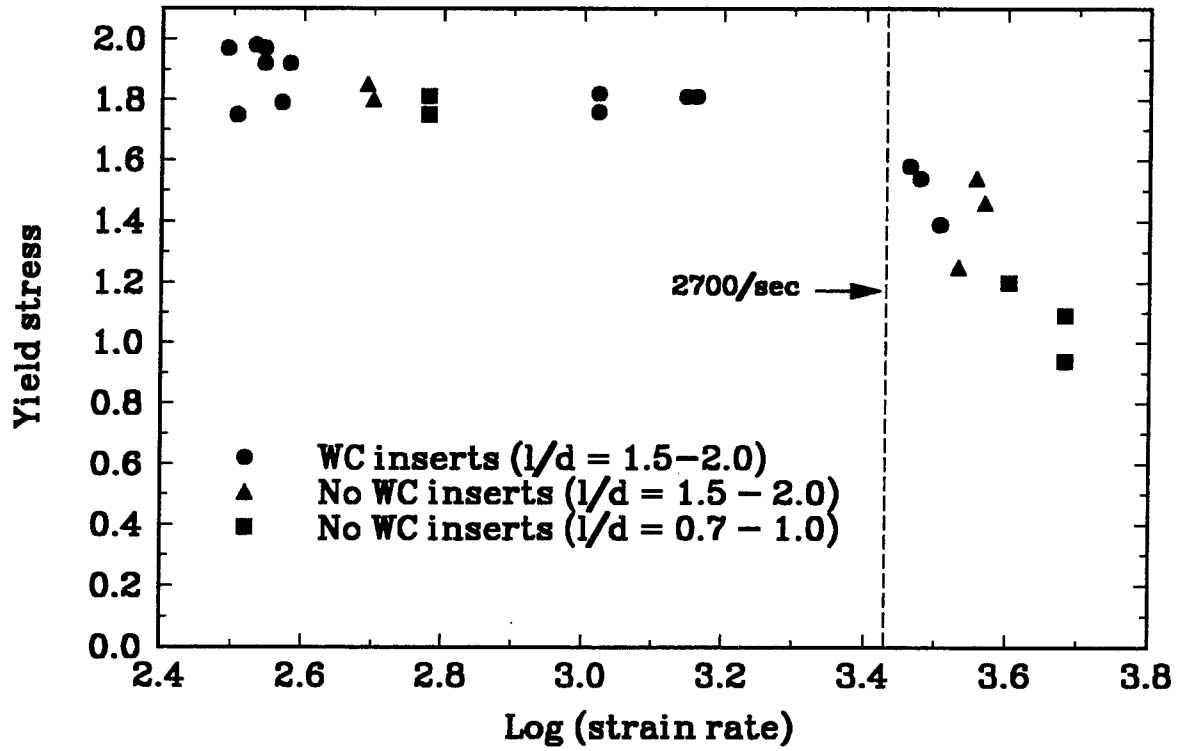**Figure 43: Strain-strain rate curve reduced from strain gage signals in Figure 40.**

Figure 44: Yield stress versus strain rate from dynamic compression tests.

The dynamic compressive stress-strain response in Figure 42 is very similar to the quasi-static compressive stress-strain response in Figure 20. The material exhibits an elastic-perfectly plastic response with yielding occurring at approximately 2% elastic strain. One notable difference between the quasi-static and dynamic responses was a substantial decrease in ductility. The ductility measured from the dynamic tests was never greater than 0.5%. This would tend to indicate that the maximum stresses near microscopic defects in the dynamic tests are closer to the critical values necessary to propagate the defects than the maximum stresses in the quasi-static tests.

Freund has numerically calculated the stress intensity factors near a crack tip loaded dynamically[4]. For a material with a Poisson's ratio of 0.3, the numerical calculations indicate that the dynamic stress intensity factor will be 30% greater than the quasi-static value. This is an illustration of the phenomenon of dynamic overshoot. If the material obeys a strain rate independent crack initiation criterion, then it will take less applied loading to propagate a defect dynamically than quasi-statically. This could only be verified by performing dynamic fracture tests on the $Zr_{41.25}Ti_{13.75}Cu_{12.5}Ni_{10}Be_{22.5}$ metallic glass.

From Figure 44, it appears that the dynamic compressive yield stress is within 5% of the quasi-static value for strain rates below 1500/sec. However, for strain rates greater than 3000/sec, the compressive yield stress appears to decrease monotonically with strain rate (strain rate softening). At first this was believed to have been due to adiabatic heating of the specimen, but thermal measurements indicated that no heating occurred prior to the onset of yielding (Figure 41).

During the dynamic compression tests, it was observed that the WC inserts were failing in tests conducted at strain rates above 3000/sec. If the WC inserts were failing before the specimens failed, then the observed strain rate softening could be due to the failure of the inserts. To test this theory, the WC inserts were removed and the compression tests repeated. By removing the inserts, the stress concentrations at the end

of the specimen might not be reduced which may cause premature failure. The results from these tests in Figure 44 indicate that removing the WC inserts did not alter the observed yield stress of the specimens at strain rates below 1500/sec, while still exhibiting the same softening behavior above 3000/sec. Therefore, it was decided that the WC inserts should be removed from the dynamic compression tests since they were not affecting the test results.

No other observations were made during the dynamic compression tests that might explain the apparent strain rate softening. Therefore, it became necessary to reassess the conditions under which the dynamic compression tests were performed to rule out any possible artifacts in the testing system that might be responsible for the apparent strain rate softening.

There are three basic, underlying assumptions used in the reduction of split Hopkison pressure bar test data. They are:

(1) The specimen undergoes homogeneous deformation during the experiment.
(2) The various stress pulses (e.g., reflected and transmitted) encountered in the split Hopkinson bar undergo minimal dispersion.
(3) The bars remain elastic at all times and the ends of the bars in contact with the specimen remain flat and parallel throughout the experiment.

For the strain rates above 3000/sec, the magnitude of the incident stress pulse was 400 GPa, well below the 2.5 GPa yield stress of the elastic bars. Therefore, assumption (3) was not violated. Verifying that the other two assumptions were not violated required using analyses developed by Ravichandran and Subhash.

4.5 Limiting Strain Rate for a Metallic Glass Specimen in a Kolsky Bar

Ravichandran used a simple analysis to establish the conditions under which a specimen must be tested to obtain homogeneous deformations consistent with assumption (1)[5]. This analysis assumed that there must be some minimum time, τ, which was required for the waves reflected back and forth inside a specimen to equilibrate. Let this time be a

multiple of the transit time, t_o, which is the time it takes for a wave to propagate from one end of the specimen to the other. In other words:

$$\tau = \alpha t_o, \tag{4.13}$$

where α represents a nondimensional number (the number of times the pulse is reflected back and forth within the specimen). The transit time is calculated as follows:

$$t_o = \frac{c}{L}, \tag{4.14}$$

where c is the longitudinal bar wave velocity for the specimen and L is the length of the specimen. Therefore, the time to failure, t_f, for metallic glass specimen should at least be greater than or equal to τ:

$$t_f \geq \tau = \alpha t_o. \tag{4.15}$$

Assume that the metallic glass specimen is linearly elastic until failure, which is reasonable given the limited ductility observed dynamically. Then, the nominal strain rate in the specimen can be approximated by:

$$\dot{\varepsilon} = \frac{\varepsilon_t}{t_f}, \tag{4.16}$$

where ε_f is the failure strain of the metallic glass, which is approximately equal to the yield strain. The limiting strain rate, $\dot{\varepsilon}_l$, for a specific length of metallic glass specimen is obtained by using equations (4.14), (4.15), and (4.16) as follows:

$$\dot{\varepsilon}_l = \frac{\varepsilon_f c}{\alpha L}, \tag{4.17}$$

The value of the nondimensional parameter α depends only on the shape of the incident pulse. From an analysis of one-dimensional wave propagation in the elastic bars and specimen using the method of characteristics[5], it was determined that for typical incident pulses the gradient of stress along the length of the specimen was within 5% of the mean stress in the specimen when $\alpha = 4$. This meant that for the metallic glass specimens used for the dynamic compression test, which had lengths of 5 mm or less and a

longitudinal bar wave velocity of 3925 m/s, the limiting strain rates were 3925/sec when the failure strain was at least 2%. Although this value is larger than the 3000/sec strain rate at which the softening began to occur, it was still close enough that it was decided to repeat the tests using specimens with aspect ratios of 0.7 to 1, which would increase the limiting strain rate to above 8000/sec and eliminate any questions about the homogeneity assumptions.

It has already been observed quasi-statically that by lowering the aspect ratio the yield stress and ductility increase because a plain strain stress state is approached. Therefore, the conditions appeared encouraging for these tests. In Figure 44, it can be seen that the yield stress results from these tests were identical to the test results for the longer specimens. In addition, the specimens appeared to be no more ductile than the longer specimens. Thus, it was concluded that the plane strain stress state was not being approached as the aspect ratios of the test specimens were reduced below 1 and that the inhomogeneity of the stress field was not responsible for the apparent softening behavior.

4.6 Effects of Dispersion in a Kolsky Bar at High Strain Rates

Ceramics have exhibited the same apparent strain rate softening behavior as the $Zr_{41.25}Ti_{13.75}Cu_{12.5}Ni_{10}Be_{22.5}$ metallic glass at strain rates above 2700/sec[6]. Dispersion effects were also analyzed by Ravichandran to determine if they would account for the apparent softening behavior of ceramics[5]. Because of dispersion effects, the amplitude and duration of a stress pulse changes as it propagates in a bar. The extent of geometrical dispersion depends on the dominant frequency components contained in the pulse that is being propagated, which is determined by the duration and shape of the pulse[7,8].

To obtain a quantitative measure for the minimum pulse duration needed to minimize the effects of dispersion, one must consider the fundamental frequency of a

typical input pulse that is being propagated in a cylindrical bar. The fundamental frequency for the pulse, ω_0, is defined as:

$$\omega_o = \frac{2\pi}{T},$$

(4.18)

where T is the period of the pulse[7,8]. The typical input pulses encountered in the dynamic compression tests are not purely sinusoidal but composed of multiple frequencies which are taken to be integer multiples of the fundamental frequency, ω_0. Associated with each of the frequencies is a characteristic propagation velocity, c_p (the phase velocity), defined as:

$$c_p = \frac{\omega}{2\pi}\Lambda.$$

(4.19)

The phase velocity is a function of the ratio a/Λ and can be obtained from the dispersion relation[7-9]. Here, a is the radius of the bar and Λ is the wavelength associated with a particular frequency component. The value of c_p for large wavelenghts can be obtained from the Rayleigh approximation[9]:

$$\frac{c_p}{c_o} = 1 - v^2\left(\frac{a}{\Lambda}\right)^2,$$

(4.20)

where v is Poisson's ratio.

The extent of dispersion during propagation of longitudinal pulses in a cylindrical bar is also a function of the ratio a/Λ and it has been shown that for $a/\Lambda > 0.1$, the distribution of displacement and axial stress across the cross section of the bar becomes highly nonuniform, i.e., it exhibits variations greater than 5%. Hence, the data obtained from the surface measurements on the bar, e.g., strain gages, will not provide an accurate measure of the strain (stress) at the input end of the bar for pulses with high-frequency components. This also violates the assumption that the wave propagation in the bar is one-dimensional.

In order to minimize the effects of dispersion, the dominant frequency component in the frequency spectrum of the input pulse in a cylindrical bar should be such that $a/\Lambda <$ 0.1. Using equations (4.18) and (4.19), this condition can be rewritten as:

$$\left(\frac{c_o}{c_p}\right)\frac{\omega}{\omega_o} < 0.1, \tag{4.21}$$

where ω_o is the fundamental frequency associated with the bar. This frequency is given by:

$$\omega_o = 2\pi\left(\frac{c_o}{a}\right). \tag{4.22}$$

For the Kolsky bars used in the dynamic compression experiments,

$$a = 6.35 \text{ mm}$$
$$v = 0.3$$
$$c_o = 4970 \text{ m/s}$$

Thus, plugging these values into equation (4.22) yields $\omega_o = 4.92 \times 10^6$ rad/s. Using the value for c_p at $a/\Lambda = 0.1$ from equation (4.20) and (4.21), a limiting value of 4.88×10^5 rad/s for the fundamental frequency of the pulse (ω) is obtained.

Assuming that the time to failure coincides with the peak of the input pulse, and from symmetry, the time to failure t_f will be T/2. The minimum time to failure t_f should be at least 6.44 μs to minimize dispersion. Using the failure strain of 2% for the $Zr_{41.25}Ti_{13.75}Cu_{12.5}Ni_{10}Be_{22.5}$ metallic glass, the limiting strain rate would be 3100/sec. This is approximately the strain rate at which the apparent strain rate softening begins. Since the reflected pulse is also affected by dispersion, it is not unreasonable to believe that the strain rates like the stresses are also underestimated. So, the true strain rates are probably much higher than 3000/sec which would mean that the strain rate softening occurs well beyond the calculated limiting strain rate.

There are two methods to correct the dispersion problem. The first is to directly correct for the dispersion in the signal[9]. This requires that a sufficient number of data points be sampled so that the contribution of each significant frequency component can be

extracted by means of a Fourier transform. At the sampling rates used in the dynamic compression experiments, approximately 80 data points could be obtained for strain rates above 3000/sec. Unfortunately, this is not enough data to properly characterize the signal in terms of its significant frequency components. Therefore, dispersion in the signal can not be corrected directly.

The second method involves placing a strain gage on the surface of the specimen to directly measure the specimen strain[6]. In order to interpret the corresponding stresses, a linearly elastic material response must be assumed. This assumption appears to be reasonable given that the $Zr_{41.25}Ti_{13.75}Cu_{12.5}Ni_{10}Be_{22.5}$ metallic glass exhibits linearly elastic behavior up to yield and that the ductility of the specimen is very limited.

A strain gage from JP Technologies was placed on the surface of a dynamic compression test specimen and tests were repeated for strain rates above 3000/sec and at approximately 230/sec. For strain rates of 230/sec, the specimen did not fail and the deformation was purely elastic. The strains were recorded from the specimen strain gage and compared with the strain derived from the transmitted pulse assuming a linearly elastic response (Figure 45). From these results it appears that the strains from the specimen strain gage are within 5% of the strains derived from the transmitted pulse with the greatest deviation occurring at the peak strain level. This is not unexpected since strain gage signals are rarely accurate to within 10% of the actual strain depending on the strength of the adhesion between the gage and the specimen surface. The strain rate was computed by curve fitting the linear portion of the strain signal from the specimen strain gage.

After elastically loading the specimen at low strain rates, the specimen was reloaded at a strain rate above 3000/sec. A typical result can be seen in Figure 46 where the strain rate was determined to be approximately 3400/sec. From these results it is obvious that the strain derived from the transmitted signal does not correlate with the strain from the specimen strain gage. In fact, the strain from the strain gage has a
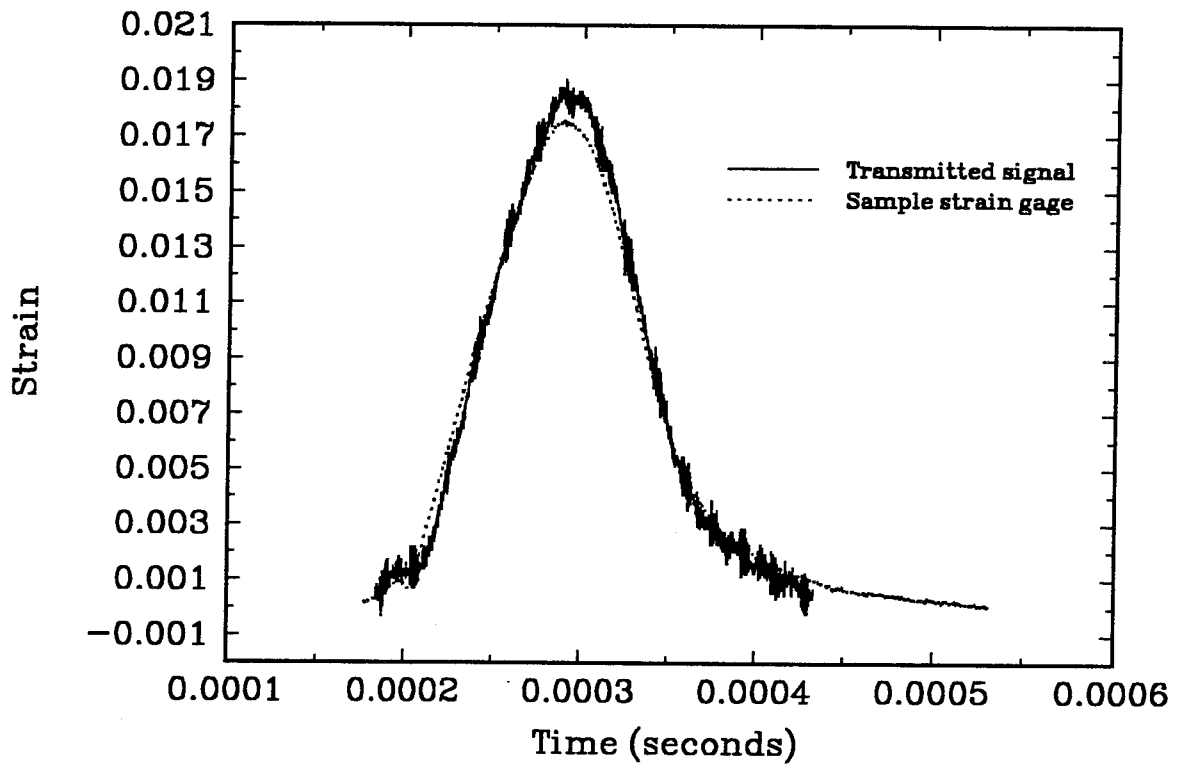
Figure 45: Dynamic strain response from the specimen strain gage and derived from the transmitted signal for a strain rate of 230/sec.

bandwidth of approximately 10 μs while the strain derived from the transmitted signal has a bandwidth of about 14 μs. This difference in bandwidths was also observed in high strain rate compression tests conducted on ceramics and attributed to dispersion effects.
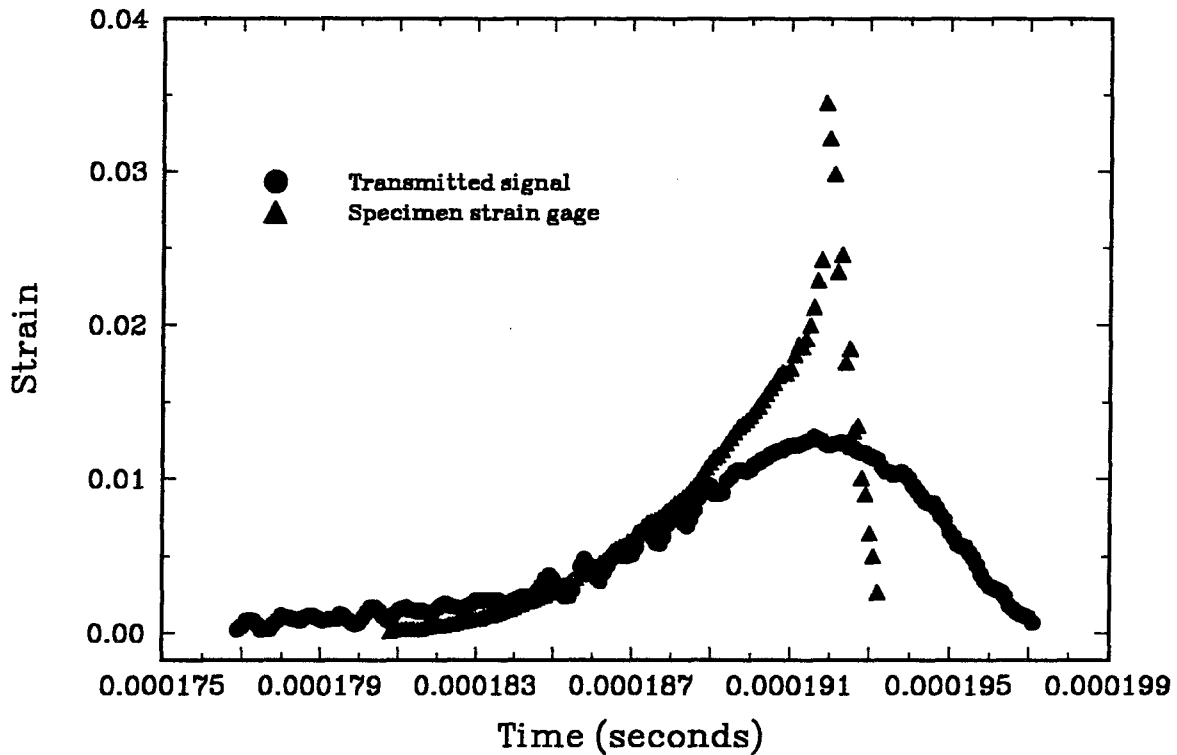

Figure 46: Dynamic strain response from the specimen strain gage and derived from the transmitted signal for a strain rate of 3400/sec.

The strain response from the specimen strain gage shows a dramatic increase in strain rate at approximately 2.0% strain, which is most likely due to the initiation of shear banding. Therefore, this was taken to be the yield strain of the specimen. The peak strain derived from the transmitted bar is approximately 1.3%, a value 35% below the yield strain. The differences in peak strain were also observed in the high strain rate experiments conducted on ceramics and attributed to dispersion effects.

The yield stress was therefore calculated to be approximately 1.9 GPa, which is within 5% of the value derived from the transmitted signal at strain rates below 3000/sec. This yield stress can be seen in Figure 47 plotted against the data from Figure 44 along

with another data point obtained using a strain gage on a specimen tested at a strain rate of approximately 4400/sec. The data points obtained using specimen strain gages are larger than any of the yield stresses derived from the transmitted signal at strain rates above 3000/sec, clearly indicating that dispersion effects are responsible for the apparent softening behavior observed at strain rates above 3000/sec.
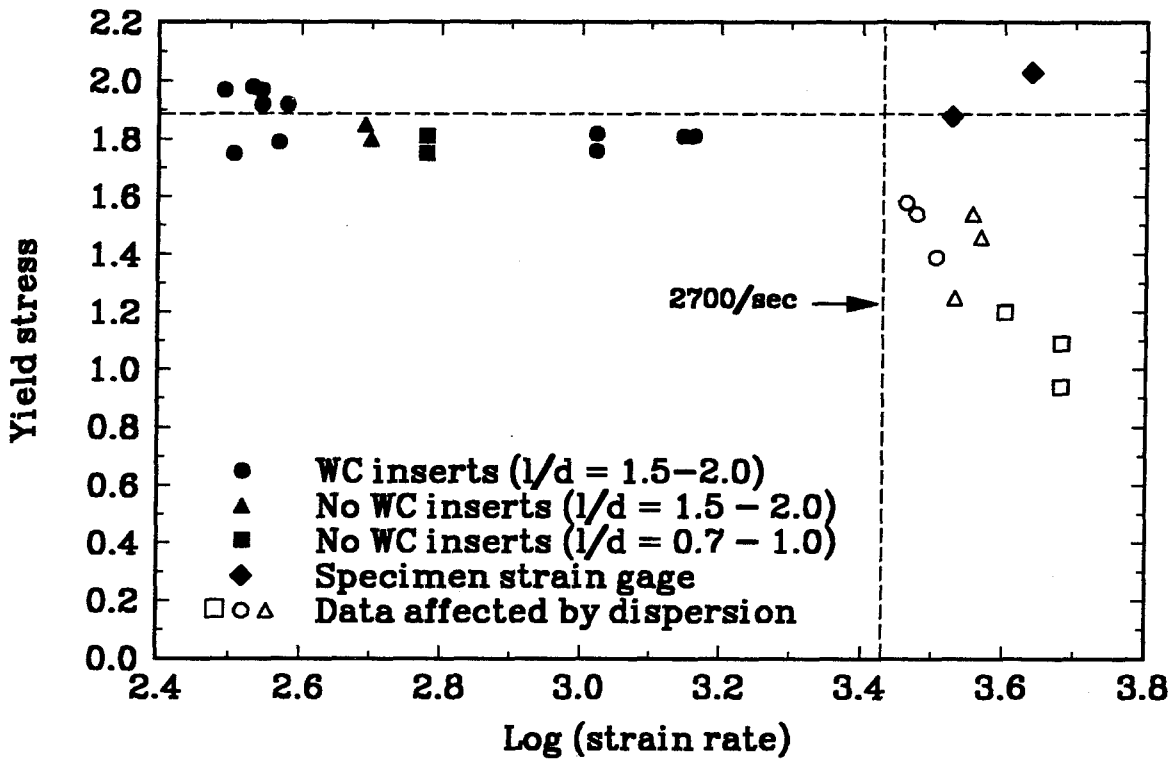

Figure 47: Data from Figure 44 plotted against specimen strain gage data.

Although peak strains of 3.5% were measured from the specimen strain gage, it is difficult to interpret these corresponding load levels. Obviously, if shear banding has occurred, the stresses can not be derived assuming a linearly elastic behavior. Furthermore, the strain would appear to be accumulated at rates of approximately 30,000/sec. It has been postulated that strain rates of this order or higher might occur inside a shear band during dynamic deformation. Although it is unreasonable to assume that the strain gage could resolve strains inside a shear band, it does indicate that there is some type of post-yield behavior such as shear band deformation occurring.
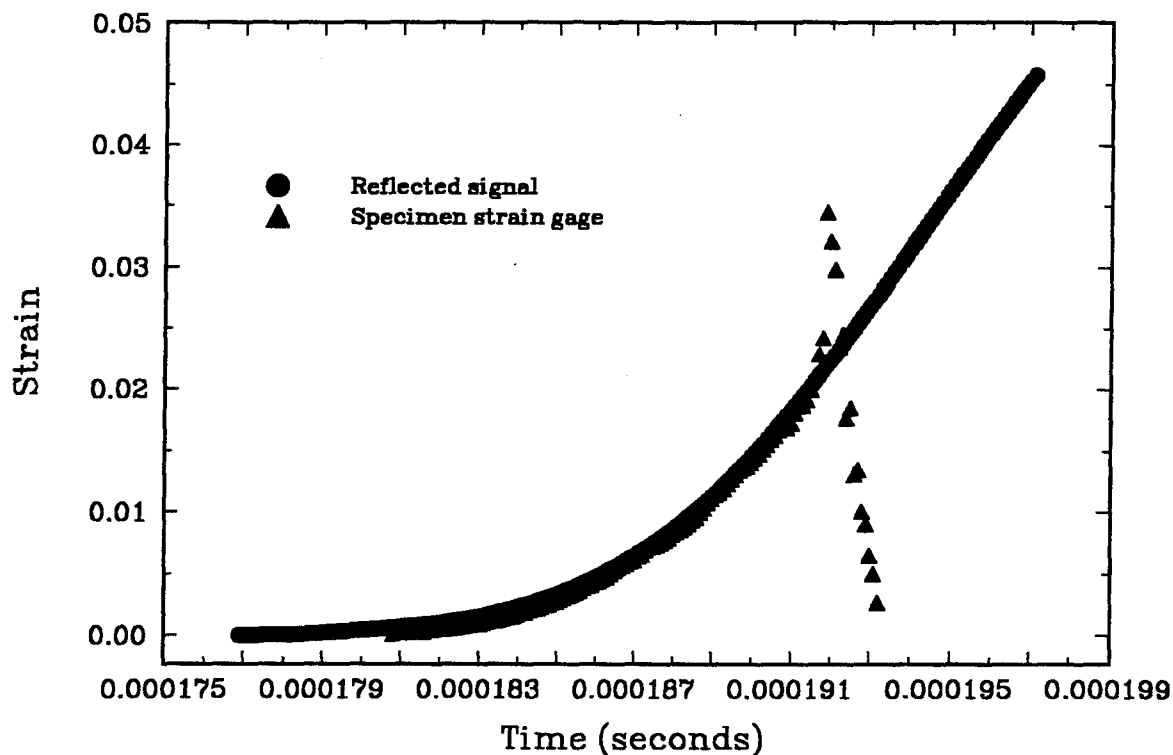
Figure 48: Dynamic strain response from the specimen strain gage and derived from the reflected signal for a strain rate of 3200/sec.

While the strain derived from the transmitted signal is affected by dispersion, the strain derived from the reflected signal does not appear to be as sensitive (Figure 48). In fact, up to yielding the two signals appear to be identical. This would indicate that although the yield stresses in Figures 44 and 47 might be affected by dispersion at strain rates above 3000/sec, the strain rates should be correct. Given that the typical reflected signal is similar to the incident signal, as seen in Figure 40, with a period twice as large as that of the transmitted signal, it appears reasonable that the reflected signal would be insensitive to dispersion.

References

[1] Kolsky, H., Proceedings of the Royal Society of London, **B62**, 676 (1949).

[2] Zehnder, A.T. and Rosakis, A.J., Journal of the Mechanics and Physics of Solids, **39**, 385 (1991).

[3] Rosakis, A.J., Mason, J.J., and Ravichandran, G., to appear in Journal of Mechanical Behavior of Materials.

[4] Freund, L.B., Dynamic Fracture Mechanics, Cambridge University Press, New York (1990).

[5] Ravichandran, G. and Ghatuparthi, S., Journal of the American Ceramic Society, **77**, 263 (1994).

[6] Staehler, J.M., Predebon, W.W., Pletka, B.J., and Lankford, J., Journal of the American Ceramic Society, 76, 536 (1993).

[7] Davies, R.A., Philosophical Transactions of the Royal Society of London, **A240**, 375 (1948).

[8] Follansbee, P.S. and Frantz, C., Journal of Engineering Materials and Technology, **105**, 61 (1983).

[9] Kolsky, H., Stress Waves in Solids, Dover Publications, New York (1963).

CHAPTER 5

Conclusions and Future Work

5.1 Quasi-static Yield Behavior of $Zr_{41.25}Ti_{13.75}Cu_{12.5}Ni_{10}Be_{22.5}$ Bulk Metallic Glasses

5.1.1 Yield criterion

The quasi-static yield behavior of $Zr_{41.25}Ti_{13.75}Ni_{10}Cu_{12.5}Be_{22.5}$ bulk metallic glasses has been characterized. Compression, tension, and torsion tests have indicated that the $Zr_{41.25}Ti_{13.75}Ni_{10}Cu_{12.5}Be_{22.5}$ metallic glass obeys a von Mises yield criterion, which supports Masumoto's findings that the $Pd_{78}Cu_6Si_{16}$ metallic obeys a von Mises yield criterion. Von Mises materials exhibit isotropic, pressure insensitive yield behavior. This yield behavior would indicate that some type of shear defect like dislocations or disclinations is the micromechanism responsible for yielding in metallic glasses. The $Zr_{41.25}Ti_{13.75}Ni_{10}Cu_{12.5}Be_{22.5}$ metallic glass also exhibits an elastic-perfectly plastic yield behavior in compression and torsion tests.

The failure surfaces for quasi-static uniaxial compressive and torsional stress states were oriented along directions predicted by slip line field theory. This provides some additional evidence that the $Zr_{41.25}Ti_{13.75}Ni_{10}Cu_{12.5}Be_{22.5}$ metallic glass exhibits an elastic-perfectly plastic yield behavior and obeys a von Mises yield criterion. However, uniaxial tension tests indicated that the orientation of the failure surface did not correspond to the slip line field solution and may be sensitive to pressure. Numerical simulations and more detailed investigations of the orientation of shear bands with respect to hydrostatic pressure may be necessary to resolve this issue. In all three cases, failure is precipitated by highly localized viscous deformation within shear bands which was confirmed by scanning electron microscopy.

5.1.2 Ductility

The ductility of the $Zr_{41.25}Ti_{13.75}Ni_{10}Cu_{12.5}Be_{22.5}$ metallic glass is strongly dependent on stress state. In tension, there is no apparent macroscopic ductility because the shear band deformation causes a plastic instability that can not be constrained. However, in uniaxial compression there appears to be substantially more ductility. The compressive ductility varied from negligible plastic strain for 7 mm diameter rods cast in evacuated quartz tubes up to 10% true plastic strain for 2.5 mm diameter rods cast in copper molds. Plane strain compression tests indicated that 2.5 mm diameter rods possessed compressive ductilities of over 30% true plastic strain. Attempts were to increase ductility in uniaxial compression by adding boron to the metallic glass, but instead concentrations greater than 1 a.t. % boron embrittled the specimens. In torsion, the specimens exhibited ductility of the same magnitude as the 7 mm diameter rods cast in evacuated quartz tubes that were used in the compression tests. The torsional ductility was also verified from shear stress measurements and optical examination of the torsional failure surface to exhibit an elastic-perfectly plastic behavior.

It has been proposed that the concept of micro-fracture stress could be used to explain the observed differences in the ductility of metallic glasses. Ductility could be removed by decreasing the micro-fracture stress below the maximum longitudinal stress, i.e., fracture processes can occur at lower applied stress levels than slip processes. Ductility may also be increased by loading metallic glasses in stress states like plane strain which are more conducive to slip processes than fracture processes.

However, the concept of micro-fracture stress needs to be refined in order to reflect the true nature of ductile deformation and failure in metallic glasses. These refinements require that quasi-static and dynamic fracture tests be performed in shear stress states rather than in uniaxial stress states in order to better quantify the competition between fracture and slip processes that is responsible for the observed differences in the ductility of metallic glasses.

It has been observed that the micro-fracture stress depends on the microstructure of the glass. Although x-ray diffraction patterns and densities of compression specimens were obtained at various quench rates and metalloid concentrations, no changes could be detected at the resolutions of the measurement techniques. The resolution of the x-ray analysis was not limited by the measurement device, but rather by the uncertainty in locating the specimen's true peak position due to significant contributions to the peak of the diffracted signal from the glass slide that the specimen was glued onto. X-ray measurements can be improved to 0.03^o if the x-ray beam is focussed on a smaller specimen area thereby removing the contribution of the glass slide from the diffracted signal. Also, the resolution of density measurements can be improved by an order of magnitude if a scale is used with a resolution of 10 μg instead of the 100 μg resolution used for this work. In addition, high resolution transmission electron microscopy investigations may also detect microstructural differences at an atomistic scale.

Properly quantifying the dependence of ductility on quench rate and metalloid concentration will require fabricating a set of fracture specimens whose quench rates and metalloid concentrations can be accurately controlled. The metalloid concentration can be easily controlled since it is a function of composition and not of the manufacturing process. Whether or not the quench rates can be controlled will depend on the plane strain fracture toughness of the $Zr_{41.25}Ti_{13.75}Cu_{12.5}Ni_{10}Be_{22.5}$ metallic glass, which will dictate the minimum specimen thickness required to run a valid plane strain fracture test. Furthermore, if the specimens are thick enough, then the quench rates will be too inhomogeneous through the thickness of the specimen to be able to quantify their effect on fracture processes.

If a concept similar to the micro-fracture stress can be used to determine the ductility of a metallic glass, then it is likely that some type of dilitational defect like vacancies is responsible for determining ductility in metallic glasses. It is not unlikely that there might be multiple types of defects responsible for the yield behavior of metallic

glasses. The activation of slip in metallic glasses might depend on the strength of the elastic bonding near some type of shear defect, while the micro-fracture stress might depend on the quantity of free volume associated with some type of dilatational defect.

5.2 Dynamic Yield Behavior of $Zr_{41.25}Ti_{13.75}Cu_{12.5}Ni_{10}Be_{22.5}$ Bulk Metallic Glasses

5.2.1 Strain rate dependence of yield stress

For the first time, dynamic tests have been conducted on a metallic glass at strain rates on the order of 10^2-10^3/sec. From these tests, it appears that the yield stress of the $Zr_{41.25}Ti_{13.75}Cu_{12.5}Ni_{10}Be_{22.5}$ metallic glass does not depend on strain rate. This result is not unexpected since the micromechanisms for yielding in metallic glasses are much different than in conventional polycrystalline metals and ceramics, where the growth and motion of defects like dislocations and microcracks are sensitive to strain rate.

However, the ductility of the $Zr_{41.25}Ti_{13.75}Cu_{12.5}Ni_{10}Be_{22.5}$ metallic glass does appear to depend on strain rate. This dependence may be due to the increase of stress concentrations near microscopic defects. As the strain rate increases, a phenomenon known as dynamic overshoot occurs near the tips of cracks where the dynamic stress intensity factor can be 30% greater than the quasi-static value. For a material whose fracture initiation criterion is independent of strain rate, dynamic overshooting would effectively increase the stress concentrations near microscopic defects thereby reducing the ductility of dynamically loaded specimens by favoring fracture over slip processes.

In order to properly quantify the differences in the ductility of metallic glasses, it is imperative that dynamic and quasi-static fracture tests be conducted on the $Zr_{41.25}Ti_{13.75}Cu_{12.5}Ni_{10}Be_{22.5}$ metallic glass. These tests should generate Mode II crack tip stress fields instead of Mode I in order to assess a critical shear criterion which would be a more appropriate criterion to evaluate the ductility of metallic glasses. In addition, measurements should be made of the deformation fields near crack tips for quasi-

static and dynamic fracture specimens, as well as the temperature fields near the tip of cracks propagating in the dynamic fracture specimens. These measurements will provide a better understanding of the strain rate dependent competition between slip processes and fracture processes in metallic glasses.

5.2.2 Thermal measurements

Thermal measurements of shear banding processes in metallic glasses have been made for the first time. These measurements indicate that temperature increases due to adiabatic heating occur only after the onset of shear band deformation. Furthermore, temperatures near the melting point of the $Zr_{41.25}Ti_{13.75}Cu_{12.5}Ni_{10}Be_{22.5}$ metallic glass may be approached within the shear band after the specimen has failed. Since only a single detector was used for the thermal measurements, it was impossible to verify the thermal distribution near the shear band. Verification can only be obtained using an array of thermal sensors which could detect the inhomogeneous temperature distribution associated with shear banding. Then, more definite conclusions can be drawn about the temperatures that may be generated inside a shear band.